Compact Ku-band Transmitter Design for Satellite Communication Applications:

From System Analysis to Hardware Implementation

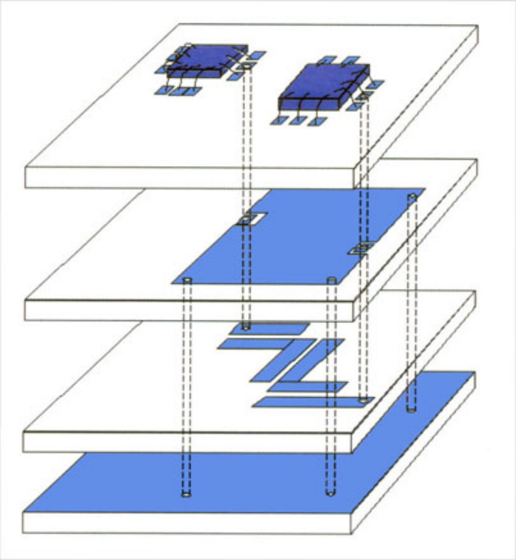

Chang-Ho Lee
Joy Laskar

Compact Ku-band Transmitter Design for Satellite Communication Applications

From System Analysis To Hardware Implementation

This page intentionally left blank

Compact Ku-band Transmitter Design for Satellite Communication Applications

From System Analysis To Hardware Implementation

Chang-Ho Lee
RF Solutions

Joy Laskar
Georgia Institute of Technology

KLUWER ACADEMIC PUBLISHERS
NEW YORK, BOSTON, DORDRECHT, LONDON, MOSCOW

eBook ISBN: 0-306-47530-8
Print ISBN: 0-7923-7698-6

Created in the United States of America

Visit Kluwer Online at: http://kluweronline.com
and Kluwer's eBookstore at: http://ebooks.kluweronline.com

To Our Family

This page intentionally left blank

Contents

PREFACE xi

1. INTRODUCTION 1

2. KU-BAND TRANSMITTER ARCHITECTURE 7
   2.1 DESIGN CRITERIA 7
      2.1.1 Modulator Design Criteria 7
      2.1.2 Frequency Translator Design Criteria 9
      2.1.3 Power Amplifier Design Criteria 9
   2.2 UP-CONVERSION TOPOLOGIES 11
      2.2.1 Direct Up-conversion Scheme 11
      2.2.2 Double Up-conversion Scheme 14
      2.2.3 Double Up-conversion with Offset Oscillator 17

3. TRANSMITTER SYSTEM SIMULATION MODEL 19
   3.1 INTRODUCTION 19
   3.2 SYSTEM MODEL DEVELOPMENT 19
   3.3 TRANSMITTER MODULE IMPLEMENTATION PROCEDURE 25

4. REVIEW OF KU-BAND MIXERS 27
   4.1 MIXER DESIGN PRINCIPLES 27
   4.2 MIXER PERFORMANCE PARAMETERS 29
      4.2.1 Conversion Gain 29
      4.2.2 Conversion Compression 30
      4.2.3 Isolation 30
      4.2.4 Dynamic Range 30

4.2.5 Dc Offset ... 30
4.2.6 Intercept Point ... 31
4.2.7 Noise Figure ... 31
4.2.8 Spurious Response ... 31
4.3 DEVICE TECHNOLOGIES FOR KU-BAND MIXER 32
4.3.1 Schottky Barrier Diode ... 32
4.3.2 GaAs Metal Semiconductor Field Effect Transistors ... 34
4.3.3 GaAs High Electron Mobility Transistors ... 35
4.3.4 Heterojunction Bipolar Transistors ... 36
4.4 KU-BAND MIXER TOPOLOGIES 39
4.4.1 Diode Mixer Topologies ... 40
4.4.2 Active FET Mixer Topologies ... 44
4.4.3 Passive FET Mixer Topologies ... 51
4.4.4 Other Topologies ... 52
4.5 COMPARISON OF KU-BAND MIXER 55
4.6 CONCLUSIONS 57

5. REVIEW OF KU-BAND VCOs 59
5.1 OSCILLATOR DESIGN PRINCIPLES 59
5.1.1 Feedback Oscillator (Two-port Model) ... 59
5.1.2 Negative Resistance (One-port Model) ... 60
5.2 VCO DESIGN PRINCIPLES 62
5.3 VCO PERFORMANCE PARAMETERS 63
5.3.1 Phase Noise ... 64
5.3.2 Load Pushing and Pulling ... 65
5.3.3 Thermal Stability ... 66
5.3.4 Post-Tuning Drift ... 66
5.4 KU-BAND VCO MMIC 67
5.4.1 YIG-Tuned oscillator ... 67
5.4.2 Varactor Tuned Oscillator ... 73
5.4.3 Tunable Active Inductor Controlled Oscillator ... 78
5.5 KU-BAND GAAS MESFET VCO DESIGN 86
5.6 KU-BAND ALGAAS/GAAS HBT VCO 88
5.7 CONCLUSIONS 88

6. TRANSMITTER MMIC FOR SATELLITE COMMUNICATIONS APPLICATIONS 91
6.1 INTRODUCTION 91
6.2 TRANSMITTER MMIC DESIGN CRITERIA 92
6.3 DUAL GATE MIXER 93
6.3.1 Mixer MMIC Design ... 93
6.3.2 Measured Performance ... 95
6.4 VOLTAGE CONTROLLED OSCILLATOR 99

6.4.1 VCO MMIC Design 99
6.4.2 Measured Performance 101
6.4.3 LO Buffer Amplifier MMIC 105
6.5 IF AMPLIFIER MMIC AND RF AMPLIFIER MMIC 108
6.6 DRIVER AMPLIFIER MMIC 111
6.6.1 Driver Amplifier Design 111
6.6.2 Measured Performance 113
6.7 POWER AMPLIFIER DESIGN 115
6.7.1 Power Amplifier Design Principles 115
6.7.2 Linear Power Amplifier Review 115
6.7.3 Power Amplifier Design 116
6.7.4 Measured Performance 118
6.8 CONCLUSIONS 119

7. TRANSMITTER MODULE DESIGN 121
7.1 INTRODUCTION 121
7.2 STRIP LINE BAND PASS FILTER 121
7.2.1 Strip Line Filter Design Principles 121
7.2.2 LTCC-based Strip Line Filter Design 124
7.2.3 Measured Performance 129
7.3 MODULE DESIGN 130
7.4 MODULE MEASUREMENT RESULTS 132
7.5 CONCLUSION 137

8. CONCLUSION 139

BIBLIOGRAPHY 141

INDEX 159

This page intentionally left blank

Preface

As the wireless communication of voice, video and data grows, the increasing demand for channels and bandwidth is driving communication transceiver systems toward microwave and millimeter-wave frequencies. To satisfy the significant worldwide demand for higher data rates and wide band transmission, applications of microwave communication systems that use satellite systems have been expanding.

There is a growing market for both fixed and mobile Ku-bad transceiver systems. The international telecommunication union (ITU) assigned orbital slots for direct broadcast system (DBS) and designated Ku-band (12~18GHz) for transmission, so there is an increasing use of the Ku-band frequency range, which is compatible with North America's very small aperture terminal (VSAT) for satellite communications. The expanding use of satellite communications in the Ku-band has created the need for low cost and highly reliable Ku-band transceivers. The present North America VSAT system uses Ku-band with a transmission frequency of 14~14.5GHz. One of the critical elements in the direct satellite communication system is a compact, low-cost transmitter block. Also introduction of Ku-band direct-to-home (DTH) satellite television service has created an enormous market for wireless transmission of digital signals. These kinds of services developments have created a rapidly growing market for radio frequency integrated circuits (RFICs) for wireless transceiver system.

In recent decades, VSAT networks have spread throughout the world. The demand for small transceivers has increased because of their portability. Because an outdoor unit is mounted on an antenna, it must be small and weigh little. In recent years, directly modulated transmitters have been proposed that eliminate any frequency conversion and thus diminish the size of the transceiver. However, their incompatibility with VSAT networks that are already in operation largely limits them to experimental use. In this book, we emphasize the miniaturization and integration of conventional transceivers to meet the need of most existing VSAT networks. The drawbacks of most commercially available transceivers are their relatively large size, weight, and separately located modules. For example, the low noise amplifier (LNA) of the transceiver is left alone on the feed while the rest is fastened to the antenna rack placed on the ground. Therefore, additional RF cables and dc lines are needed to link it with the main body of the transceiver. By improving the circuit's design and a more deliberate circuit layout, we seek to minimize the size of each module to cut down the total size of the transceiver. One obstacle is the large and heavy cavity filter that cannot be integrated into other MIC layouts directly. To address this issue, a low temperature co-fired ceramic (LTCC)-integrated coupled strip-line filter has been incorporated to replace the discrete cavity filter.

This book will review approaches to and topologies of Ku-band transmitters and study their advantages and disadvantages and determine the critical design criteria in order to enhance system performance. Some of the original contributions of this book are:

- Systematic topology analysis and system model development for Ku-band transmitters;
- First fundamental analysis of phase noise using a reflection coefficient line for voltage controlled oscillator (VCO) design and implementation;
- First demonstration of the low phase noise performance at high drain bias using reflection coefficient line analysis;
- The best reported phase noise performance for a GaAs metal semiconductor field effect transistor (MESFET) VCO MMIC;
- First development and characterization of miniaturized multi-layer integrated strip-line Ku-band filters using coupled-line topologies;
- First demonstration of a functional ultra-compact LTCC-based transmitter module for Ku-band satellite communication applications featuring an integrated filter and monolithic microwave integrated circuit (MMIC) chipsets using a low-cost commercial GaAs MESFET process.

This book is divided into eight chapters. Chapter 1 offers a brief introduction of satellite communication systems. Chapter 2 reviews the transmitter architecture and, through comparative analysis, identifies the design criteria for up-conversion topologies. In Chapter 3, a system model for a transmitter is developed and a thorough system level analysis is performed to define the required design parameters for a Ku-band transmitter that can meet VSAT specifications. Chapter 4 is devoted to the review of mixer design principles, device technologies, and topologies for a Ku-band mixer. This discussion also will suggest the most suitable technology and topology for commercial Ku-band mixer designs. Chapter 5 will review approaches and topologies of GaAs MESFET Ku-band VCOs and study their advantages and disadvantages. A comparison will be conducted between GaAs MESFET Ku-band VCO and AlGaAs/GaAs heterojunction bipolar transistor (HBT) Ku-band VCO designs. Chapter 6 summarizes the design and technology issues of each building block and the design and measurements of the compact monolithic integrated circuits (IC) for a transmitter. Chapter 7 describes the design and measurements of LTCC-based BPF and LTCC-based entire transmitter module. Chapter 8 summarizes the measured transmitter performance and offers transmitter module design recommendations.

The authors are deeply indebted to many people for their guidance, support, and contribution to this writing project. The authors also have benefited greatly from the collaboration and support of Yamacraw Design Center and Packaging Research Center at the School of Electrical and Computer Engineering at Georgia Institute of Technology, and TriQuint Semiconductor for their MMIC fabrication, and National Semiconductor Corporation for their LTCC fabrication.

This page intentionally left blank

Chapter 1

Introduction

The growth of wireless communications is causing an increasing demand for channels and bandwidth, which drives the wireless transceivers toward microwave and millimeter-wave frequencies. To satisfy the significant worldwide demand for higher data rates and wideband transmission, applications of microwave communications systems using satellite systems are expanding. The era of satellite communications began in the early 1960's after the first launch of communications satellites such as Telstar and Relay in 1962, Syncom in 1963, and INTELSAT 1 and MOLNIYA 1 in 1965 [1]. From then on, the field of satellite communications has continued to grow rapidly. Satellites became dramatically larger, capable of increased capacity, and employed rapidly developing lightweight electronics technology, spacecraft control and power generation and storage devices. Significant development went into sophisticated space-borne regional and spot-beam dual polarized antennas at both C- and Ku-band to increase payload capacity through frequency reuse techniques. Next, VSAT networks and applications and DBS systems and technology were introduced. Today, communications satellites carry about one third of voice and essentially all international television traffic [1]. Significant advances in video compression and data protocol enhancement technology have made possible previously very expensive satellite communications services such as digital DBS, digital DTH, and internet access at lower cost. At the same time, we are entering a new and potentially revolutionary era in satellite communications. A large number of commercial systems are being planned and introduced to provide an array of voice, data, and video services that promise to radically change global telecommunications.

In summary, satellite technology is a preferred choice for a variety of telecommunications applications such as television broadcast distribution and basic voice and data communications, where the terrestrial infrastructure is either insufficient or nonexistent. It is also possible to address the emerging wideband multimedia applications with new advances in VSAT technology, extending terrestrial infrastructure seamlessly over large geographic areas.

Satellite communications services operate over the following assigned spectrum allocations as summarized in Table 1.1 [2]:

Table 1.1. Spectrum allocation for satellite communications

Frequency band	Frequency range	Satellite Service
L-band	1.5 ~ 1.65 GHz	Mobile satellite service (MSS), UHF TV
S-band	2.4 ~ 2.8 GHz	MSS, NASA deep space research
C-band	3.4 ~ 7.0 GHz	Fixed satellite service (FSS)
X-band	7.9 ~ 9.0 GHz	FSS military communication
Ku-band	10.7 ~ 15.0 GHz	FSS, Broadcast satellite service (BSS)
K-band	18 ~ 26 GHz	BSS, FSS
Ka-band	26.0 ~ 31.0 GHz	FSS, Local multipoint distribution service (LMDS)

Satellite communications are delivered through a network architecture that can be divided into three categories: point-to-point (mesh), point-to-multipoint (broadcast), and multipoint interactive (VSAT) [3]. The VSAT category is a sophisticated communications technology that allows for the use of small, fixed satellite antennas to provide a highly reliable communication between a central hub and almost any number of geographically dispersed sites, as shown in Figure 1.1. VSATs are taking on an expanding role in a variety of interactive, online data, voice, and multimedia applications. Such a network can provide a variety of services, including internet access, multimedia conferencing, video conferencing, video-telephony, distance learning, and voice transmission [4].

Commercial VSAT systems operate in C- and Ku-band; however, a demand for much wider bandwidth make Ka-band frequencies much more attractive for future commercial VSAT systems. The short wavelengths at higher frequencies have the advantage of allowing compact terminals and antennas to support high bandwidth applications. Because of the demand for bandwidth, the up and down links have moved from the C-band to the Ku-band and have now moved up to the K- and Ka-band. There are also a host of wide band systems being introduced for Ka-band, such as Astrolink, Spaceway and Teledesic, which intend to provide multimedia services to desktop computer-size terminals. Both the narrow band and wide band systems appear attractive because they offer much higher capacity and relatively low user costs compared to traditional systems. In the future, as the bandwidth demand continues to escalate, the carrier frequencies will move up to even higher bands. Recently, several companies announced proposals to build satellite systems in the Q and V bands to supplement the Ka-band wide band systems now in various stages of development [1].

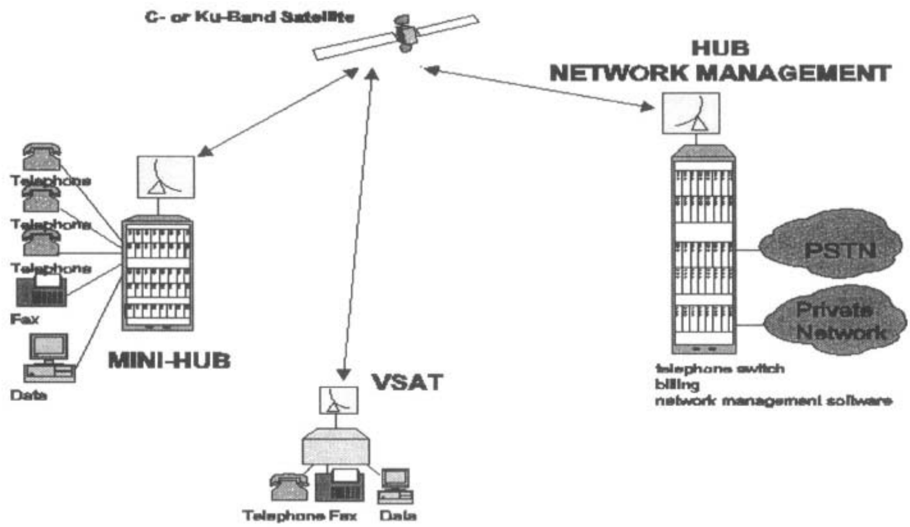

Figure 1.1. An illustration of the VSAT networks

The North American market for both fixed and mobile Ku-band transceiver systems is still growing. The ITU has assigned orbital slots for DBS and has designated the Ku-band for transmission, so there is an increasing use of the Ku-band frequency range, which is compatible with present North America's VSAT for satellite communications. The expanding use of satellite communications in the Ku-band has created the need for low-cost and reliable Ku-band transceivers. Also, the introduction of Ku-band DTH satellite television services has created an enormous market for wireless transmission of digital signals. The development of such services has created a rapidly growing market for RFICs intended for wireless transceiver systems. One of the critical elements in the satellite communications system is a compact, low-cost transmitter block.

To satisfy the significant worldwide demand for higher data rates and broadband transmission, applications of satellite communication systems in the Ku/Ka-band range are expanding due to its large available bandwidth [5]. However, the lack of economical high frequency components for low cost home transceivers remains a barrier to development of this application and its market. The earth transmission station uses an outdoor unit (ODU), which operates as a transmitter to convert baseband signal to Ku-band and amplify the output signal before it is fed to an antenna. Because it must be mounted on the antenna, the ODU needs to be small and light [6]. Therefore, since one key building block in a VSAT network is the ODU, the design and implementation of the transmitter module is crucial. The main emphasis of this book is on the design and integration of ODU to meet the need of most existing VSAT networks. The drawbacks of most commercially available transceivers are their relatively large size, heaviness, and separately located modules. The implementation of a compact transmitter module is the key issue for reduction in cost, size and system complexity. By improving circuit design and integrating all the components into a single MMIC chip set, the size of each module can be minimized to reduce the total size of the transceiver. One obstacle to a compact transceiver module is the large and heavy cavity filter that cannot be easily integrated into the module [7]. To address this issue, a LTCC-integrated coupled strip-line filter has been incorporated to replace the discrete cavity filter. This book will also review approaches and topologies of Ku-band transmitters and study their advantages and disadvantages to determine the critical design criteria to enhance system performance.

There are several objectives for this book. The first objective is to build the system model for the Ku-band transmitter to predict the overall system performance. The second objective is to analyze the phase noise of the VCO using reflection coefficient line analysis and design a low phase noise oscillator suitable for use in satellite communications applications. The third objective is to design the front-end image-rejection band pass filter (BPF) using LTCC coupled strip-line topology for compactness and comparable performance to discrete ceramic filters. The last objective is to design and implement the entire transmitter chain using a commercial semiconductor foundry process and to characterize each block for Ku-band satellite communications applications.

This book offers the design and development of a functional compact LTCC-based transmitter module featuring an integrated filter and MMIC chipsets using a low-cost commercial 0.6 μm GaAs MESFET process with a f_t of 20 GHz. Most of the LTCC-based modules demonstrated so far [8,9,10] were dedicated for phased-array applications. The feasibility of implementing a LTCC integrated filter has been demonstrated in [11,12] for L-band application. The same concept is now extended for Ku-band applications [13]. This book demonstrates that a functional low-cost Ku-band satellite transmitter module can be implemented using commercial GaAs MESFET and LTCC processes despite such major challenges as the closeness of the design frequency to the f_t of the device technology and the loss and bandwidth requirement of the filter. This book also demonstrates that this transmitter module is suitable for the satellite ODUs with data rate up to 32 Mbps and an adjacent channel power ration (ACPR) of 42 dB.

This page intentionally left blank

Chapter 2

Ku-band Transmitter Architecture

2.1 Design Criteria

The typical transmitter module can be divided into three blocks: (1) the modulator, (2) the frequency converter, and (3) the output power amplifier. The basic operations of a transmitter are as follows. The digital data is first encoded, and then the independent I and Q channels of data are combined by the some form of modulator, and the resultant modulated signal is mixed to the RF carrier frequency by the frequency up-converter block. Then, after some filtering, the up-converted signal drives the output power amplifier (PA), which drives the amplified output signal to the antenna. The antenna radiates the signal into the air, and then the transmission is complete.

2.1.1 Modulator Design Criteria

Modulation accuracy is an important design issue for the modulator. The channel performance and simplicity of quadrature phase shift keying (QPSK) modulation make it suitable for use in satellite communications systems [14]. In QPSK, the transmitted digital symbols are mapped to four distinct transmitter carrier phases that are uniformly distributed in the interval $[0, 2\pi]$. QPSK has four constellation points, which are associated to signal carrier phases of $\pi/4$, $3\pi/4$, $5\pi/4$, $7\pi/4$, and thus have a maximum theoretical spectral efficiency of 2b/s/Hz [15]. An important issue in QPSK modulator design is the phase and gain match of the I/Q paths. The imperfection of the phase and gain leads to cross-talk between the two data streams modulated on the quadrature phase of the earner [16]. Because of the linear modulation characteristics, the resultant signal is not a constant envelope signal. Therefore, it requires the use of a linear PA with consequent power inefficiencies.

In the late 1970's, QPSK and its modified version offset QPSK (OQPSK) have been extensively employed in conjunction with fixed point, satellite and, to a less extent, terrestrial point-to-point microwave links. In the 1990's, a modified version of QPSK, namely, $\pi/4$-shift differential QPSK (DQPSK) was adopted as the modulation standard for the IS-54 North American digital cellular (NADC) and the Japan digital cellular (JDC) digital cellular systems. When using differential phase encoding at the transmitter, the receiver does not need to produce a coherent estimate of the transmitter carrier phase in order to detect phases of the transmitted signal. $\pi/4$-shift DQPSK uses the four differential phase shifts of $\pi/4$, $3\pi/4$, $5\pi/4$, $7\pi/4$, rather than the absolute carrier phase values of QPSK, and this has reduced envelope fluctuation. QPSK can also be transmitted in another differential fashion, often referred to simply as DQPSK, using differential phases of 0, $\pi/2$, π, $3\pi/2$, with considerably more envelope fluctuation than $\pi/4$-shift DQPSK. The envelope fluctuation of $\pi/4$-shift DQPSK, although much improved with respect to that of DQPSK, will nevertheless result in spectral spreading in a nonlinearly amplified channel.

To minimize this spreading, amplifier linearization techniques have been proposed. Exponential schemes employ the modulations by which the information symbols modulate the angle of the carrier in such a way that its phase becomes continuous. The modulated signal has a constant envelope at the output of the transmitter, and thus these modulation formats are referred to as constant envelope modulation schemes.

There are two main advantages of having constant envelope property. First, constant envelope signals are less sensitive to amplifier nonlinearities than other modulation schemes with fluctuating envelopes. On the contrary, non-constant envelope signals suffer from spectral sidelobes regrowth and spreading due to the nonlinear amplifier effects that degrade the overall performance. Secondly, constant envelope signals are more resistant to adjacent channel interference (ACI) because their spectrum is more compact than that of the non-constant envelope signals. Among the large number of constant envelope modulation schemes, gaussian minimum shift keying (GMSK) has been most widely used because of its excellent spectral and simple implementation structure. As is well known, GMSK employs a gaussian premodulation filter before its MSK modulator so that a compact spectrum with suppressed sidelobes is obtained. GMSK has been a very popular modulation scheme for mobile radio telecommunication standard for several wireless personal communication system (PCS), including group special mobile (GSM), digital enhanced cordless telecommunications

(DECT), and industry scientific and medical (ISM) unlicensed band application. [16]

2.1.2 Frequency Translator Design Criteria

Spectral emission is the major design criteria for the frequency translator. Suppression of unwanted local oscillator (LO) and sideband signals are the important design issue for the up-converter design. The various possible solutions and trade-offs in the design of field effect transistor (FET) up-converter building blocks will be discussed in Chapter 4. Critical parameters for the up-converter are conversion gain, noise figure, and rejection of spurious and unwanted signals such as sideband and second harmonics of the intermediate frequency (IF). Any up-converter produces an output spectrum that contains the LO signal, the upper and lower sidebands produced by the harmonics of the IF. Conventional microwave systems use a BPF to select the desired sideband before it is fed to an amplifier. This book discusses the various possible solutions and trade-offs made during the design of an MMIC up-converter. Particular attention is paid to the realization of the LTCC-based compact coupled-line BPF for the LO and image signal rejection. Good conversion gain with a high gain compression point must be obtained while keeping the LO output power to a minimum. This is required to obtain a good ratio of output power to LO power at the up-converter output with limited achievable LO rejection. The two commonly available devices for providing the mixing function on an MMIC are the FETs and the diodes.

The most suitable configuration for up-conversion is the FET mixer topology. Three circuit configurations are considered to find the optimum circuit topology from these constraints. These configurations are distinguished from one another by the way the IF and LO signals are fed to the different terminals of the FET. In the first case, the IF and LO can both be applied to the gate. In the second case, the IF is applied to the gate and LO to the source. In the third case, the IF is applied to the source and LO to the gate. In all cases, the RF signal is taken from the drain of the FET. Of these three, the first one was found to be the most suitable because it has a high IF input impedance, thus enabling a high IF bandwidth. Also, when biased close to pinch off, it gives a good conversion gain and minimizes the amplification of the LO signal [17].

2.1.3 Power Amplifier Design Criteria

PA is the component that takes the signal to be transmitted and amplifies it to the necessary level needed to drive the antenna for a particular power output level. The PA is the largest power consumer, usually because the amount of power that needs to be sent to the antenna is itself very large. Because the power output specification itself is often larger than the power consumption of the rest of the blocks in the RF system, and the power consumption of the PA will be greater than the specified power output, the PA is decidedly the major power consumer of the transmitter system. Output power level and linearity are the design specifications for the PA design. The output PA is used to boost the upper sideband output power and contains a high-pass filtering network in its input matching network to reduce the level of IF leakage to the output. Amplifier efficiency must be increased while meeting system linearity specifications. Signals with time-varying envelope, such as QPSK and other spectrally efficient modulation formats, provide the greatest challenge because of the need to avoid spectral regrowth and to preserve modulation accuracy. The amplifier linearity challenges with such systems as multicarrier code division multiple access (CDMA) are very severe because the peak-to-average-ratio is particularly high. Amplifier efficiency is also affected by the fact that to conserve power and reduce interference, wireless transmitters are typically used at power levels well below their maximum output capability. Frequently amplifier efficiency falls off dramatically from its peak value at maximum power [18]. It is crucial to maintain good efficiency at lower output power levels.

2.2 Up-conversion Topologies

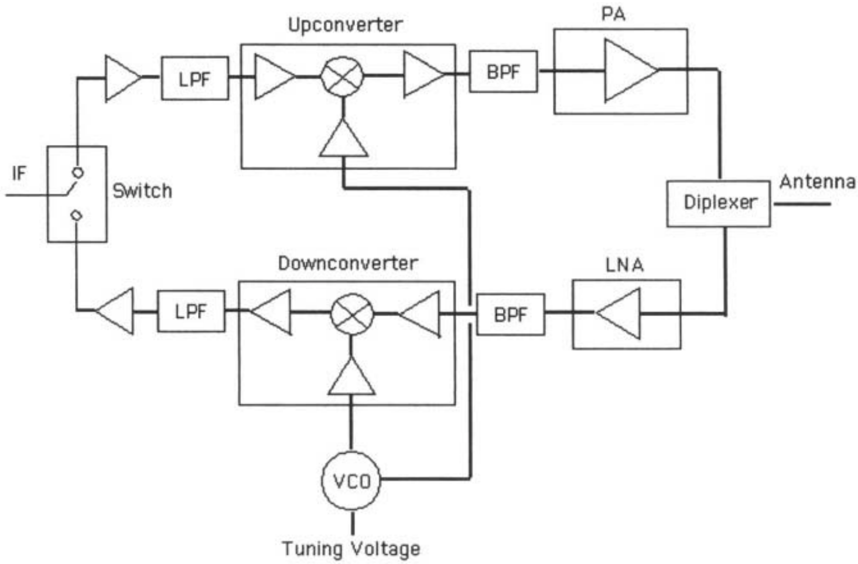

Figure 2.1. Schematic diagram of a typical Ku-band transceiver.

Figure 2.1 shows the typical schematic diagram of a Ku-band transceiver. In this section, the topologies for the modulator and frequency translator were investigated. In general, the transmitter performs modulation, up-conversion, and power amplification; in some cases the first two are combined. The up-conversion topologies can be divided into two categories: the direct conversion scheme and the double conversion scheme.

2.2.1 Direct Up-conversion Scheme

The direct conversion transmitter uses an I/Q modulator and performed frequency translation in one step as shown in Figure 2.2. In this case, the transmitted carrier frequency is equal to the LO frequency, so modulation and up-conversion occur in the same circuit. In other words, the baseband I/Q signal is directly modulated onto a carrier through multiplication by the LO signal. Since the frequency translation is performed in one step, the needs for IF filtering and image rejection can be eliminated.

This scheme has the advantage that no harmonics on the IF are present at the output, because one LO is used. Since no IF exists, an IF filter is not required in this architecture. Moreover, this architecture eliminates the need for any image rejection because no image signals are created by a single step frequency translation.

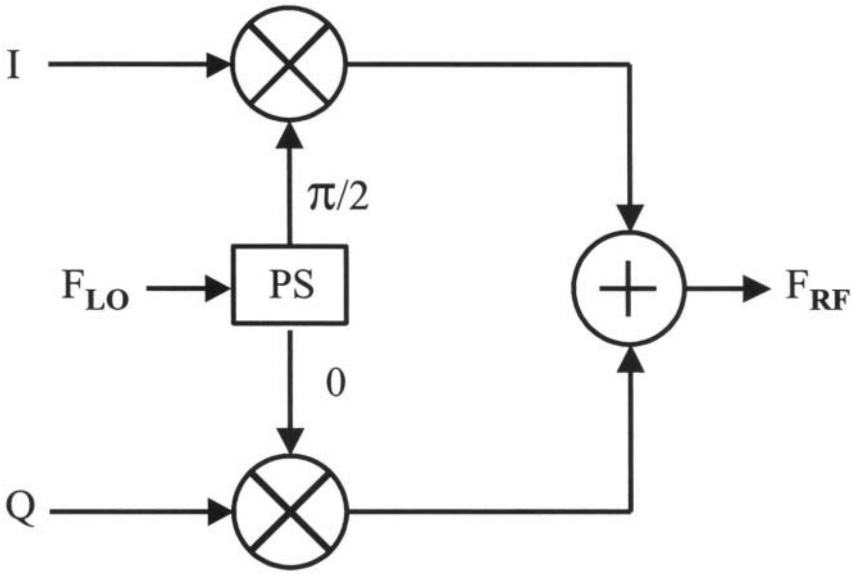

Figure 2.2. Schematic diagram of direct conversion modulator.

This scheme further lowers the requirements of the BPF before the PA that reduces unwanted harmonics and noise from the up-conversion process. It requires fewer components but is harder to implement. Also, this architecture suffers from a VCO pulling, which is the disturbance of the LO frequency through interaction with the PA. The output of the modulator, the PA, and the local oscillator all run at the same frequency, namely the RF frequency. As a result, the output of the LO may be pulled by the large signal emitted from the PA. This has the effect of modulation (or altering) the VCO frequency. The modulated RF signal at the output of the transmitter (PA) would couple back to the VCO and cause modulation distortion. Without exceptional isolation between the PA and VCO, integration of the PA with the VCO in a single-step transmitter may be difficult to eliminate the VCO pulling problem. Despite various isolation techniques, the VCO can still be corrupted by the output signal from the PA. This is because the PA output is a modulated waveform with a high power and a spectrum centered at the LO frequency. This problem is worsened if the PA is turned on and off periodically to save power. In addition, the radiated LO results in generation of a dc offset by self-mixing in the up-conversion mixer. Therefore, it requires a BPF before or after the PA for a better performance. The inclusion of this filter before the PA may allow a lower performance of the RF filter, which attenuates all energy outside of the transmit band. If, however, the BPF before the PA is removed to achieve higher integration, a higher performance RF filter may be required after the PA. This requirement may lead to a larger insertion loss through the PA and filter and reduces the efficiency of the PA by lowering the output power at the antenna for a given input power. Thus a trade-off exists between integration and power consumption. The BPF before the PA may be integrated, but the performance of the on-chip RF BPF is limited by the RF front-end PA since power consumption increases. Minimizing the spurious signal and noise created by the up-conversion process is therefore necessary to reduce power consumption. Also, poor LO-RF isolation of the surface mount package of the transmitter will allow the carrier to leak and be present in the output spectrum. Thus, making 40 dBc carrier suppression is a very difficult task.

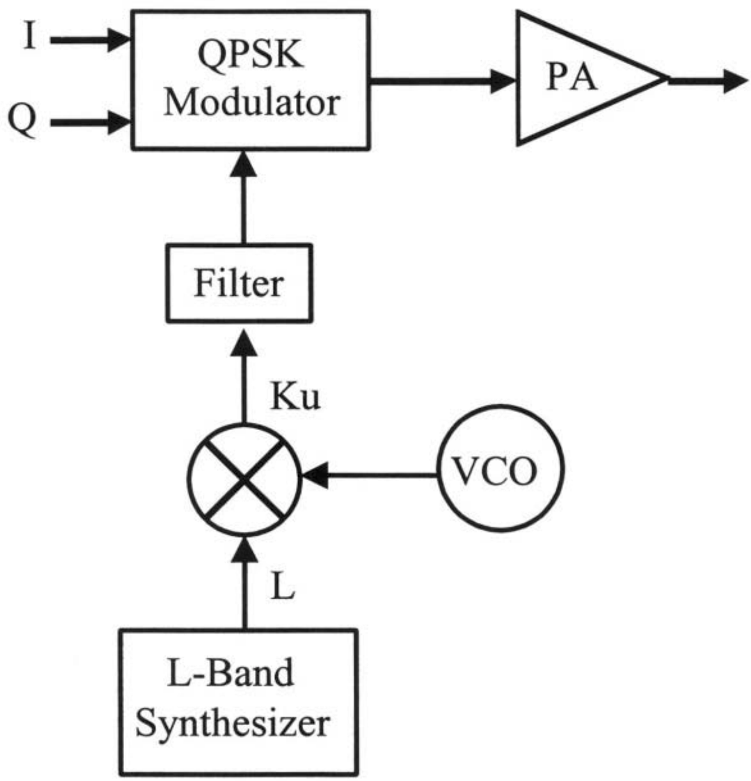

Figure 2.3. Ku-band direct up-conversion block diagram using VCO.

For the Ku-band direct conversion system, there are two possible topologies to implement the Ku-band synthesizer. The first topology is up-converting an L-band signal by mixing with a Ku-band VCO, as shown in Figure 2.3. The second option is to multiply the L-band signal into a Ku-band signal by eight, as shown in Figure 2.4. The direct conversion scheme using a multiplier has the advantage that it does not need a Ku-band VCO that is hard to implement with good phase noise performance, but it needs reduced step size compared to the direct conversion scheme incorporating Ku-band VCO. In addition, the multiplier results in extra conversion loss therefore it needs higher input power to keep the output power at the same level.

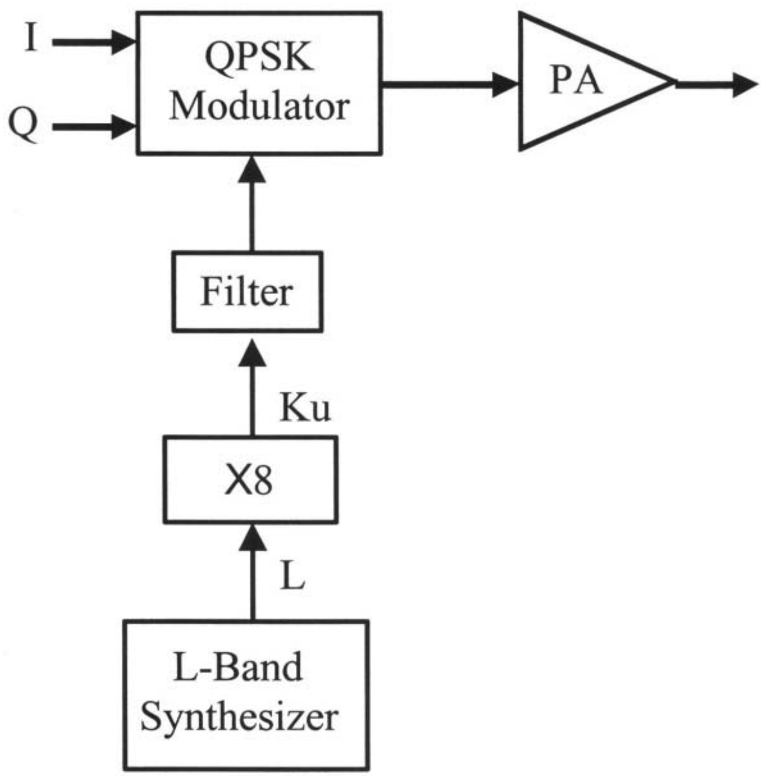

Figure 2.4. Ku-band direct up-conversion block diagram using multiplier.

2.2.2 Double Up-conversion Scheme

The double up-conversion scheme is to up-convert the baseband signal in two steps so that the PA output spectrum is not affected by the LO frequency. The baseband signal is modulated by the first LO signal and then up-converted to the desired RF frequency signal by the second LO, as shown in Figure 2.5.

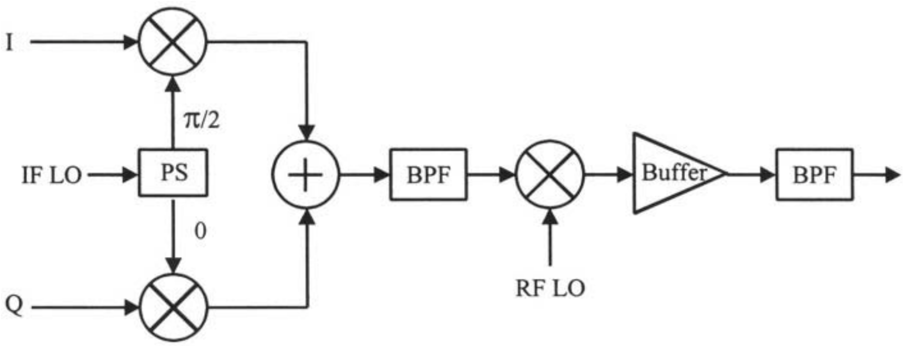

Figure 2.5. Schematic diagram of double conversion modulator.

The digital data first passes through a digital-to-analog converter (DAC) and is then filtered to suppress distortion introduced by the DAC. Frequency translation to a fixed IF is then performed by the I/Q mixers after which the signals are summed. The signal then passes through an off-chip low pass filter to suppress LO2 harmonics that may violate the spectral mask requirements and cause distortion in the PA. The signal is then frequency translated to RF by a mixer and a RF channel select frequency synthesizer. A discrete RF BPF attenuates the image created by the second mixer and filters any additional spurious that may violate the spectral mask requirements. The desired output power level is achieved by providing gain with a PA. Finally, a BPF removes energy transmitted outside of the desired band. The VCO for both LO1 and LO2 are typically realized with high Q discrete components that are able to produce a low phase noise oscillator. The IF filtering requirements can be relaxed if the intermediate frequency is selected so that none of the LO2 harmonics fall indirectly in the transmit or receive band where emission specifications are usually the most stringent. Furthermore, increasing the IF will push the image band further away from the desired signal, allowing more image rejection by the IF filters. The difficulty in double conversion transmitters is that BPFs are required to filter the unwanted intermodulation products. A double-conversion scheme needs more components than the direct conversion scheme because of the need for IF and image filtering. An advantage of the double up-conversion over the direct conversion approach is that, since quadrature modulation is performed at lower frequencies, I/Q matching is superior, which leads to less cross-talk between the two bit streams. Also, a channel filter maybe used to limit the transmitted noise and spurious signals in adjacent channels. It also has no VCO pulling problem and less LO radiation.

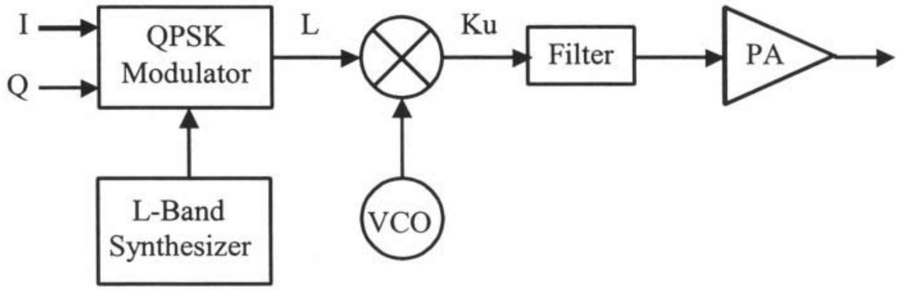

Figure 2.6. Ku-band double up-conversion block diagram.

For the Ku-band double up-conversion scheme, the baseband signal is modulated to an IF signal (950 ~ 1450 MHz) with the IF LO. The IF low pass filter (LPF) must remove the IF harmonics. The modulated IF signal is then up-converted to the RF frequency (14 GHz) by the Ku-band (13 GHz) LO as shown in Figure 2.6. The BPF is used to reject the undesired sideband. The requirements on the filter depend on the spectral distance between the two sidebands. Using a filter to attenuate the high sideband can be a very simple solution and consume little power, however, the filter can be difficult to realize and can have a large physical off-chip dimension [19]. To address this issue, an LTCC-integrated strip line filter has been incorporated to replace the discrete cavity filter. The up-converted signal is filtered and amplified by the driver amplifier and PA. It has a simple topology and less complex component than the direct conversion scheme.

This conventional double up-conversion has been adopted for its compatibility with VSAT networks that are already in operation and to achieve the required LO suppression as well as to reduce module size. Note that since baseband and IF signals are strong, the noise of the mixers is much less critical than in the receiver case. As mentioned, one of the sidebands is filtered out. This makes the recovery of the signal in the receiver much easier. This process is called single sideband (SSB) up-conversion. In the VSAT system, the unwanted sideband must be rejected by more than 30 dBc [19]. In general, the transmitter output spectrum must satisfy a system-specific spectral mask.

2.2.3 Double Up-conversion with Offset Oscillator

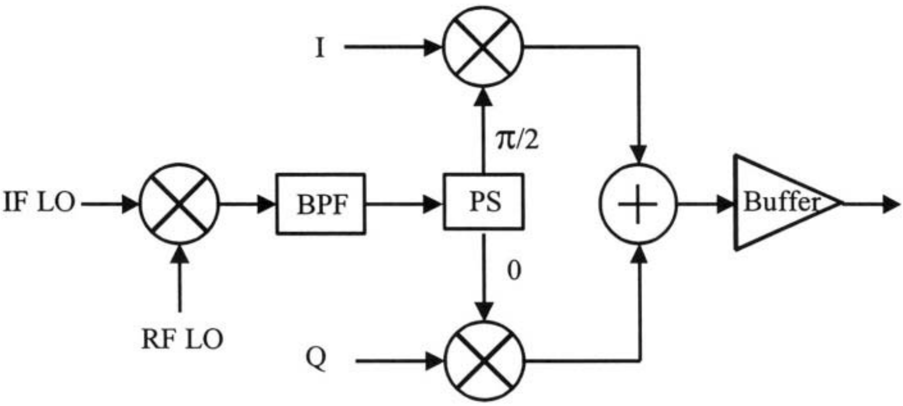

Figure 2.7. Schematic diagram of double conversion modulator with offset oscillator.

This architecture is based on a double up-conversion concept as shown in Figure 2.7. The RF LO is down converted by IF LO. The IF LO must be carefully planned to avoid harmonics in the RF spectrum. Also the phase shifter should be carefully designed. This concept of an offset oscillator is used in several RF products for time division multiple access (TDMA)/CDMA systems [19]. The VCO pulling problem may be eliminated in single step transmitters with the use of an offset mixing scheme in which two local oscillators, LO1 and LO2 (similar to the LO1 and LO2 of the two-step case), are first mixed to generated the desired RF channel select local oscillator. This LO is then mixed with the baseband data signal to generate the RF data signal. This method avoids the VCO pulling problem of single step architectures because neither VCO is operating at the RF carrier frequency.

One method for reducing the filtering requirements in the transmit path is to use the filtering inherent in a phase locked loop (PLL) in order to reduce the harmonics and noise generated in the frequency translation process [20]. A typical PLL transmitter is based on the two-step transmitter. A quadrature modulator translates the baseband signal to a fixed IF, after which the IF signal is translated to radio frequency (RF) by the PLL. The transmitter PLL is similar to the frequency synthesizer PLL, except that the reference frequency is replaced by an IF signal and the dividers are replaced by a down conversion mixer. In the phase detector, the IF signal is compared with the down converted mixer in the feedback path. The phase detector is followed by the charge pump and discrete loop filter before the transmit VCO is reached. The discrete VCO then feeds the PA directly. A RF filter is not necessary because noise and distortion introduced by the quadrature modulator and frequency synthesizers are filtered by the band pass action of the PLL. Significant power savings can occur because the RF filter loss is removed. Depending on the specification, filters may be needed after the quadrature modulator and after the feedback mixer. Full integration of a PLL based transmitter will minimize power advantages. The power savings occur because a high performance, discrete VCO can be designed to transmit very little unwanted energy. An integrated VCO could not achieve this performance, thus requiring a front-end RF filter. Once again integration and low power are conflicting requirements. PLL based transmitters are inherently limited with regards to multi-standard operation because such transmitters only operate with constant envelope modulation schemes [21].

Chapter 3

Transmitter System Simulation Model

3.1 Introduction

An accurate transmitter system simulation model, which provides an effective design method for implementation of a Ku-band transmitter module, has been developed. Development of an accurate system simulation model for a Ku-band transmitter by the use of a commercial computer aided design (CAD) tool is needed to: (1) study the transmitter topologies for satellite communication systems; (2) determine the critical design criteria in order to enhance overall system performance; and (3) anticipate the overall system performance accurately prior to the actual system development. This model has been verified with physical transmitter output spectrum and overall transmitted gain and ACPR measurements.

3.2 System Model Development

A system simulation model has been built using commercial microwave system/circuit design CAD tool for the proposed Ku-band transmitter module to derive the specification of RF building blocks in order to meet the output power spectrum, linearity, and ACPR as well as the filter requirement. Behavioral model for each RF building block in the transmitter is modeled by specifying gain, 1-dB compression point, third order intercept point (IIP3), return loss, and noise figure.

Figure 3.1 shows the system simulation block diagram for a Ku-band QPSK transmitter. A pseudo-random binary data generator is fed to a data splitter that generates I/Q data streams. These I/Q data streams are used to modulate a QPSK modulator. The output from the QPSK modulator has been set at an IF frequency of 1 GHz with an output power of -18 dBm and was applied to the up-converter module.

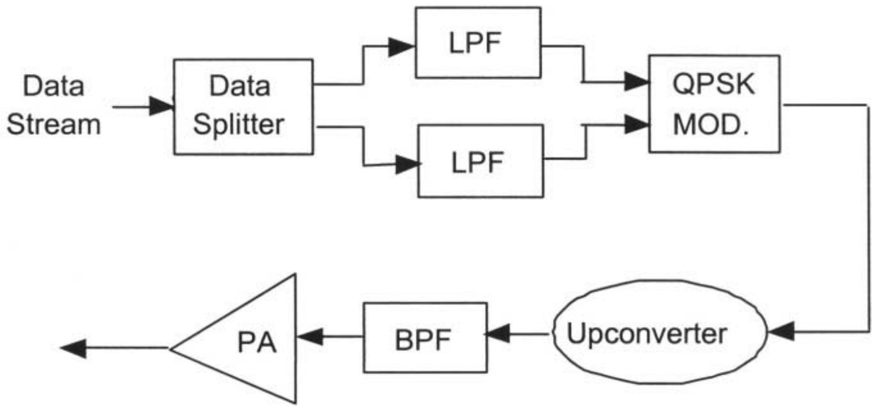

Figure 3.1. System simulation block diagram for a Ku-band QPSK transmitter.

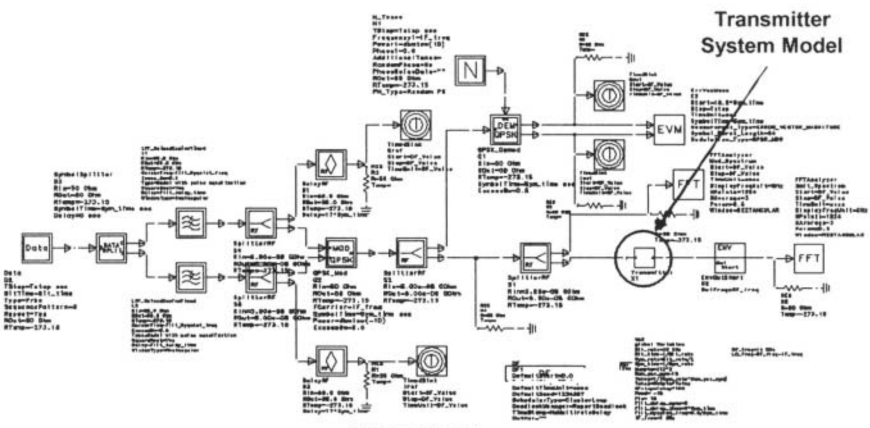

Figure 3.2. QPSK Simulation setup for Ku-band transmitter.

Figure 3.2 shows the system simulation set-up for QPSK transmitter. This system simulation set-up contains an up-converter model under circuit envelope co-simulation. QPSK simulation outputs include transmitter power spectrum, ACPR, and constellation diagrams. The 32 kbps QPSK signal is generated by using I/Q bit data streams and the data splitter and then is applied to a 1 GHz QPSK modulator. The modulated IF signal out of the modulator is applied to the top-level model of a transmitter. The transmitter is modeled by using the components provided by the commercial microwave system design CAD tool platform. All measured characteristics of the developed chipset, and filter and wirebond losses have been incorporated in the simulation platform. This simulation platform uses circuit envelope simulation to interface the data generator and IF modulator with the RF building blocks. The envelope simulation facility has also been used to get an estimate of ACPR of the transmitter module. The transmitter module was aimed to provide output power of more than 24 dBm with an input power level of approximately -20 dBm. The required design specifications for each RF building blocks have been derived from AC simulation. From a linearity perspective, the output power of any RF building block should satisfy the input linearity requirement of the subsequent block in the transmitter chain.

The schematic of the implemented double conversion transmitter architecture of each RF building block is shown in Figure 3.3. The transmitter system chain consists of an up-converter MMIC, a PA MMIC, and a LTCC BPF. The up-converter MMIC consists of an IF amplifier, a dual-gate mixer, a low phase noise VCO, a LO buffer amplifier and a RF amplifier. The PA MMIC consists of a driver amplifier and a power amplifier. The gain requirement of the up-converter was determined by the IF power available from the IF amplifier and the available LO power. The required output power of the up-converter was determined from the input power required to put the driver amplifier and power amplifier in compression while overcoming the losses in the BPF and bond wires between MMICs and BPF.

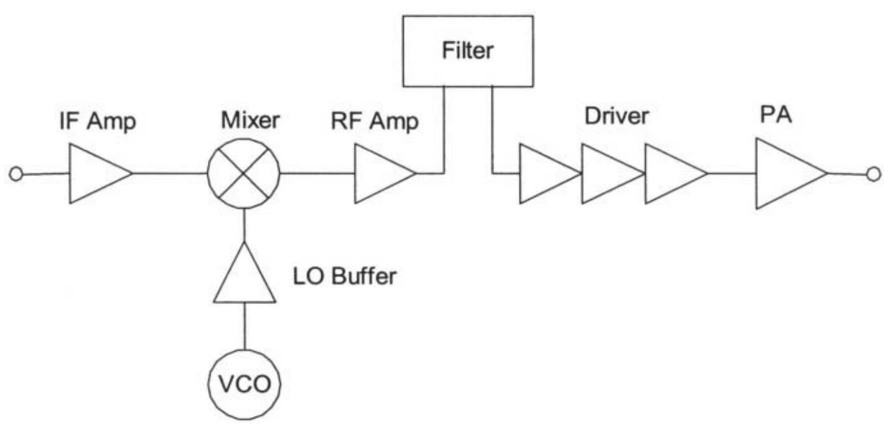

Figure 3.3. Block diagram of the monolithic Ku-band up-converter module.

The MMIC transmitter specifications were derived by examining all the functions required for the transmitter chain. Cascading high gain amplifiers at the output of the BPF are used to create an overall gain as high as 30 dB over RF output bandwidth of 500 MHz (14 ~ 14.5 GHz). Gain and power-level requirements for each block were examined until a compromise was found that would meet the system performance.

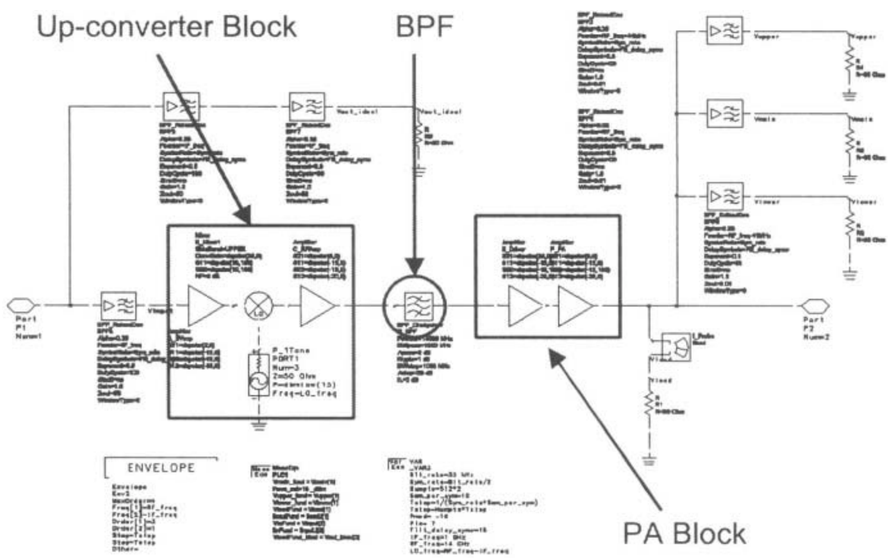

Figure 3.4. System block diagram of the transmitter.

Figure 3.4 shows the system block diagram for the implemented transmitter. The modulated IF signal is filtered with a root raised cosine filter and then is applied to the up-converter block with circuit envelope simulation. The circuit envelope simulation allows circuits with transient or digitally modulated RF signals to be simulated much more efficiently than existing time and frequency domain simulators by exploiting the benefits of both techniques.

This envelope simulation set-up includes a pair of filters for generating an undistorted signal for error vector magnitude calculation as well as a set of filter banks so that the effects of receive side filtering in the main and adjacent channel can be included. This envelope simulation shows the power spectrum at the load at the output of the transmitter as well as the upper and lower ACPR, main channel output power, and power gain. The modulated spectrum and transmitted spectrum are shown in Figure 3.5 and the QPSK constellation is demonstrated in Figure 3.6.

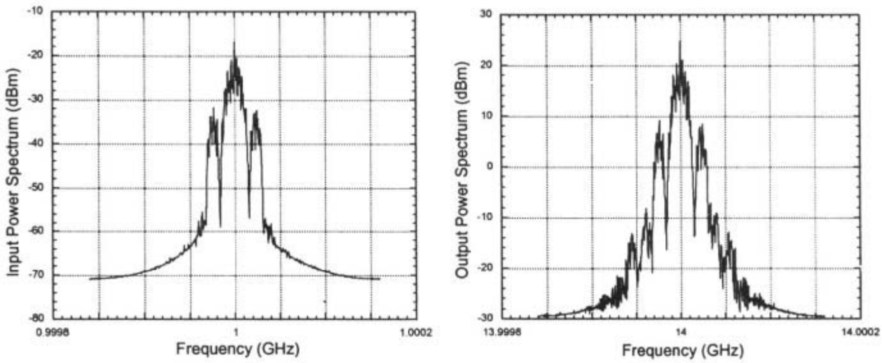

(a) (b)

Figure 3.5. Simulation results of the power spectrum (a) Modulated power spectrum (1 GHz), (b) Transmitted power spectrum (14 GHz).

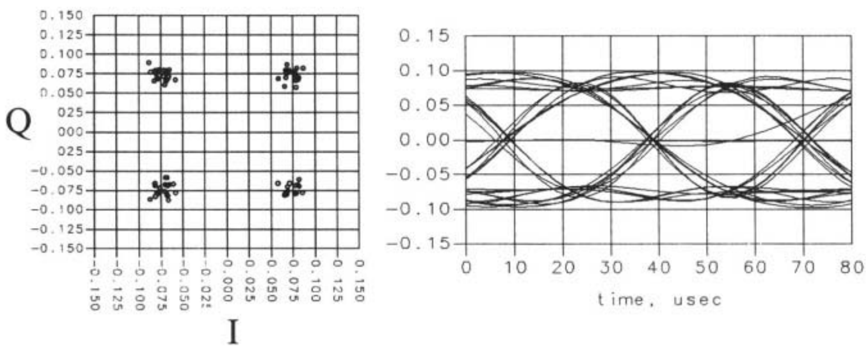

(a) (b)

Figure 3.6. Simulation results of the QPSK constellation diagram (a) QPSK constellation, (b) Eye diagram.

The link budget is calculated by AC simulation, as shown in Figure 3.7. Link budget analysis computes the transducer power gain from the input to the output of each component as well as the overall noise figure. The link budget data from the simulation is generated sequentially in the same order as the transmitter chain components. Figure 3.8 shows the gain budget diagram and noise figure diagram. Table 3.1 shows the standard specification for Ku-band VSAT service.

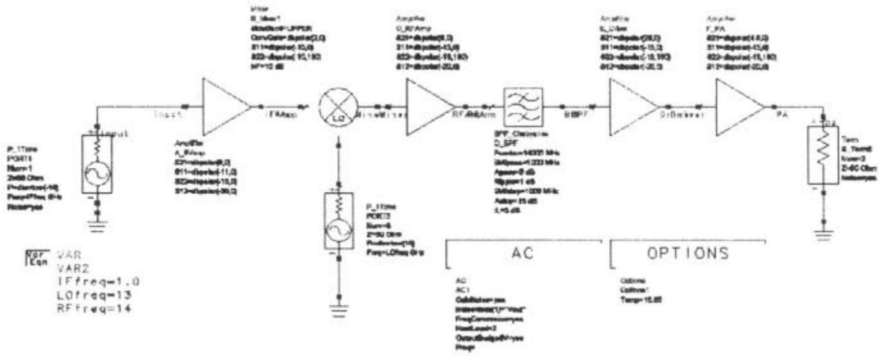

Figure 3.7. Link budget simulation set-up for transmitter.

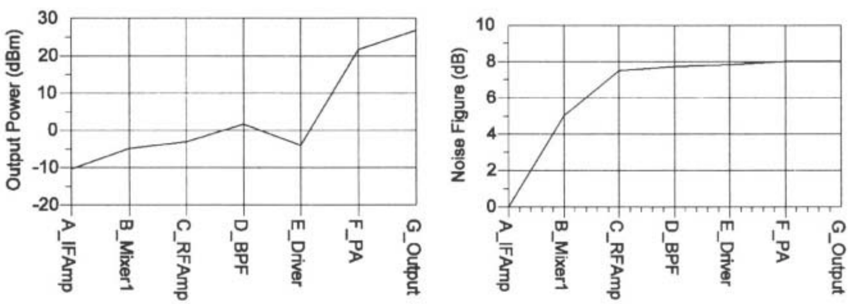

(a) (b)

Figure 3.8. Simulation results of the link budget and noise figure of the transmitter (a) Link budget, (b) Noise figure.

Table 3.1. Summary of Ku-band VSAT service specifications [22]

Parameter		Specification
Modulation Scheme		QPSK
Multiplexing Scheme		TDMA (Frame Efficiency : 89.5 %)
Data Rates		16 ~ 4096 Kbps
Coding Scheme		½ FEC (Convolutional encoding/Viterbi Decoding)
Bit Error Rate		$< 10^{-10}$ under clear sky conditions $\leq 10^{-8}$ under degraded sky conditions
Frequency Band	Uplink	14.00 ~ 14.50 GHz
	Downlink	10.95 ~ 11.2 GHz 11.45 ~ 11.7 GHz
RF Frequency Stability		1×10^{-7}
RF out-of-band Emission		23 ~ 26 dBc
Spurious		< -30 dBc
Phase Noise		-60 dBc @ 100 Hz offset -70 dBc @ 1 KHz offset -80 dBc @ 10 KHz offset -90 dBc @ 100 KHz offset

3.3 Transmitter Module Implementation Procedure

Figure 3.9 graphically depicts the sequence of the transmitter module development procedure. First, the topology study for transmitter was performed and a decision was made determining the transmitter topology. The system model was developed to verify the chosen topology. Through this system model, the critical design criteria were determined for optimum system performance. With these design specifications, each MMIC chip set was designed and implemented with a commercial MMIC process. At the same time, the band pass filtering structure was studied and designed to meet our system specifications. Next, each MMIC and filter was fully characterized.

To see overall system performance based on the implemented RF component characteristics in the transmitter link, the simulation model was developed. With these measured performances, a system simulation is performed to see if these implemented MMIC and filter can meet our application specification. If it does not meet the desired specifications, new design criteria are determined and the design trade-offs can be made. Finally, the compact transmitter module can be obtained that will meet our design specification.

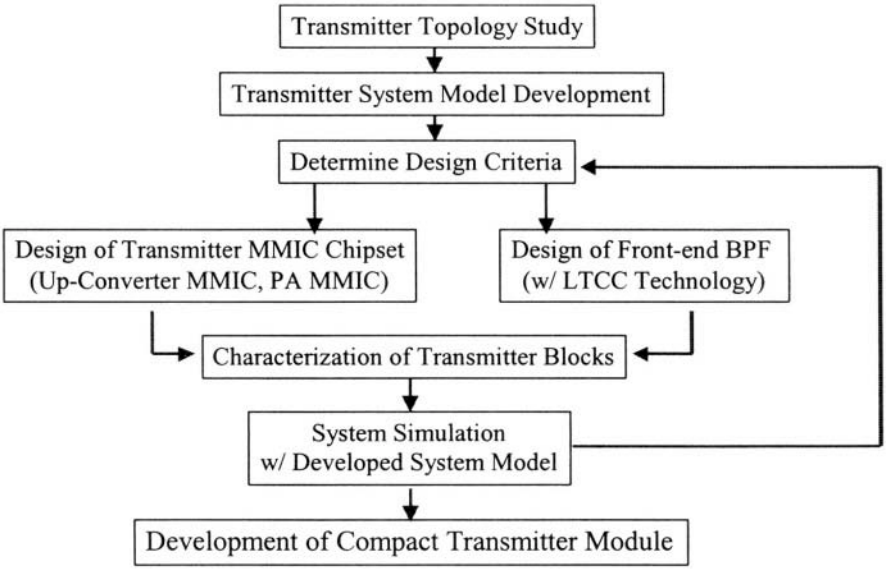

Figure 3.9. Transmitter module development procedure.

In conclusion, an accurate transmitter system model has been developed on commercial microwave system design CAD tool platform to predict the transmitter system performance such as link budget, output power, transmitted power, ACPR, and modulation constellation. This model has been verified with the physical transmitter output spectrum and overall transmitted gain measurements. It provides an efficient design procedure that can accurately predict the performance of the overall transmitter system.

Chapter 4

Review of Ku-band Mixers

4.1 Mixer Design Principles

A mixer, or frequency converter, has the function of converting a signal from one frequency to another with minimum loss of the signal and minimum noise performance degradation. The operation of the mixer can be analyzed either by its multiplication function or its operation as a switch. Since linear, time-invariant systems cannot produce outputs with spectral components not present at the input, mixers must be either nonlinear or time-varying elements in order to provide frequency translation [23].

A mixer, which consists of any device capable of exhibiting nonlinear performance, is fundamentally a multiplier. An ideal mixer multiplies a signal by a sinusoid, shifting it to both a higher and lower frequency, and selects one of the resulting sidebands. A modulated signal that has a carrier frequency ω_s, usually called the RF signal, represented by

$$S_{RF}(t) = a(t)\sin(\omega_s t) + b(t)\cos(\omega_s t) \tag{4.1}$$

is multiplied by the LO signal which is a pure, unmodulated sinusoid at frequency ω_p

$$f_{LO}(t) = \cos(\omega_p t) \tag{4.2}$$

By the following trigonometric identity:

$$(A\cos\omega_1 t)(B\cos\omega_2 t) = \frac{AB}{2}[\cos(\omega_1 - \omega_2)t + \cos(\omega_1 + \omega_2)t] \tag{4.3}$$

The following IF signal can be obtained

$$\begin{aligned} S_{IF}(t) = \frac{1}{2}a(t)(\sin((\omega_s + \omega_p)t) + (\sin((\omega_s - \omega_p)t)) + \\ \frac{1}{2}b(t)(\cos((\omega_s + \omega_p)t) + (\cos((\omega_s - \omega_p)t)) \end{aligned} \tag{4.4}$$

The output in the ideal mixer is composed of modulated components at the sum and difference frequencies. Either of these frequencies can be selected by the IF filter. In the receiver system, the difference-frequency component is desired, therefore the sum-frequency component is rejected by filters. Unfortunately, no physical nonlinear device is a perfect multiplier. Thus it generates noise and produces a vast number of spurious frequency components. Even if the LO voltage applied to the mixer is a clean sinusoid signal, this signal is distorted by the nonlinearities of the mixer device, causing the LO signal to have harmonics.

Those nonlinearities can also distort the RF signal, resulting in RF harmonics. In general, the IF is the combination of all possible mixing products of the RF and LO harmonics. To select the appropriate response and eliminate the spurious response, filters are usually used. Every mixer, even an ideal one, has a second RF frequency that can create a response at the IF. This type of spurious response is called the image. It occurs at the frequency $2f_{LO}$ - f_{RF}. It is possible to create combinations of mixers and hybrids that do reject the image response [24].

Multiplication of two input signals in the time domain results in output signals at the sum and difference frequencies of the input, signals whose amplitudes are proportional to the product of the RF and LO amplitudes. Hence, if the LO amplitude is constant (as it usually is), any amplitude modulation in the RF signal is transferred to the IF signal. Also an undesired transfer of modulation from one signal to another can be occur through nonlinear interaction in mixers. This result in cross-modulation, and its suppression through improved linearity is an important design consideration. [23].

Another way to consider the operation of a mixer is as a switch that is switched at a LO frequency ω_p [25]. Diodes used in mixers can be idealized as switches operated at the LO frequency ω_p. This is a good approximation of the mixing process for a diode mixer. The simplified mixer model as a switch is shown in Figure 4.1. The RF signal appearing at the IF load is interrupted by the switching action of the diode, which is caused by LO. It can be shown from the modulation theorem that the sum and difference frequencies appear at the IF port along with many other products. The desired output can be separated from the others by filtering.

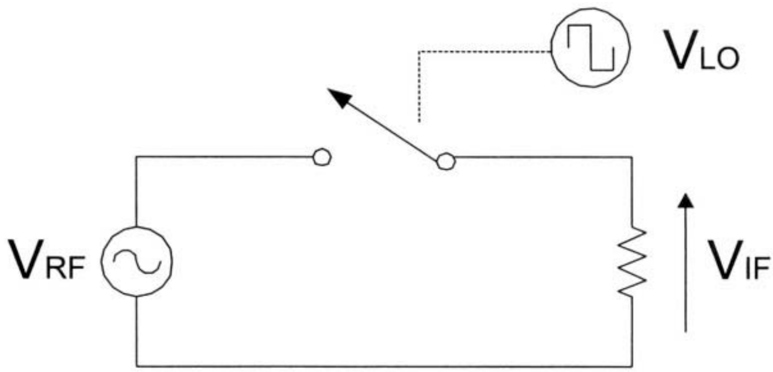

Figure 4.1. Switching Mixer.

Ideally, a mixer performs this frequency conversion with perfect fidelity and thus generates no intermodulation distortion products (IMD). Other desirable characteristics include high isolation between all three ports and a low noise figure. Ideally all of these characteristics are obtained with minimal loss or preferably gain while performing frequency conversion.

4.2 Mixer Performance Parameters

4.2.1 Conversion Gain

Conversion gain is a measure of the efficiency of the mixer in providing frequency translation between the input RF signal and output IF signal. Conversion gain of the mixer is equal to the ratio of the IF single side band output to the RF input level. Mixers using the Schottky barrier diode are passive components and consequently exhibit conversion loss. Mixers using active devices often exhibit conversion gain. High mixer gain is not necessarily desirable because it reduces stability margins and can increase distortion.

4.2.2 Conversion Compression

Conversion compression is a measure of the maximum RF input signal for which the mixer will provide linear operation. Normally, the IF output signal is equal to a constant ratio of the RF input signal level. As the RF level increases further, there will be a greater change in the constant ratio. The conversion loss will increase as the RF input level increases. The IF output level does not exactly follow the increase in RF output level. The compression point is the value of the RF signal at which a calibrated departure from the ideal linear curve occurs. Usually, a 1-dB or 3-dB compression value is specified.

4.2.3 Isolation

Isolation is a measure of the circuit balance within the mixer. When the isolation is high, the amount of the "leakage" or "feed thru" between the mixer ports will be very small. The LO to RF isolation is the amount the LO drive level is attenuated when it is measured at the RF port. The LO to IF isolation is the amount the LO drive level is attenuated when it is measured at the IF port. High LO-RF isolation is a key mixer performance parameter for direct-conversion applications because it is related to the amount of dc offset produced by the LO self-mixing at the RF port. Because of the unilateral characteristics of three terminal devices, an active balun approach can offer enhanced LO-RF port isolation [26].

4.2.4 Dynamic Range

Dynamic range is the power range over which a mixer provides useful operation. The upper limit of the dynamic range is determined by the conversion compression point. The lower limit of the dynamic range is determined by the noise figure of the mixer. Since the mixer noise figure is proportional to its conversion loss, the lowest conversion loss is desirable in order to obtain the largest dynamic range.

4.2.5 Dc Offset

Dc offset is a measure of the unbalance in the mixer. For the ideal mixer, the dc offset is zero. Dc offset defines the IF voltage output when the mixer is used as a phase detector and only the LO signal is applied and the RF port is terminated in 50 ohms.

4.2.6 Intercept Point

Two-tone intercept point intermodulation distortion is a measure of the third-order products generated by a second input signal arriving at the RF port of a mixer along with the desired signal. A popular method of determining the suppression capability of the mixer is the "third-order intercept" approach. The third-order intercept point is a theoretical point on the RF input versus the IF output curve where, as RF input is raised, the desired input signal and third-order products become equal in amplitudes. The two-tone third-order intercept point is also used to characterize mixer linearity. Distortion in mixers is manifested as IMD, which involves mixing between multiple RF tones and the harmonics of those tones. If two RF signals f_1 and f_2 are applied to a mixer, the nonlinearities in the mixer will generate a number of new frequencies, resulting in the IF spectrum [24]. Figure 4.2 shows all intermodulation products up to third order.

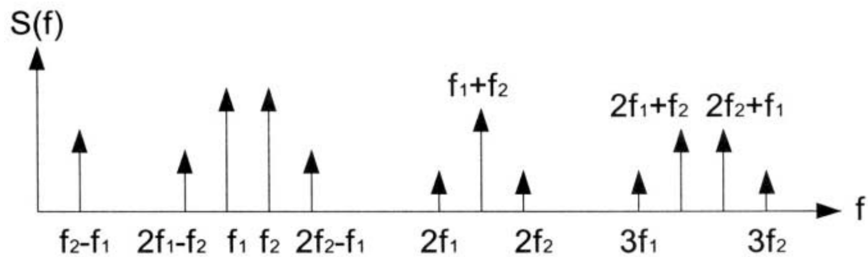

Figure 4.2. IF spectrum of intermodulation products up to third order.

4.2.7 Noise Figure

Noise figure is defined as signal-to-noise ratio (SNR) at the input port divided by the SNR at the output port. In a passive mixer whose image response has been eliminated by filters, the noise figure is usually equal to the conversion loss. In active mixers, the noise figure cannot be related easily to the conversion efficiency. The noise figure of an active mixer depends strongly on the characteristics of the design.

4.2.8 Spurious Response

A mixer converts a RF (or IF) signal to an IF (or RF) signal. Considering the harmonics of both the RF and LO, the resulting set of frequencies is

$$f_{IF} = mf_{RF} \pm nf_{LO} \tag{4.5}$$

where m and n are integers. If a RF signal creates an in-band IF response other than the desired one, it is called a spurious response. Usually the RF, IF, and LO frequency ranges are selected carefully to avoid spurious responses, and filters are used to reject out-of-band RF signals that may cause in-band IF responses. IF filters are used to select only the desired response. Many types of balanced mixers reject certain spurious responses where m or n is even. Most singly balanced mixers reject some, but not all, products where m or n is even; doubly balanced mixers reject all responses where m or n are even [24].

4.3 Device Technologies for Ku-band Mixer

The primary devices used for mixers are Schottky barrier diodes and FETs. Bipolar Junction Transistors (BJTs) are also used occasionally, but FET devices are usually preferred because of their superior ability to handle large signals, higher frequency range, and lower noise. Schottky barrier diodes have the advantage of low cost and do not need dc bias. Unlike FETs and bipolar transistors, diodes are two-terminal devices and thus can be reversed. This allows them to be used in configurations that are impractical for three-terminal devices like FETs or BJTs,

4.3.1 Schottky Barrier Diode (SBD)

A Schottky barrier diode is the dominant device used in mixers. Because Schottky diodes are inherently capable of fast switching and have very small junction capacitances, they can be used in very broadband mixers. Schottky diode mixers usually do not require matching circuits, so no tuning or adjustments are needed. But, the MMIC Schottky barrier diodes generally have a higher conversion loss than those used in discrete hybrid mixers because of a higher series resistance. [27].

The Schottky barrier diode consists of a rectifying metal-to-semiconductor junction. The semiconductor consists of a thin epitaxial layer grown on a heavily doped substrate. The metal contact is anode, and an ohmic cathode contact is made to the substrate either directly to the bottom of the chip or to the top side by etching away the epitaxial layer [24]. Figure 4.3 shows the structure of a typical Schottky barrier diode.

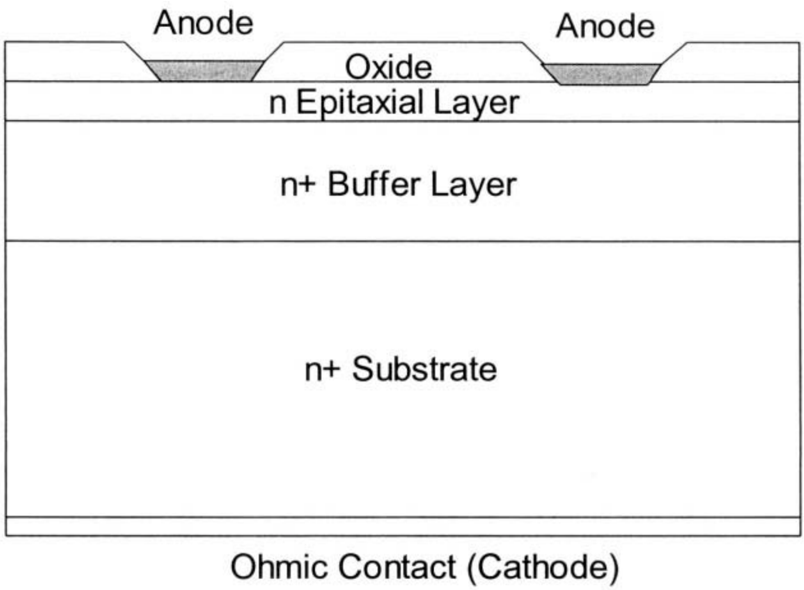

Figure 4.3. Cross section of the Schottky barrier diode chip.

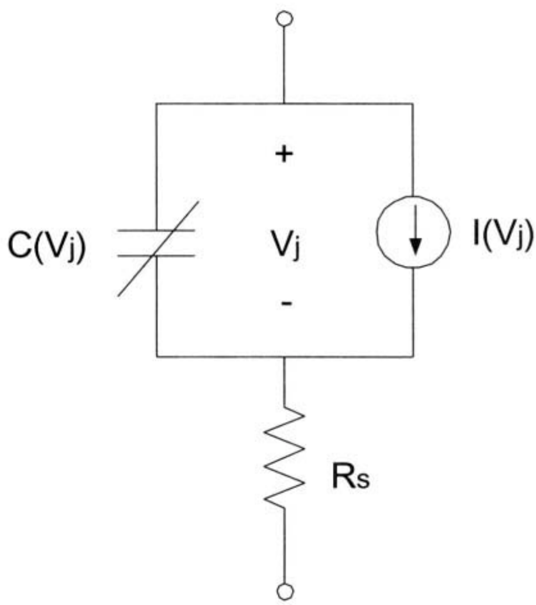

Figure 4.4. Equivalent circuit of the Schottky barrier diode.

The equivalent circuit of the diode, including the nonlinear junction capacitance and the fixed, linear series resistance, is shown in Figure 4.4. The junction I/V characteristics are given by the exponential expression

$$I(V_j) = I_0(\exp(\frac{qV_j}{\eta kT}) - 1) \tag{4.6}$$

where q is electron charge, K is Boltzmann's constant, and T is absolute temperature in Kelvins. η is the ideality factor, usually in the range of 1.05 to 1.25, and accounts for the nonideality junction. I_o is the current parameter, proportional to junction area.

The capacitance C(V) is given by the expression [24]

$$C(V) = \frac{C_{j0}}{(1 - \frac{V}{\phi})^{\gamma}} \tag{4.7}$$

where C_{j0} is the zero-voltage junction capacitance and the ϕ is the built-in potential of the junction. γ depends on the doping profile of the epitaxial layer. It is 0.5 if the epilayer is uniformly doped.

The cutoff frequency of a Schottky diode is

$$f_c = \frac{1}{2\pi R_s C_{j0}} \tag{4.8}$$

where R_s is measured at dc and C_{j0} at any convenient low frequency. f_c is depending on the type of diode and semiconductor material.

4.3.2 GaAs MESFETs

A MESFET is a junction FET having a Schottky barrier gate. Although silicon MESFETs have been made, they are now obsolete and all modern MESFETs are fabricated on GaAs. The gate's length is usually less than 0.5 µm, and may be as short as 0.1 µm. This short gate length, in conjunction with the high electron mobility and saturation velocity of GaAs, results in a high-frequency, low-noise device [24].

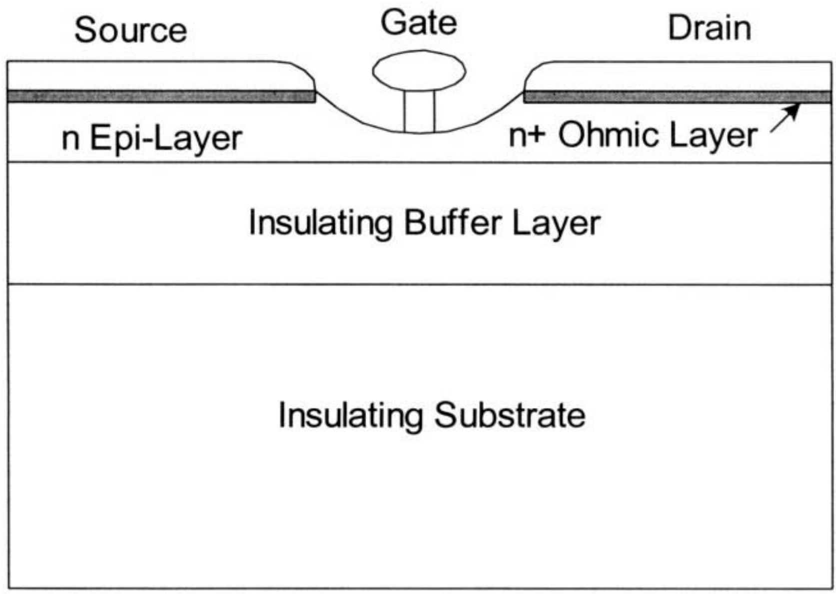

Figure 4.5. Cross section of recessed-gate MESFET.

Figure 4.5 shows a cross section of GaAs MESFET. The channel is moderately doped epitaxial layer grown on an undoped substrate. Because n-type GaAs has higher mobility than p-type GaAs, all conventional GaAs MESFETs use n-type material for the channel. A dc voltage applied to the channel creates a longitudinal electric field. In normal operation, the field is strong enough to accelerate the electrons to their saturated drift velocity, creating an electron current from the source to drain. The Schottky barrier formed by the gate creates a depletion region that extends part way into the channel at zero gate bias. Varying the gate-to-source voltage modulates the depletion depth and hence the thickness of the conductive channel; the channel current varies accordingly. As in the Schottky diode, the gate voltage also varies the depletion capacitance.

4.3.3 GaAs High Electron Mobility Transistors (HEMTs)

A HEMT is a junction FET that uses a heterojunction (a junction between two dissimilar semiconductors), instead of a simple epitaxial layer, for the channel. The discontinuity of the band gaps of the materials used for the heterojunction creates a layer of charge at the surface of the junction. The charge density can be controlled by the gate voltage. Because the charge in this layer has a very high mobility, high-frequency operation and very low noise are possible. HEMTs require specialized fabrication techniques, such as MBE, and thus are very expensive to manufacture [24]. HEMT heterojunctions are invariably realized with III-V semiconductors; AlGaAs and InGaAs are common. HEMTs are used for mixers in the same way as conventional GaAs FETs. Because the gate I/V characteristics of a HEMT are generally more strongly nonlinear than that of a MESFET, HEMT mixers usually have greater intermodulation distortion than FETs. The nose figure (NF) of a HEMT mixer usually is not significantly lower than that of a GaAs FET, however. Figure 4.6 shows the cross section of one type of HEMT. There are many degrees of freedom in the design of such devices. For example, the number of heterojunction, the thickness of layers, and the fabrication of Al or In in AlGaAs or InGaAs devices are all variable and can be used to optimize the device.

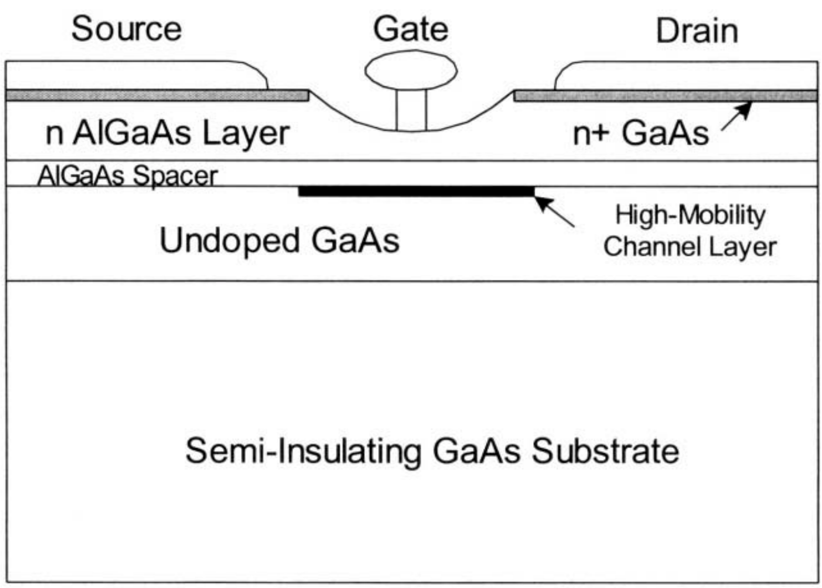

Figure 4.6. Cross section of a simple HEMT.

4.3.4 Heterojunction Bipolar Transistors (HBTs)

HBT structures are mainly characterized by an emitter-base heterojunction (single HBT) or both emitter-base and collector-base heterojunction (double HBT). The E-B heterojunction permits a very high base doping level leading to a lower base resistance value than BJT.

Low frequency noise in microwave HBTs results from the superimposition of both 1/f noise (at very low frequency) and generation-recombination noise (at high frequency) associated with trapping-detrapping effects. III-V HBTs are noiser than IV-IV ones due to their largest traps densities [28].

For n-p-n HBTs we need a discontinuity in the valence band such that the holes have a higher energy in the emitter than in the base. To make good quality heterojunctions, the two materials should be lattice matched. Some possible combinations that fulfill the lattice-matching condition are AlGaAs/GaAs and Si/SiGe.

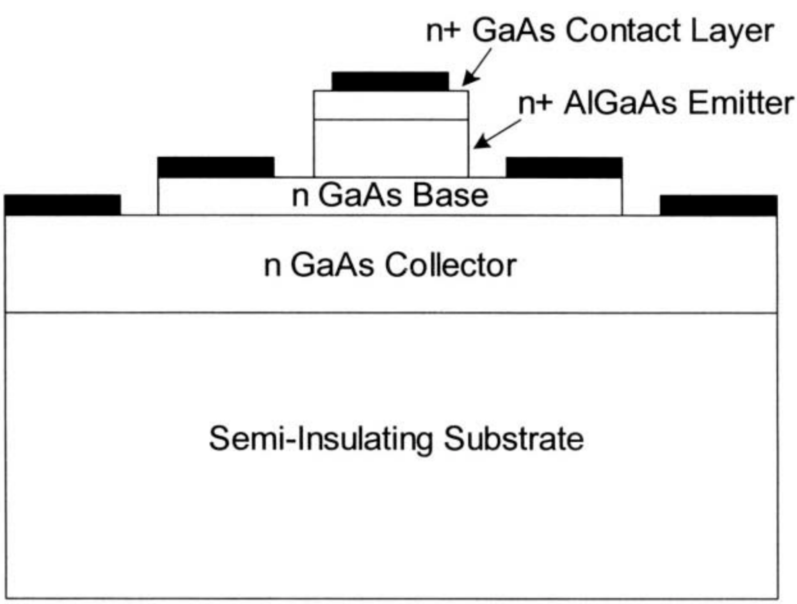

Figure 4.7. AlGaAs-GaAs HBT structure.

- **AlGaAs/GaAs HBTs**

One of the most researched material combinations is AlGaAs-GaAs, with an AlAs fraction of 20 ~ 30 %. A disadvantage of GaAs is its short electron lifetime, 10^{-9}s as compared with 10^{-6}s for Si. However, if the base is thin enough, the transit time through the base is small compared with the lifetime, and recombination is negligible. GaAs-based HBTs have the following advantages compared with silicon: (1) a greater electron mobility, resulting in higher cutoff frequencies; (2) a greater bandgap, and hence less thermal generation of charge carriers; (3) the possibility of using a semi-insulating substrate, which eases the isolation of devices; (4) the possibility of integration with optoelectronic components [29].

Compared with GaAs MESFETs, GaAs HBTs also have some advantages: (1) higher transconductance and output current; (2) more uniform threshold voltages; (3) less low-frequency noise; (4) absence of backgating [29]. Recently with GaAs HBTs, cutoff frequencies of 100 GHz have been reached comparable with those of the best MESFETs. Figure 4.7 shows the structure of a recent AlGaAs HBT.

- **SiGe HBTs**

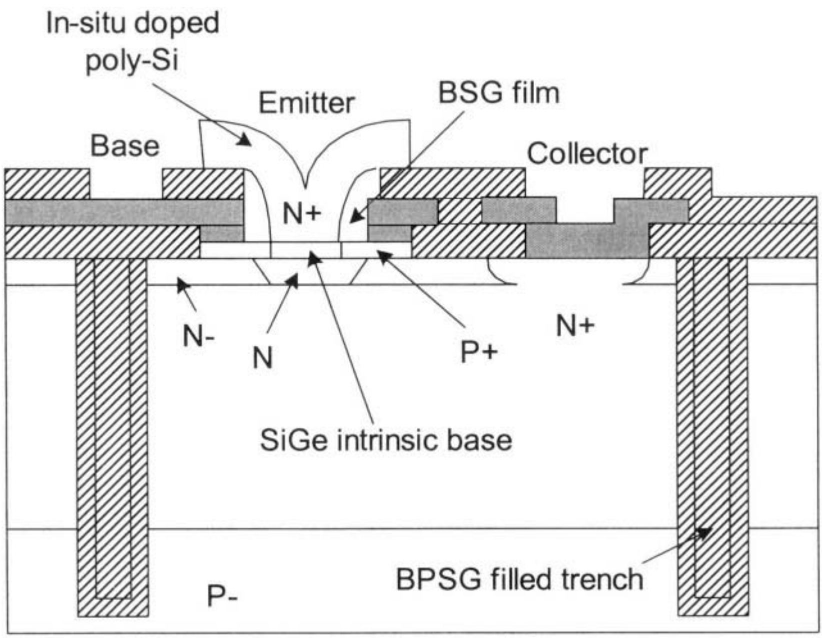

Figure 4.8. Schematic cross-section of a self-aligned SiGe HBT.

Recent improvements in $Si_{1-x}Ge_x/Si$ HBTs have increased cutoff frequencies to 50 ~ 200 GHz, approaching those of III-V HBTs and even HEMTs. A significant problem with Si based MMICs [30-32] is the lack of a semi-insulting Si substrate. High resistivity silicon has been used [31], however these substrates are often more costly than their III-V counterparts and are not always compatible with standard, industrial Si production lines [33,34]. In this transistor, which has been receiving much attention recently, the base is made of an alloy of silicon with about 10 % germanium. Since Ge has a bandgap of 0.7 eV, as compared with 1.1 eV for Si, the alloy will have a lower gap than the Si emitter. The problem is that the lattice constant of Ge differs strongly from that of Si. This could result in crystal defects at the interfaces. However, if the Ge content is not too high and the base layer not too thick, say 0.1μm or less, the SiGe layer is strained to match the Si crystal lattice and defects are absent. The bandgap difference can therefore not be more than about 0.04 eV.

The SiGe HBT technology has the great advantage of being compatible with standard Si technology. A possible disadvantage could be that the lower bandgap in the base means higher thermal generation of electron-hole pairs, making the transistor more sensitive to temperature variations [29]. Figure 4.8 shows the schematic cross-section of a Si/SiGe HBT.

For mobile communication system applications SiGe-HBTs offer some important advantages over other devices. First, SiGe-HBTs exhibit superior high frequency performance by extremely high f_{max} and f_t values of 160 GHz and 116 GHz, respectively. Besides this, SiGe-HBTs have excellent noise behavior. Second, SiGe-HBT fabrication is compatible with Si bipolar technology. Third, the thermal conductivity of Si is three times higher than that of GaAs. Fourth, the best high frequency performances can be obtained at low voltages, e.g. $V_{ce} = 1 \sim 3$ V, demonstrating the low-power potential. Fifth, SiGe-HBTs have a real advantage in power applications over Si-BJTs due to their low base sheet resistance down to 500 ohm/μm^2 [35].

4.4 Ku-band Mixer Topologies

At the present time, Schottky diode mixers are the most commonly used mixers in microwave systems. However, they have relatively poor intermodulation and spurious response properties because of their strongly nonlinear characteristics. Because monolithic diodes fabricated in FET-compatible technologies are often relatively poor, MMICs favor the use of FETs. And the development of high performance FET variants, such as HEMTs, promises improved noise figures and gain of FET mixers, while Schottky diode mixers have reached the limit of their performance. FET resistive mixers offer noise figure and conversion loss comparable to diodes, but much lower intermodulation. References [36-38] show that three-terminal devices, such as MESFETs and HEMTs, when used as mixing elements can achieve better performance and require less LO power than diode mixers [39].

4.4.1 Diode Mixer Topologies

Traditionally diode mixers have been used for broadband applications, because diodes can have very small junction capacitances that rarely limit the bandwidth of a diode mixer. However, FET mixers have the primary advantage of conversion gain instead of conversion loss in the case of the diode mixers. Because the diode mixer operates on the diode's on/off states, the conversion loss is more sensitive to process variations. It also requires a high LO signal to drive the mixer [40]. A diode mixer is sensitive to many frequencies outside of those at which it is designed to operate. The most famous of these is the image frequency, which is found at the LO sideband opposite the input, or RF frequency. The mixer is also sensitive to similar sideband on either side of each LO harmonic. These responses are usually unwanted.

- **Single Diode Mixer Topology**

Single diode mixers are occasionally used for simple, low-cost applications where performance need not be high. These mixers are rarely used at frequencies below the millimeter-wave region. Although single-diode mixers are practical and are widely used in millimeter-wave receiver applications, they have some undeniable faults. The most obvious difficulty is the need for a filter diplexer or other device to allow LO injection [41]. Figure 4.9 shows the equivalent circuit of a single diode mixer.

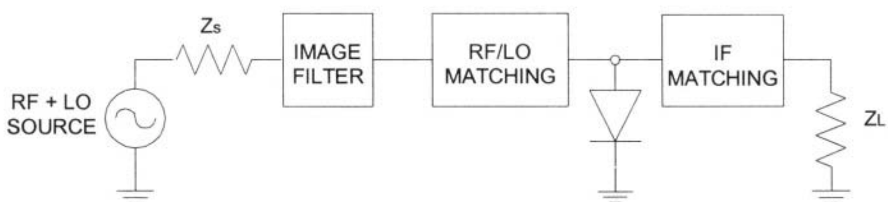

Figure 4.9. Equivalent circuit of a single-diode mixer.

- **Balanced Diode Mixer Topology**

Most diode mixers used at microwave and the lower millimeter-wave frequencies are balanced. The advantages of the balanced diode mixers over single-diode mixers are (1) the inherent rejection of spurious responses and intermodulation products; (2) LO/RF and LO/RF-to-IF isolation without the need for filters; and (3) rejection of AM noise in the LO. The disadvantages are (1) greater LO power requirements; (2) generally higher noise figure and conversion loss because of difficulties in biasing and matching individual diodes; and (3) few types of balanced mixers that exhibit all these characteristics [42]. Furthermore, in cases where the LO and RF bands overlap, balanced mixers are essential because it is impossible to separate the LO from RF using filters.

- **Singly Balanced Diode Mixer Topology**

A singly balanced mixer consists of two mixers combined by either a 180° or a 90° hybrid. Figure 4.10 shows a singly balanced mixer using 180° and 90° hybrids. The LO and RF are applied to one pair of mutually isolated ports, and single-diode mixers are connected to the other pair of ports. The diodes in the two mixers must be connected to the ports in such a way that their polarities are opposite [42]. The IF outputs of the individual mixers can be connected via another hybrid, or more commonly, they can be connected directly in parallel.

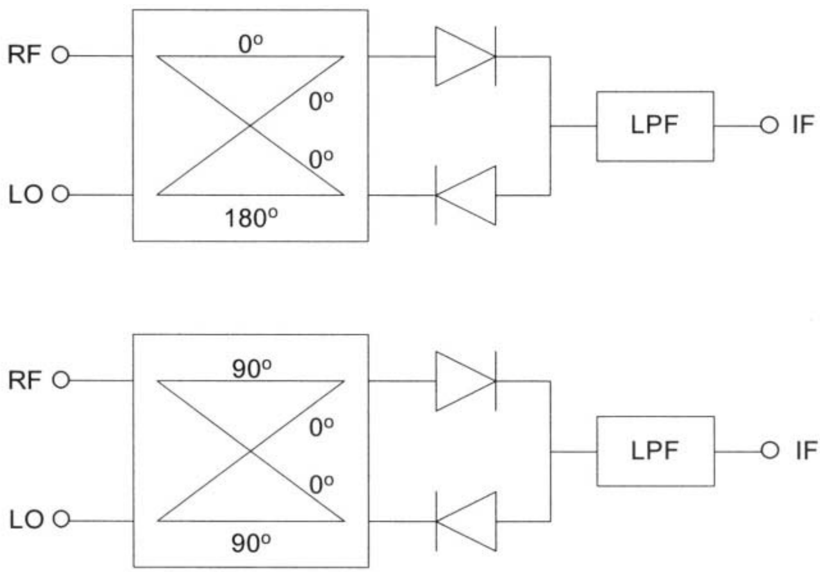

Figure 4.10. Singly balanced mixers using (a) 180-deg and (b) 90-deg hybrids.

- **Doubly Balanced Diode Mixer Topology**

A double balanced diode mixer has widespread application because of its inherently broad bandwidth, good isolation between ports, low spurious signal generation, excellent LO noise rejection and superior intercept point [43].

The two most common types of doubly balanced diode mixers are the ring mixer and the star mixer. The ring mixer is more amenable to low-frequency applications, in which transformers can be used. The star mixer is used primarily in microwave applications, because it is more amenable to operation with microwave baluns. There is no significant difference in the properties or performance of these mixer types.

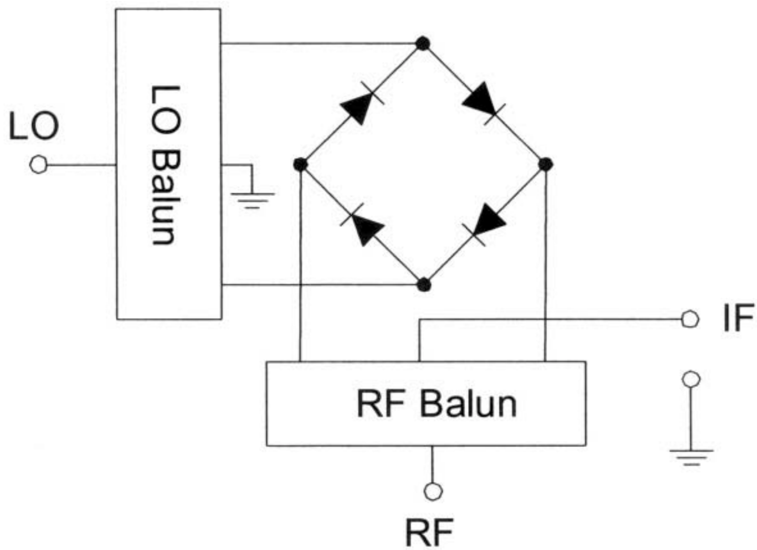

Figure 4.11. Doubly balanced diode-ring mixer.

Figure 4.11 shows the most common configuration for a doubly balanced diode ring mixer. It is best understood as a switching mixer in which the diodes are viewed as a switches controlled by the LO.

The frequency mixing process can be described as

$$V_{IF}(t) = s(t)V_{RF}(t) \tag{4.9}$$

where s(t) is a symmetrical square-wave switching function. As such, s(t) has no dc component, so the IF contains no RF component. Furthermore, s(t) has no even harmonics, so mixing with even harmonics of the LO is impossible. Similar consideration can be used to show that mixing with even RF harmonics also cannot occur [24].

Mixing occurs between the fundamental frequency of s(t) and $V_{RF}(t)$. The resulting IF current excites both transformers in an even mode; consequently, no IF voltage is developed across their secondaries and the transformers are invisible at the IF.

Two key advantage of the star mixer are broad IF bandwidth and a symmetrical balun structure that enhances the mixer's spur and isolation performance. All four diodes are connected together by a ring to form a star mixer [44,45].

In a star mixer, one terminal of each of four diodes is connected to a common node; this node is used as the IF terminal. Figure 4.12 shows a version of a star mixer that uses a high-frequency balun and, therefore, is useful at microwave frequencies. Marchand balun is remarkably broadband and is sometimes used in mixers having decade bandwidths [42]. Because the star mixer operates via the same principle as the ring mixer, the spurious-response properties of the star mixer are the same as those of the ring mixer.

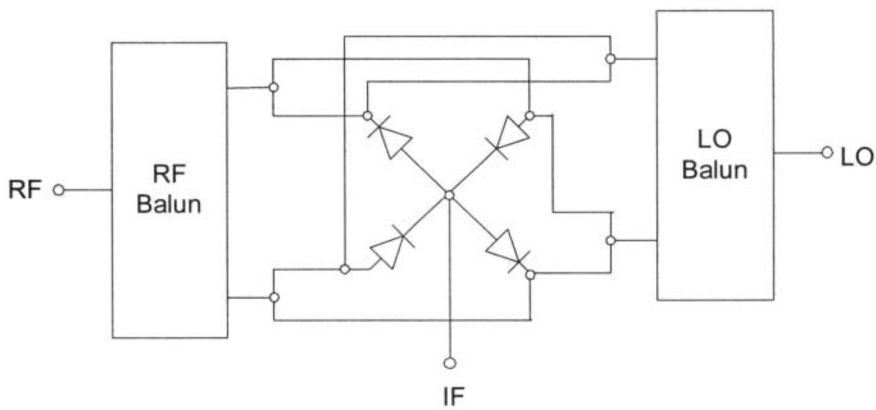

Figure 4.12. A doubly balanced star mixer for use at microwave frequencies.

- **Double Doubly Balanced Diode Mixer**

Mixers with low intermodulation products and a high third-order intercept (IP3) point are the key components of receivers with a high dynamic range. So far, the FET resistive mixer owns the highest IP3 performance. Double doubly balanced mixers (DDBM) are another candidate for high dynamic range application. It is the only mixer in which RF and IF bandwidths can overlap and without the loss of isolation between its RF, IF, and LO signals.

Most of the DDBM designs require separate RF, LO, and IF baluns and double-ring diodes, and are realized using hybrid implementation [46,47]. Figure 4.13 shows the circuit schematic diagram of DDBM.

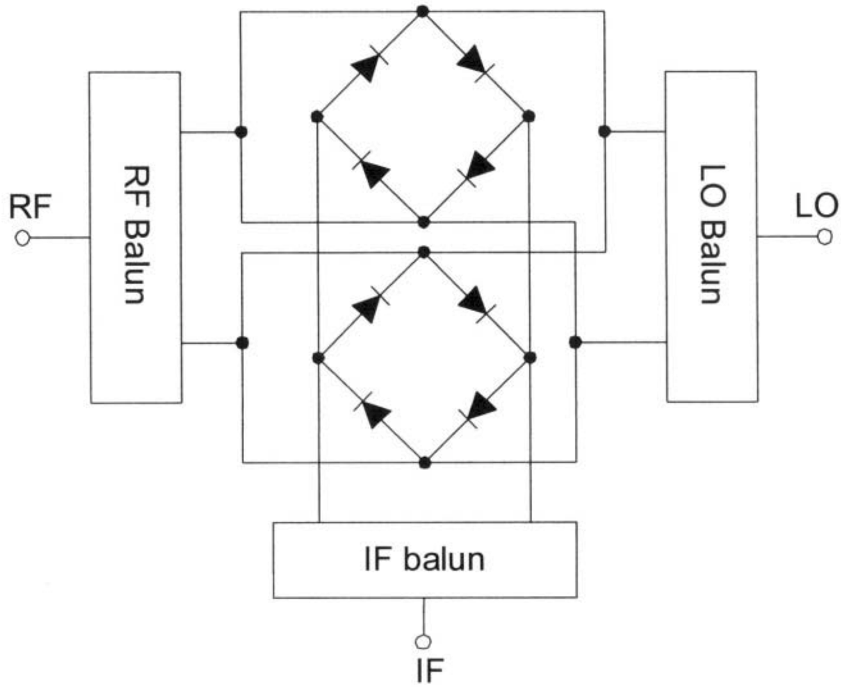

Figure 4.13. Schematic diagram of DDBM.

4.4.2 Active FET Mixer Topologies

In active FET mixers, the dominant nonlinearities are associated with the channel resistance R_{ds}, gate-to-source capacitance C_{gs}, and the transconductance g_m. Although the nonlinearities of R_{ds}, and C_{gs} are significant, usually the predominant nonlinearity used is that associated with g_m. Based on the maximum conversion gain, the optimum bias point was near the pinch-off or forward turn-on voltages, as expected for a standard FET-like device [48]. In the active mode, the device is used in a range of circuit configurations resembling those for small-signal amplifer design. A FET mixer operating in active mode can have a number of advantages over the diode mixer depending on its configuration. These include: (1) the possibility of conversion gain, (2) lower LO power, (3) the potential for LO signal isoaltion in a dual-gate FET by applying LO and signal to different gates, and (4) high reverse isolation, i.e. IF-signal and IF-LO, due to the unilateral properties of the FET [41].

- **Single-Gate Mixer**

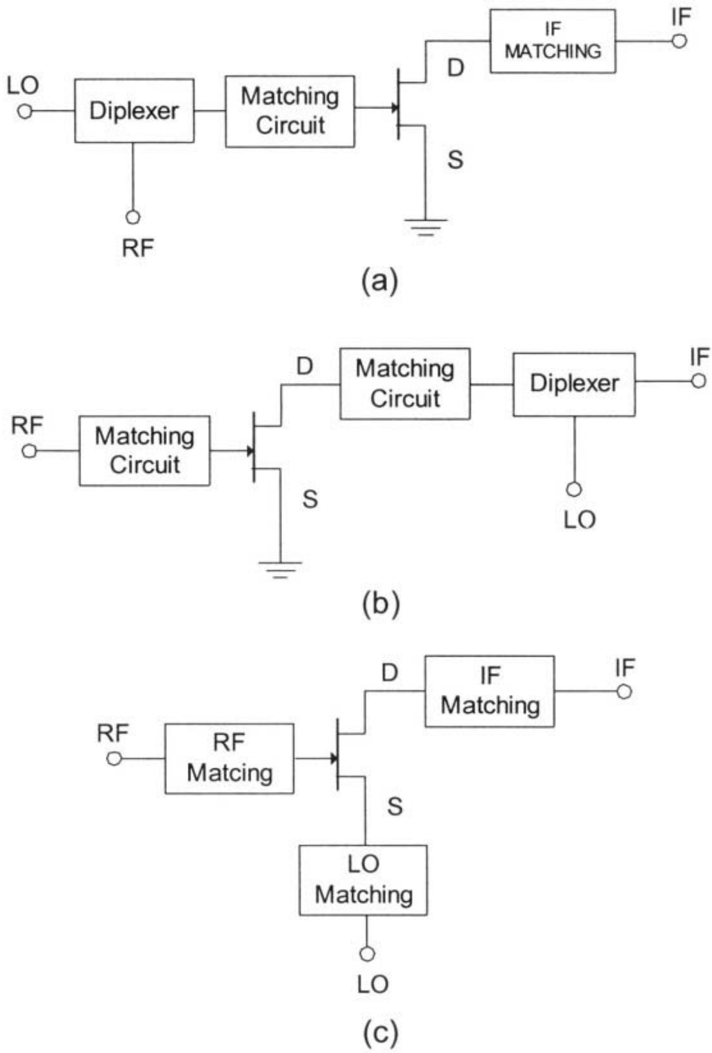

Figure 4.14. FET-based mixers are generally categorized into one of the three types; (a) gate mixer; (b) drain mixer; (c) source mixer.

Single-gate FETs have consistently provided better noise temperature and conversion gain than dual-gate FETs, although dual-gate mixers often have slightly lower distortion. Single-gate mixers have one major disadvantage in comparison to dual-gate mixers: It is much more difficult in single-gate devices to achieve good LO-to-RF isolation.

The FET-based mixers are generally categorized into one of three topologies: (1) gate [40], (2) drain [49], and (3) source mixing mixers [50]. An example of each topology is shown in Figure 4.15.

For the gate mixer, both LO and RF signals are applied to the gate of the mixer, while the IF is extracted from the drain terminal. The MESFET or HEMT is biased near pinch-off such that the applied LO signal varies the FET transconductance over a highly nonlinear region. Frequency conversion occurs primarily due to the nonlinear FET transconductance and thus a gate mixer is sometimes referred to as a transconductance mixer.

For the drain mixer, the LO signal is applied at the drain terminal, RF at the gate terminal, and the IF is extracted from the drain. Similar to the gate mixer, this mixer requires filtering to diplex the IF from the LO. The mixer operates with the FET drain-source voltage set near the knee of the linear and saturated regions of the I-V curve with a gate source bias of less than 0 V. At the bias condition, and with a LO signal applied to the drain, the FET transconductance and output resistance are both nonlinear and contribute to mixing. Compared to the gate topology, some improvement in noise performance has been reported with the drain topology [51]. In conventional FET mixer structure that involves "gate mixing" [52,53] or "drain-mixing" [49,54] topology, independent port matching for each signal is impossible because the LO and IF (or RF) signals share the same port. Such cases usually require hybrid circuits to gain sufficiently isolation between the LO and IF (or RF) signals. Such hybrid circuits, however, involve Lange couplers, power dividers, balun circuits and several anti-phase input signals [55-58] that greatly increase the complexity of the mixer circuit.

- **Dual-Gate Mixer**

The dual-gate FET (DGFET) is a four-terminal device that is usually operated in a common source configuration. Dual-gate FET mixers have one major advantage over single-gate: LO-RF isolation. The LO and RF signals can be applied to separate gates; because of low capacitance between the gates, which is manageable parasitic in the layout of the dual-gate FET [59], the mixer has good RF-to-LO isolation without the use of large filtering networks. Thus, it is often practical to use a single-device dual-gate FET mixer in applications where a balanced mixer would be needed [42,46]. Figure 4.15 shows the dual-gate FET mixer. The dual-gate device is represented by two single-gate FETs in series.

Many designs use dual-gate FETs as a means of achieving LO-to-RF isolation, but matching a dual-gate FET over a wide frequency band is difficult, and maintaining stability from spurious oscillations is also a problem [60]. The LO rejection to the RF port of the dual-gate FET mixer is good. The LO rejection to the IF port of the dual gate mixer is not high, but the LO is relatively simple to filter out of the IF [61]. A dual-gate mixer is simple to implement. Neither a filter diplexer nor an input hybrid are necessary to combine RF and LO signals as in a single gate mixer. The dual-gate FET was modeled as two single-gate FETs in series. The FET near the drain is operated in a linear mode, and the FET near the source is operated in a saturated mode [62].

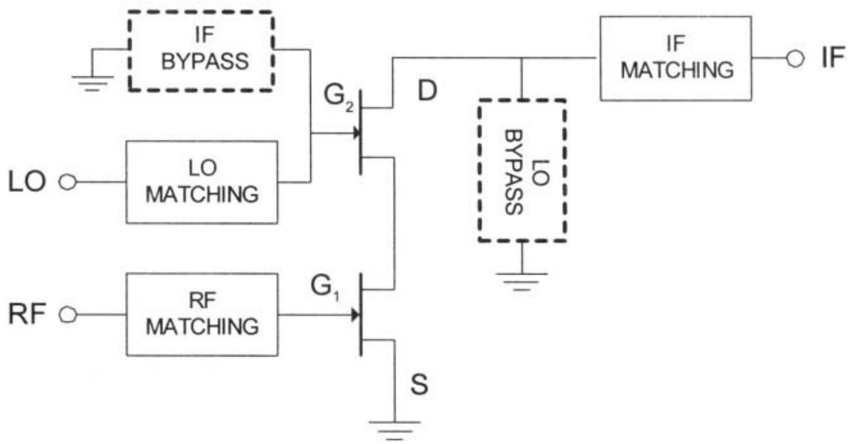

Figure 4.15. Dual-gate FET mixer.

Since the dual-gate device operation is nonlinear, a model that can accurately and efficiently predict large-signal performance is required. The device can be represented by either physical models or equivalent circuit models. The physical models are based on the device physics and usually describe the carrier transport mechanisms [63]. Physical models have the inherent ability to describe the operation of the device under any condition. The difficulty with all physical models is the determination of the physical parameters necessary to describe the device. Semiconductor device manufacturers are often unwilling to release this information. Thus, it is difficult to verify the accuracy of a physical simulation. Most of the microwave circuit design techniques are based on equivalent circuit models [64].

The DGFET is modeled as two single-gate FETs (SGFETs) in a cascode configuration, as shown in Figure 4.16. The complexity of the equivalent circuit increases as the operational frequency is increased because the effects of parasitic elements become significant and have to be included. A large signal equivalent circuit requires the determination of the behavior of the nonlinear elements within the circuit. This can be achieved by deriving the circuit elements from small-signal S-parameters over the range at which the applied bias device is operating. Methods for deriving the equivalent circuit of the DGFET from S-parameters are complicated because of the large number of elements required to describe the device. The procedure has been simplified at the expense of accuracy [15,16].

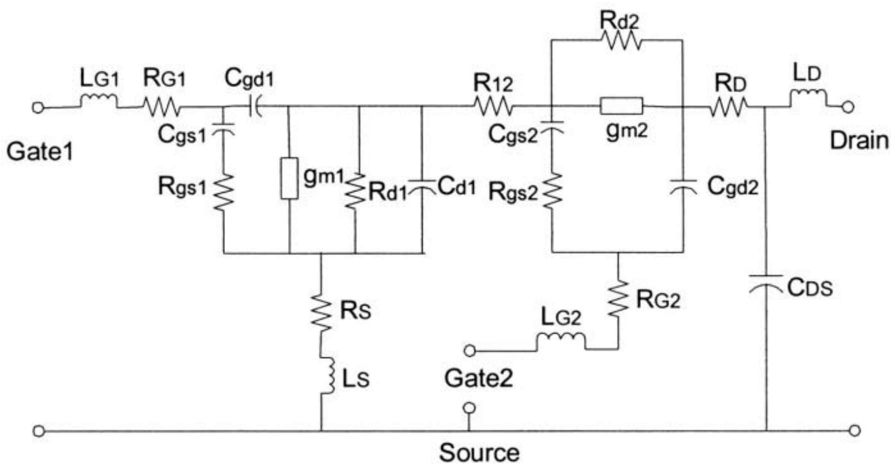

Figure 4.16. Equivalent circuit of the DGFET.

In the mixer design for the up-converter, the dual-gate FET was modeled using two single-gate FETs arranged in a common source and a common gate configuration, with the drain of the first FET connected to the source of the second FET, as shown in Figure 4.17. Depending on the bias conditions, the two FETs operate under different modes [65]. The gate bias for the first FET and the second gate bias were both set to be negative for low current. The drain characteristics for the pair can be approximated by combining the characteristics of each intrinsic FET. The operating point can vary significantly, depending on how the FET is biased. Typically, gate 1 is used for signal injection with gate 2 biased (Vgs2 < 0 V) for FET operation in the low-noise mode. Gate 2 is also used for local oscillator (LO) signal injection. Applying the LO at gate 2 is, in effect, drain pumping the first FET; hence, FET 1 is the primary mixing element. The operation is reversed if a sufficiently high bias voltage (Vgs2 > 2 V) is applied to gate 2. Under these bias conditions, FET 1 acts as a RF preamplifier, while FET 2 becomes the primary mixing element. This is especially true in the case of the dual-gate mixer, because the additional port allows inherent LO to RF isolation and it can replace a single balanced passive approach [66]. The possibility of conversion gain rather than loss is also an advantage because the added gain may eliminate the need for the excess amplification, thus reducing system complexity.

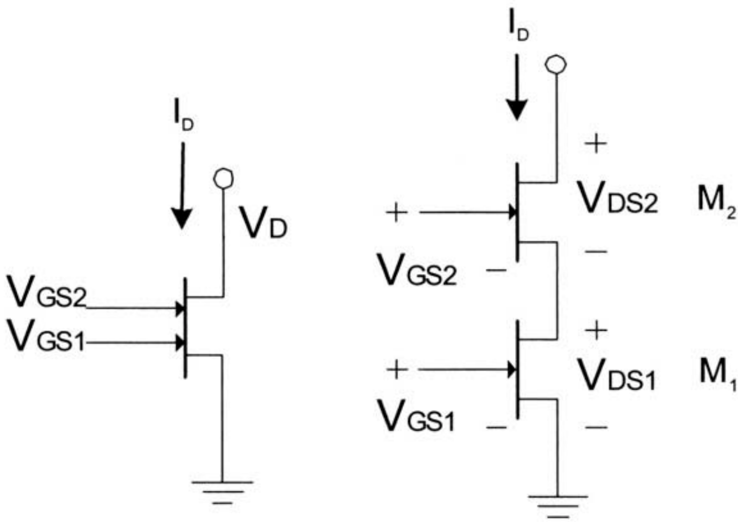

Figure 4.17. Cascode equivalent of dual-gate FET.

- **Balanced FET Mixers**

Balanced FET mixers can be realized with either single-gate or dual-gate devices. Although either type of device is useful for singly balanced mixers, dual-gate mixers are especially well suited for doubly balanced circuits. Unlike diodes, however, FETs cannot be "reversed;" the consequence of this characteristic is that balanced FET mixers often require IF hybrids [46], but diode mixers do not. This is an unavoidable situation: multiple hybrids significantly increase the size of a mixer and limit its practicality for monolithic applications.

- **Singly Balanced FET Mixers**

The single balanced mixer uses a pair of stacked FETs. The single balanced mixer makes it possible to eliminate an IF filter, which effectively reduces the chip size. Figure 4.18 shows two singly balanced FET mixers, one a 180° hybrid mixer and the other a quadrature hybrid mixer.

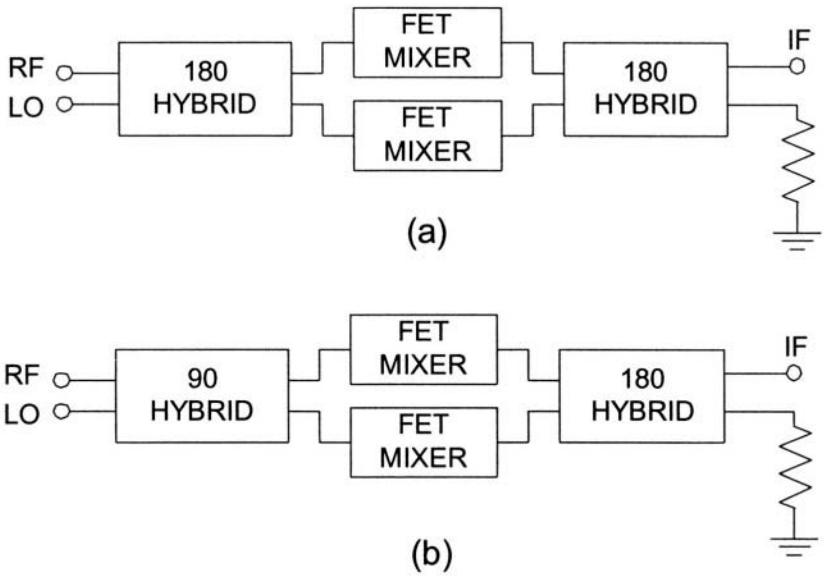

Figure 4.18. Singly balanced FET mixers : (a) 180-deg hybrid mixer; (b) quadrature-hybrid mixer.

The single-balanced (SB) mixer configuration can operate over a wider frequency band than its double balanced (DB) counterpart, although the DB mixer configuration outperforms the SB one in terms of port-to-port isolation and rejection of unwanted signals [67]. This is because one of the bandwidth limiting baluns in a DB mixer is replaced in a SB mixer by a power divider, which generally has a wider bandwidth than a balun. Consequently, both mixer configurations are used in the broadband monolithic mixer designs.

- **Doubly Balanced FET Mixers**

Since a DB mixer configuration provides isolation between all ports, it does not require filters to separate the RF, LO and IF signals. This configuration also has the advantages of LO noise and spurious signal rejection and even order spurious response rejection [39]. Figure 4.19 shows a schematic diagram of a doubly balanced dual-gate FET mixer.

In order to reduce the necessary LO drive power, an active balanced mixer [60] was designed. Balanced mixers are widely used to minimize unwanted frequencies like the leakage of the LO signal to the RF port, the LO signal to the IF port, as well as intermodulation products [68]. Balanced dual-gate FET mixers are also possible and are used in applications where the spurious response and LO-noise rejection of a balanced mixer are valuable [46]. Balanced dual-gate mixers usually require hybrids for all three ports, and thus may be relatively complicated circuits.

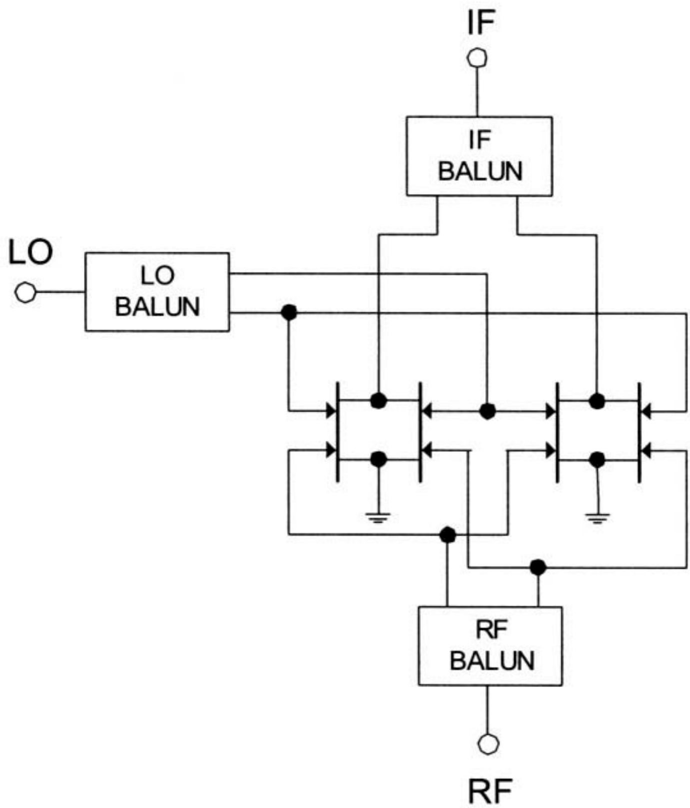

Figure 4.19. Doubly-balanced dual-gate FET mixer.

4.4.3 Passive FET Mixer Topologies

In a resistive mixer, the FET is used as a time-varying resistor, which is modulated by the LO signal. No external bias voltages are applied to the FET. The LO is fed to the FET gate, resulting in a change of channel resistance between high and low values [68]. Under this bias condition, the FET is weakly nonlinear, and thus very high IMD performance is possible. However, because the FET is unbiased and is operated as a time-varying resistor, it exhibits significant conversion loss [69]. Figure 4.20 shows the FET resistive mixer.

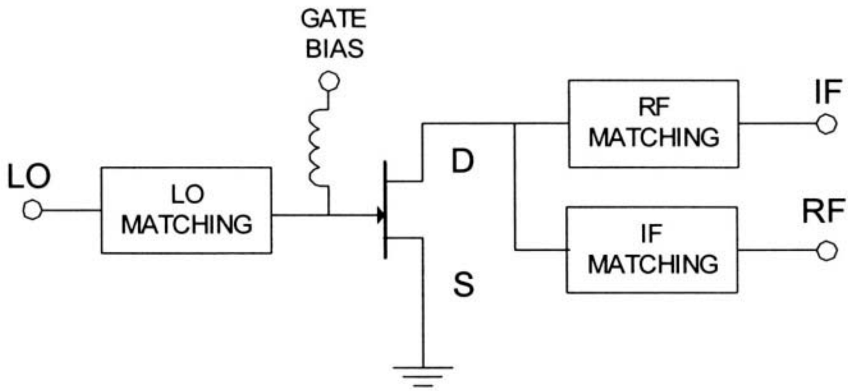

Figure 4.20. FET resistive mixer.

Both MESFETs and HEMTs can be used as mixing elements in either an active or a resistive mode. The resistive mode has the advantages of very low distortion, low 1/f noise, and no shot noise, a low noise figure, a high two-tone third-order intermodulation intercept point, separation between the LO and RF/IF-ports, and low dc power consumption when compared with a corresponding active mixer [46,70]. In addition, a resistive HEMT mixer requires lower LO power and can operate over a wider frequency range than a resistive [39,71] MESFET mixer. Also low conversion loss can be obtained at a very low LO-power using advanced InP based HEMT devices [72].

4.4.4 Other Topologies

- **Gilbert Cell Mixer**

The Gilbert cell mixer offers improved spur performance and high conversion gain in a very compact size from baseband to microwave frequencies [73-75]. Figure 4.21 shows FET Gilbert cell mixer. One of the attractive features of the Gilbert cell topology is that it achieves double balanced conversion without passive baluns that are conventionally used in diode mixers. The isolation is comparable to passive balun Schottky diode mixers, but the active Gilbert cell mixer can be realized in a much smaller area. The isolation can be further improved by adding a differential buffer stage to the LO and IF input ports of the Gilbert cell [73]. But, the Gilbert cell mixer requires at least 3 V_{be} to operate with reasonable linearity [74].

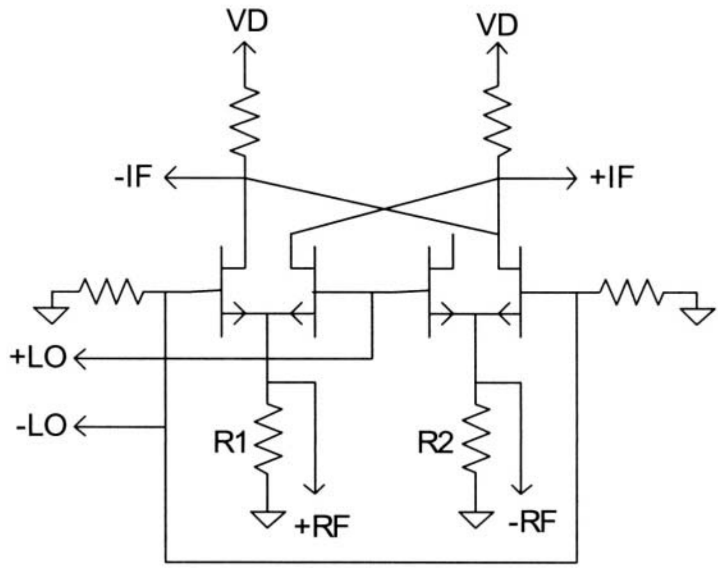

Figure 4.21. FET Gilbert Cell Mixer.

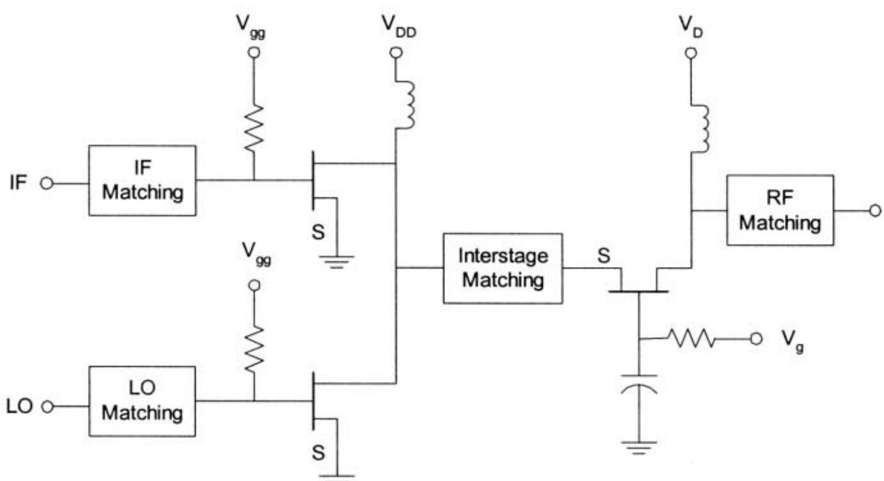

Figure 4.22. Schematic of CS/CG Mixer.

- **Common Source/ Common Gate (CS/CG) Mixer**

If a monolithic implementation is desired, the balun dimension is limited by the chip area, especially for Ku-band frequencies (below 20 GHz). Thus, active baluns or lumped element transformers are the only viable options. This active balun can be implemented by using a common-gate and common-source circuit configuration because an ideal 180° phase shift exists between both outputs. The balanced mixer presented uses this topology to perform both mixing and balun functions [76,77]. The goals for this circuit are the following; (1) have conversion gain, (2) have low LO-power necessity (3) have good rejection of unwanted harmonics and spurious frequencies, and (4) have a low noise figure in order to get the largest possible signal-to-noise ratio. This can eliminate the need for bulky balun circuitry [75,77]. Figure 4.22 shows CS/CG upconverter mixer.

- **Image Rejection Mixer**

An image rejection filter is required in the system to eliminate the image. In a low IF system, it is very difficult to implement a filter that can provide sufficient image rejection. One solution is to replace the image rejection filter with an image rejection mixer. The image-rejection mixer is realized as the interconnection of a pair of balanced mixers. It is especially useful for applications in which the image and RF bands overlap or the image is too close to the RF to be rejected by a filter. The LO ports of the balanced mixers are driven in-phase, but the signals applied to the RF ports have a 90° phase difference. A 90° IF hybrid is used to separate the RF and the image bands [78]. Figure 4.23 shows an image rejection mixer.

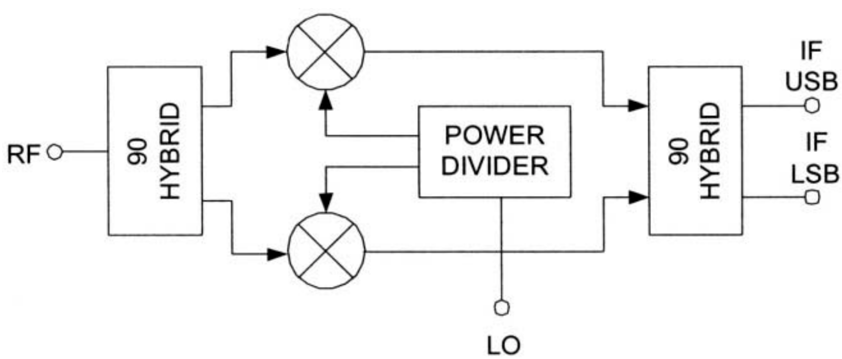

Figure 4.23. Image rejection mixer.

4.5 Comparison of Ku-band Mixer

Up until now, two types of device approaches have primarily been reported for the MMIC implementation of Ku-band satellite communication applications. One is a GaAs ion-implantation MESFET [79-81] and the other is HEMT [82,83]. The former has superiority in terms of its manufacturability while the latter has an advantage in its excellent low-noise performance. However, cost is the most significant factor in the case of consumer applications such as in Ku-band DBS frequency converters. From the standpoint of cost, GaAs ion-implementation MESFET's are favorable in comparison with HEMT's [84].

Recently, HBTs have been regarded as the preferred device IC technology for frequency converter applications because it offers both low 1/f device noise characteristics and low parasitic Schottky diodes. Compared with MESFETs and HEMTs, the HBT offers the following advantages for mixers intended for use in satellite communications application in Ku-band: (1) superior conversion gain that can reduce the number of IF stages, (2) increased 3rd order intercept point (IP_3), which means better adjacent channel interference properties, (3) low dc power consumption, which can increase battery life, (4) higher 1dB compression, which results in better signal handling capabilities (5) better intermodulation performance [85]. Both MESFET and HBT mixer conversion gain is a strong function of output resistance and transconductance, hence, the HBT offers better conversion gain [86]. But it is generally acknowledged that the HBT device has poor noise performance when compared to MESFETs or HEMT devices; thus, the small-signal applications of this device are limited. The types of noises encountered in the HBT are shot noise, flicker noise and Johnson noise. Flicker noise is inversely proportional to frequency [85]. Despite their poor noise performance, interest in applications of HBTs in high-speed digital and analog microwave circuits exists for many applications such as local multipoint distribution systems (LMDS). The potential of using HBTs in mixed-mode application is of interest because of its high transconductance, large current drive, low 1/f noise, high bandwidth, and uniform turn-on voltage [87].

In HBT, the possible combinations that fulfill good lattice-matching conditions are AlGaAs/GaAs and Si/SiGe. The GaAs HBT has demonstrated a variety of analog and microwave functions with significant advantages over advanced Si bipolar and GaAs FETs (MESFET and HEMTs) in combinations of bandwidth, power consumption, harmonic distortion, phase noise, and size.

The GaAs HBT's exponential output current/input voltage transfer characteristic is used to achieve nonlinear mixing operation.

Compared to conventional double-balanced diode mixers, the GaAs HBT upconverter mixer has advantages of low drive LO and the ability to provide positive conversion gain. Compared to similar MESFET upconverter mixer, the GaAs HBT circuit is 5 ~ 6 times smaller in overall chip area, while, compared to silicon Gilbert-cell mixer versions, the HBT upconverter mixer has more gain (7 dB) and 5 times higher output frequency performance [61]. And GaInP/GaAs HBTs are also another candidates for satellite communication applications because of their high peak power density and their usefulness for a variety of circuit types [75].

GaAs HBT technology can also provide high performance Schottky diodes, which are known to produce Schottky based mixers, with higher IP3 performance than conventional active balanced mixers such as the Gilbert cell while consuming no dc power.

Previously reported AlGaAs/GaAs HBT Schottky diode mixer MMIC's results have shown that high performance Schottky mixers can be realized with a generic GaAs HBT foundry process with little or no material-process optimization [88]. Using the same GaAs HBT IC technology, a double-double balanced Schottky mixer has been reported [89]. Compared to a previous reported double-double balanced 0.5-μm MESFET Schottky mixer designed for the Ku-band, this HBT Schottky mixer achieves the same conversion loss (10 dB) and input IP3 (20 dBm), but achieves better LO-RF (> 30 dB improvement) and RF-IF (> 10 dB improvement) isolation using lower LO power [88,89]. The requirement for lower LO drive is a significant parameter when considering proper operation of the complete converter architecture. The higher the LO drive requirement of the mixer, the more stages and dc power consumption required at the LO port from the buffer amplifier stage. This can increase the size of a monolithic integrated receiver or upconverter by 10 ~ 20 % and its total power consumption by 10 ~ 30 % [88,89].

Available silicon bipolar technologies are partly able to cover Ku-band frequency ranges, although at the expense of high power consumption, e.g. an active mixer with 280 mW power consumption [90,91]. Recently, SiGe heterojunction bipolar transistor (HBT) technologies have become commercially available that combine enhanced RF performance with the maturity of silicon technology.

[90] describes the application of SiGe HBTs with a constant germanium concentration in the base to Gilbert cell type mixers operating at Ku-band frequencies. The mixer consumes only 53 mW from a 3.6 V supply voltage with local oscillator input power of -2 dBm and a conversion gain of 16 dB was observed [90]. Recent progress has pushed the operating range of silicon bipolar well into the microwave range for applications such as optical-fiber communications at 10 ~ 20 GHz and Ka-band frequency

dividers [92]. At low frequency, the Si BJT circuits had slightly lower NF than the SiGe HBT circuits. This may be because the Si BJT parts have equal or higher low-frequency gain than the SiGe HBT parts as a result of slightly higher polysilicon resistor R_s for the Si BJT wafer. At high frequency, the SiGe HBT circuits had higher gain and lower NF than the Si BJT circuits because of the higher bandwidth that SiGe affords [92]. The SiGe HBT wafer showed a 6 to 20 % improvement in circuit gain-bandwidth and a 22 % improvement in device f_t and f_{max} over an identically processed Si BJT wafer with similar noise figure, IP3, and compression [92]. Thus, there is a consistent speed advantage for the epitaxial-base SiGe HBT circuits and devices over the epitaxial-base Si BJT circuits and devices.

4.6 Conclusions

Microwave mixers are essential components of most telecommunication, and satellite communication systems. Mixers can be designed in the active (lower conversion loss, higher noise) or passive (higher conversion loss, lower noise) modes, as required by the application. At microwave frequencies, mixers can be realized using discrete components circuitry or as MMICs. Small size, light weight, and low cost are the main reasons for the increasing demand for MMIC mixers in microwave systems.

Several different types of technology and topology for the Ku-band MMIC mixer have been reviewed. The primary devices which can be used for Ku-band mixer are Schottky barrier diode, GaAs FET (MESFET, HEMT), and HBT (GaAs, SiGe). The most common type of microwave frequency mixer uses a Schottky barrier diode. Diode mixers are useful over a remarkably broad range of frequencies. However, FET mixers have the primary advantage of conversion gain instead of conversion loss as in the case of the diode mixers [48]. The GaAS MESFET process is cheaper and more commercially available in high volume manufacture but HEMT has an advantage in its excellent low noise performance.

However, progress in the development of HBT may bring about a resurgence in the use of bipolar devices as mixers. The HBT offers superior conversion gain and intermodulation for lower dc power consumption than GaAs FET (MESFET, HEMT) mixers. Because of the lower ideality factor and lower series contact resistance of HBT Schottky diodes, lower conversion loss and higher IP3 is expected for a given LO drive level compared to MESFET or HEMT Schottky diode implementations.

The complexity of mixer designs has ranged from a single-point contact diode to structures employing eight Schottky diodes. More recent designs use single- and dual-gate FETs to replace the diode as the nonlinear element.

Several MMIC mixers (based on both diodes and FETs) have also been reported [93]. High-level monolithic integration of microwave functional modules is effective in reducing the total module size and the assembly cost. Therefore, it is essential to reduce the chip size in order to suppress MMIC chip cost. To accomplish this, circuit configurations and structures suitable for small circuitry are desirable as well as smaller circuit elements.

Usually balanced mixers are used to minimize unwanted frequencies like the leakage of the LO signal to the RF port, and the LO signal to the IF port, and intermodulation products. Since a DBM configuration provides isolation between all ports, it does not require filters to separate the RF, LO and IF signals. This configuration also has the advantages of LO noise and spurious signal rejection and even order spurious response rejection. Therefore, the DBM configuration is widely used in the design of the Ku-band monolithic mixer.

Different kinds of mixer topology are available according to its application and system requirement. If cost is not a consideration, both GaInP/GaAs and Si/SiGe HBT are well-suited for high performance mixer applications compared to other semiconductor device; and double balanced mixer topology has better performance than other topologies. In most cases, however, the determination of suitable technology and topology for a Ku-band mixer will be determined by cost, size, and performance specifications dictated by a specific applications.

Chapter 5

Review of Ku-band VCOs

5.1 Oscillator Design Principles

An oscillator is an energy conversion element that transforms dc power into ac power. To model an oscillator from the circuit point of view, two different models are used: a two-port model and a one-port model [16]. The oscillator circuit is analyzed by these two different ways of defining the oscillator circuit topology and their oscillation condition. The two-port oscillator model can be viewed as a feedback circuit because the feedback loop is closed around a two-port network. Also note that the one-port model treats the oscillator as two one-port networks connected to each other. The two models are equivalent in many cases. The constant exception is active devices, such as tunnel diodes, that have inherently only one-port. Microwave oscillators often fall in the feedback category, but the one-port model can give additional insight into their operation.

5.1.1 Feedback Oscillator (Two-port Model)

A feedback oscillator consists of an amplifier and a resonant circuit as shown in Figure 5.1. A feedback oscillator achieves instability by positive feedback.

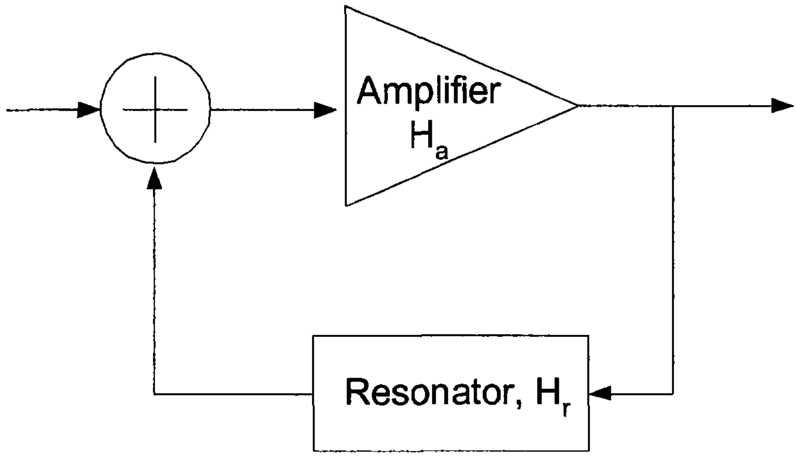

Figure 5.1. Feedback oscillator.

For steady oscillation, two conditions must be simultaneously met at ω_0: (1) The loop gain must be equal to zero, and (2) the total phase shift around the loop must be equal to zero. This relation is known as the Barkhausen criterion [94] and can be written,

$$H_a \cdot H_r = 1 \tag{5.1}$$

where H_a and H_r are the loop gain for the amplifier and resonator, respectively.

Equation (5.1) implies that the gain of the amplifier has to compensate for the loss in the resonator, and that the electrical delay through the amplifier and resonator must be equal to an integral multiple of 360°. The amplifier's input and output impedances are assumed to be equal to the characteristic impedance Z_0 (usually 50 ohms) and must be stable over a range of frequencies. In oscillators, the resonator determines the oscillation frequency and phase noise performance.

5.1.2 Negative Resistance (One-port Model)

A microwave oscillator is modeled as one-port because the real part of the port impedance is negative. A two-terminal device like a Gunn diode inherently has negative resistance, while a three-terminal device like a transistor needs appropriate feedback inside an active device to achieve the negative resistance. [95]

A negative resistance oscillator circuit consists of a resonator and an active block as shown in Figure 5.2. The resonator by itself does not oscillate because in every cycle some of the stored energy is dissipated in Z_T. The idea in the one-port model is that an active network generates impedance equal to $-Z_T$ so that the equivalent resistance seen by the resonator is lossless. In other words, the energy lost in Z_T is replenished by the active circuit with $-Z_T$, thus allowing steady oscillation. [16].

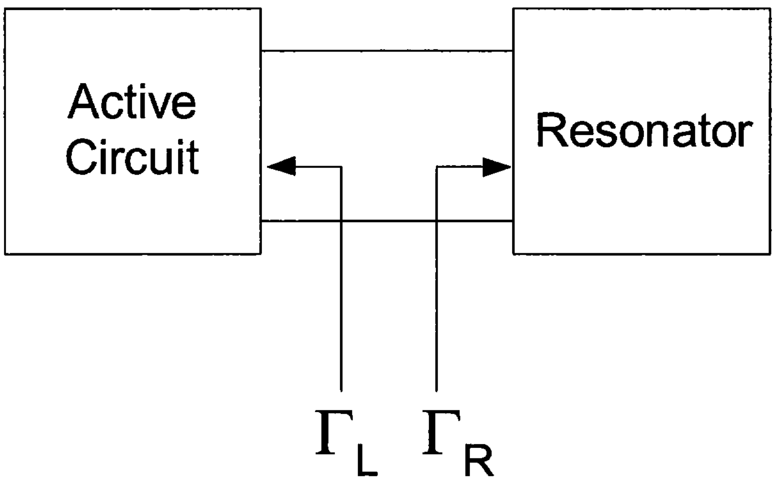

Figure 5.2. Negative Resistance Oscillator Configuration.

The conditions for oscillation are

$$K = \frac{1-|S_{11}|^2-|S_{22}|^2+|S_{11}\cdot S_{22}-S_{12}\cdot S_{21}|^2}{2|S_{12}\cdot S_{21}|}<1 \tag{5.2}$$

$$\Gamma_l \cdot \Gamma_r = 1 \tag{5.3}$$

$$Z_l + Z_r = 0 \tag{5.4}$$

where K is the Rollet stability factor, Γ_r is the reflection coefficient of the resonator circuit and Γ_l is reflection coefficient of the active block, and Z_l and Z_r are the corresponding impedance. Equation 5.2 implies that the stability factor should be less than unity for oscillation to start. Equation 5.3

means that the return loss of the resonator has to be equal to the return gain of the active block, which implies the presence of a negative resistance between the active block's input terminals. In terms of impedance, the sum of the positive resistance of the resonator and the negative resistance of the active block is zero, and the sum of their reactance to them should be zero as well. To ensure oscillation start-up, the small-signal loop gain has to be greater than one. Oscillation will grow continually until negative resistance reduces it to its steady state by the non-linear effects of the active device.

5.2 VCO Design Principles

The frequency converter block is an important component in the transmitting and receiving path of a communications system, and both require a VCO to perform the frequency conversion. The active elements of VCO must be able to generate a negative resistance or a reflection coefficient greater than unity over the desired tuning range with suitable feedback. Two feedback configurations [41] are commonly used for negative resistance generation: (1) the common-gate inductive feedback, and (2) common-source capacitive feedback as shown in Figure 5.3.

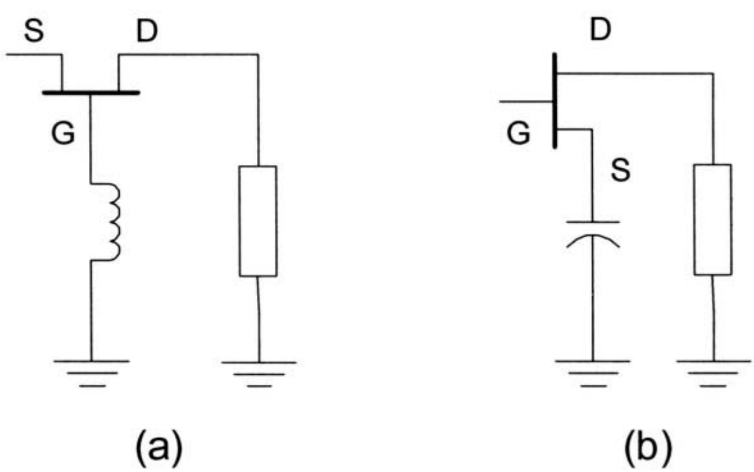

Figure 5.3. Basic feedback topologies for negative resistance oscillators (a) Common gate inductive feedback (b) Common source capacitive feedback.

For MESFET oscillators, the most widely used topology is the common-gate configuration because a common-lead inductance increases the magnitude of the input- and output-reflection coefficient to a value well above unity. To realize a VCO, one of these reactances should be able to be tuned with voltage. In most cases, output loads are connected to the MESFET drain, and frequency tuning elements are placed in either or both of the other two terminals.

Oscillation may start only when the magnitude of the output port reflection coefficient is greater than unity. The output port reflection coefficient Γ_o is related to the variable reactance reflection coefficient Γ_υ as

$$\Gamma_o = S_{11} + \frac{S_{21} \cdot S_{12} \cdot \Gamma_\upsilon}{1 - S_{22} \cdot \Gamma_\upsilon} \tag{5.5}$$

where S_{11}, S_{21}, S_{12}, and S_{22} are the S parameters of the FET in each configurations. The oscillation frequency is determined by Γ_o and load impedance. For VCO design, one or more of the immittances are made tunable by using an yttrium iron garnet (YIG), or tunable active inductor (TAI) resonators, varactor diodes. YIG resonators have a very high Q and a wide tuning range, but also have slow tuning speed and high power dissipation. The TAI shows stable, high Q performance with a large tunable range and compact layout. However, their high dc power consumption is a drawback. The varactor diode oscillator has a faster switching time but poor phase noise performance because of the low Q of the varactor diode. Designing the resonator and its tuning circuit involves a direct trade-off between tuning range and phase noise. The contribution to phase noise and frequency stability from the resonator for a certain topology is dominated by the sensitivity of its impedance with respect to tuning voltage and the strength of coupling tuning elements to the circuit. Since this sensitivity and strength of coupling determines the tuning range of the VCO, an improvement in tuning range will result in degradation in phase noise and frequency stability. This situation occurs because of poor thermal stability and possible reduction of the resonator Q.

5.3 VCO Performance Parameters

Frequency and output power are two fundamental performance parameters of an oscillator. In this section, other important performance parameters such as phase noise, pushing and pulling, thermal stability, and post-tuning drift are described.

5.3.1 Phase Noise

Phase noise is one of the most important parameters because it affects the dynamic range, selectivity, and sensitivity of a transceiver. Most oscillator noise, particularly close to the carrier, is phase or FM noise. Noise processes in semiconductor devices can modulate the phase of an oscillator and create noise sidebands in its output spectrum. For satellite and coherent communication systems, phase distortion is a very serious problem because phase information is crucial in these systems. The fundamental significance of the phase noise is that it determines the level of interference in the neighboring channel. Therefore, a typical VCO specification states values of phase noise depending on the carrier offset. The noise processes that generate low frequency noise components are of crucial concern because the resonator attenuates high frequency components of phase noise. Noise originating from the power supply and noise that is coupled to the dc bias circuit also contributes to phase noise. The phase noise characteristic describes the relationship of the carrier level to the noise level in the environment of the carrier frequency.

The SSB phase noise, $\mathcal{L}(f_m)$, is the most commonly used expression for oscillator phase noise. $\mathcal{L}(f_m)$ can be expressed as,

$$L(f_m) = 10 \cdot \log\left(\frac{P_{SSB}}{P_S}\right)[dBc/Hz] \tag{5.6}$$

where P_{SSB} is the SSB phase noise power in a 1-Hz bandwidth at offset frequency f_m away from the signal, and P_s is the carrier signal power as shown in Figure 5.4.

The phase noise of a VCO has been observed in numerous theoretical experiments, and was derived by Lesson [96]. Lesson derived the SSB phase noise equation of the oscillator by using a feedback oscillator analysis method. Lesson's equation of SSB phase noise is,

$$\begin{aligned} L(f_m) &= \frac{1}{2}\left[1 + \frac{1}{f_m^{\,2}}\left(\frac{f_o}{2Q_L}\right)^2\right]\frac{FkT}{P_{avs}}\left(1 + \frac{f_c}{f_m}\right) \\ &= \frac{FkTB}{2P_{avs}}\left[\frac{1}{f_m^{\,3}}\frac{f_o f_c}{4Q_L^{\,2}} + \frac{1}{f_m^{\,2}}\left(\frac{f_o}{2Q_L}\right)^2 + \frac{f_c}{f_m} + 1\right][dBc/Hz] \end{aligned} \tag{5.7}$$

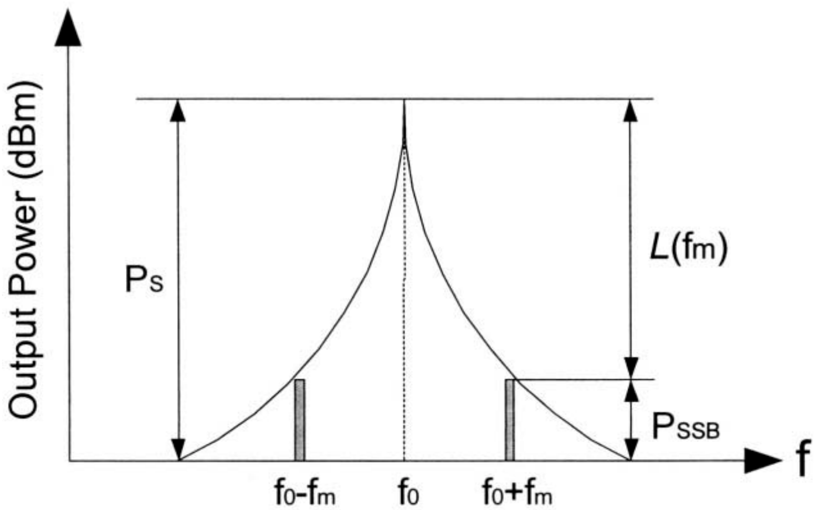

Figure 5.4. Output power spectrum of an oscillator

where f_o is the carrier frequency, f_m is the offset frequency from the carrier frequency, Q_L is the loaded quality factor of the resonator, f_c is the corner frequency of 1/f noise, F is the equivalent noise factor of the amplifier or active circuit, k is Boltzmann's constant, T is the absolute temperature in Kelvin, and P_{avs} is the signal power at the input of the amplifier.

Examining (5.7) gives the four major causes of oscillator noise: the up-converted 1/f noise or flicker frequency modulation (FM) noise, the thermal FM noise, the flicker phase noise, and thermal noise floor [97]. The most common way to reduce phase noise is by employing an active device with a low noise figure and low flicker noise, and by using a resonator with high loaded Q and choosing a low noise power supply, filtering the power supply and avoiding saturation in the active device. Using low frequency loading and low frequency feedback to reduce 1/f noise up-conversion can also be used to reduce phase noise [98]. Usually, lower phase noise can be achieved by using GaAs HBT devices because of their low 1/f noise performance with a trade-off in terms of a greater up-conversion factor than that of HEMT [99].

5.3.2 Load Pushing and Pulling

The change in oscillation frequency because of the oscillator's supply voltage is called pushing. Pushing occurs because the transistor's S-parameter and Γ_{in} changes with its dc bias voltage. Supply voltages generally drift with time, temperature, and load variations. Using the high-Q resonator can minimize pushing because higher loaded Q isolates the resonant circuit from active-device junction capacitance variation due to supply voltage [100].

The load impedance of the oscillator also affects the output level and oscillation frequency by changing the phase of Γ_{in}. Pulling is defined as the total output frequency deviation due to load perturbation. It describes the sensitivity to load fluctuations of the free-running VCOs at the VCO output. An exact derivation of the pulling figure, taking fully into account the nonlinear behavior of the oscillator admittance, has been presented in [101]. The simplified pulling figure expression [102], neglecting the nonlinear term, is

$$\Delta\omega_t = \frac{\omega_o}{2Q_e}\left(S - \frac{1}{S}\right)[Hz] \tag{5.8}$$

where ω_o is the carrier angular frequency, S is the voltage-standing-wave-ratio (VSWR) of the load, and Q_e is the external Q of the oscillator. Pulling can also be minimized by using a high-Q resonator and an additional buffer amplifier. Such a buffer amplifier also improves the output power level of the VCO.

5.3.3 Thermal Stability

Both the resonant frequency of resonator and the Γ_{in} of the transistor change with variation in oscillator temperature. This phenomenon causes the change in oscillation frequency, output power, and even termination of oscillation. For resonators, changes in their resonant frequency are caused primarily by temperature dependency of the dielectric constant and the thermal expansion of the material [41]. For the GaAs MESFET, increasing the temperature widens the reverse biased gate-channel junction that increases the depletion region resulting in drain current reduction and a consequent change in all the S-parameters [97]. Some degree of compensation can be included in the bias circuits or by using a resonator with low temperature coefficient and high Q. The thermal stability is more dependent on the resonator's frequency stability than its Q.

5.3.4 Post-Tuning Drift

The post-tuning drift in a VCO is defined as the frequency drift that occurs during the time interval required before the circuit returns to its steady-state condition after the tuning step has been applied. Bias voltages and the thermal effects are the main contributors. When the frequency of a VCO is being tuned, changes occur in the RF voltage, and in the current throughout the oscillator; slight changes also occur in the dc bias current. As a result, the junction temperature of the transistor and of the tuning elements such as a varactor all change, as do the dc voltages in blocking capacitors and the dc current in inductors. This causes impedance change and thus results in frequency change. The time interval over which this phenomenon occurs is dependent on the thermal impedance of the device. The post-tuning drift can be reduced by choosing a frequency tuning element with a fast heat dissipation.

5.4 Ku-band VCO MMIC

The GaAs MESFET is the most widely used monolithic active device for Ku-band oscillator design because of its many advantages over other technologies. Compared to Si BJT, the GaAs MESFET provides higher frequency of oscillation, higher output power because of a greater critical field and higher saturated drift velocity, higher gain due to greater electron mobility, and higher efficiency. The Si BJT usually have much lower flicker noise but only microwave integrated circuit (MIC) Ku-band Si BJT VCO designs have been done [103-105] because of its lossy substrate. The GaAs MESFET offers poorer phase noise performance than HBT but is more cost effective and more commercially available higher volume technology. Comparisons between AlGaAs/GaAs HBT and GaAs MESFET will be closely looked at in section 5.5 and section 5.6.

Currently, the three most widely used frequency tuning elements are: YIG sphere, varactor diode, and TAIs. In this section, GaAs Ku-band MESFET VCO employing each of these three types of frequency tuning elements will be reviewed and compared.

5.4.1 YIG-Tuned oscillator

YIG resonators are high Q ferrite resonators that can be tuned over a wideband by changing the biasing dc magnetic field. A YIG resonator uses ferrimagnetic resonance that can be attained from 0.5 to 50 GHz [106] depending on size, applied field, and the material composition. Therefore, the maximum possible oscillating bandwidth of a YIG-tuned oscillator is usually limited by the negative resistance frequency range of the active device. Linear tuning can be achieved using single-crystal YIG and gallium-doped YIG because their resonance is directly proportional to the applied magnetic field controlled by an electric current. The resonator consists of a YIG sphere, an electromagnet, and a coupling loop. A typical YIG sphere resonator in a MIC configuration is shown in Figure 5.5 [106].

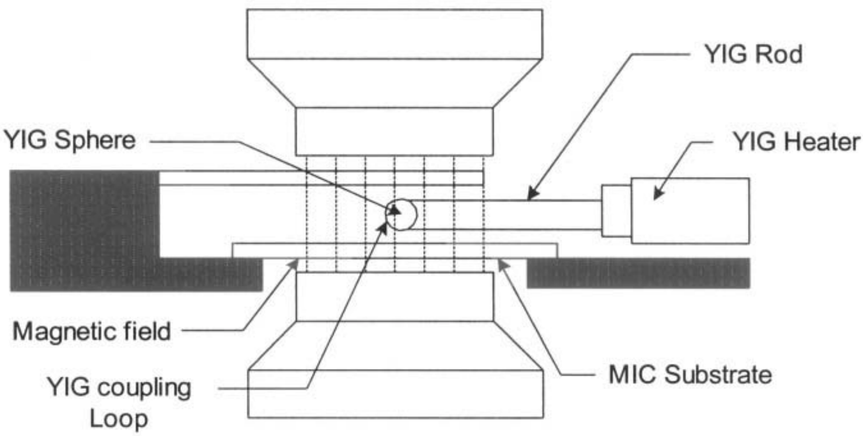

Figure 5.5. Elements of a YIG oscillator.

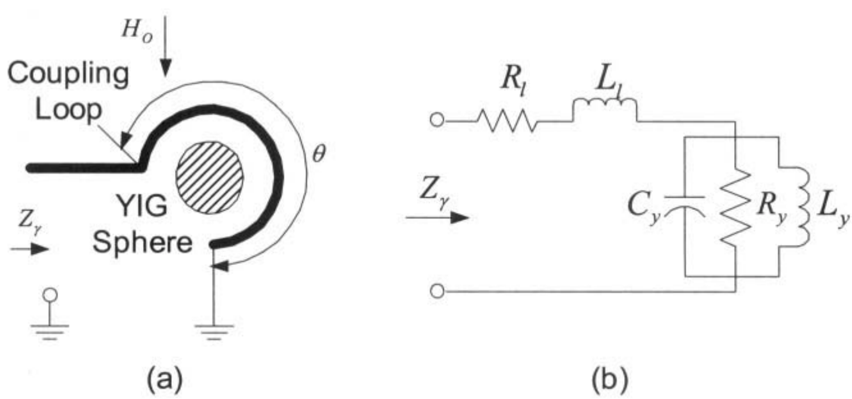

Figure 5.6. Loop Coupling Circuit (a) and equivalent circuit (b).

A sphere is the most widely used geometry for a YIG resonator because it is easily oriented in the magnetic field and easy to prepare with precision, and the resonant frequency is not strongly dependent on its orientation. The upper frequency and lower frequency limit of YIG are set by the available magnetic field and the value of the saturation magnetization, respectively. The saturation magnetization value can be increased by doping the crystal with gallium, but doping will also increase YIG resonator losses, degrading its Q factor. Coupling of the YIG resonator to the oscillator circuit is usually done by using a wire loop around the YIG resonator as shown in Figure 5.6 (a).

The YIG resonator and the coupling loop can be modeled by an electrical equivalent circuit shown in Figure 5.6 (b). The parallel resonant circuit is induced by the coupling of the YIG resonator. R_l and L_l are the resistance and inductance of the coupling loop. The equivalent circuit parameters related to the YIG resonator and coupling loop are [107]

$$L_y = \frac{R_y}{Q_u \cdot \omega_o} \tag{5.9}$$

$$C_y = \frac{1}{L_y \omega_o^2} = \frac{Q_u}{R_y \omega_o} \tag{5.10}$$

$$R_y = \mu_o \frac{V_y}{d_l^2} Q_u (2\pi\gamma)(4\pi M_s) \tag{5.11}$$

where Q_u is the unloaded Q of the YIG (> 1,000), the ω_o is the resonant frequency of the YIG, μ_o is the permeability of the free space, V_y is the volume of the YIG sphere, d_l is the diameter of the coupling loop, γ is the charge-to-mass (gyromagnetic) ratio of the electron (2.8 MHz/gauss), and $4\pi M_s$ is the saturation magnetization of the resonator (1750 gauss for pure YIG).

The input impedance of this circuit Z_y is [108]

$$Z_y = R_l + \left(\frac{R_y}{1 + Q_u^2 \left(\frac{\omega}{\omega_o} - \frac{\omega_o}{\omega} \right)^2} \right) + j \left(\omega L_l + \frac{R_y Q_u \left(\frac{\omega}{\omega_o} - \frac{\omega_o}{\omega} \right)}{1 + Q_u^2 \left(\frac{\omega}{\omega_o} - \frac{\omega_o}{\omega} \right)^2} \right) \tag{5.12}$$

The magnetic tuning circuit design is very important in deciding tuning linearity because the magnetic field determines the resonant frequency of the YIG resonator. The magnetic circuit most commonly used is a re-entrant self-shielding magnetic circuit [102].

YIG magnetic tuning dissipates large dc power, typically about 5 W at 12 GHz [102]. The tuning sensitivity of YIG is between 15 and 25 MHz/mA [102], which imply that the noise and ripple of current supply is a very important factor in the FM noise of the YIG-tuned oscillator. There are two other possible complementary types of structure. One is the permanent magnet type, which provides faster switching speed and lower power dissipation. The other is a laminated magnet circuit that has an even faster switching configuration.

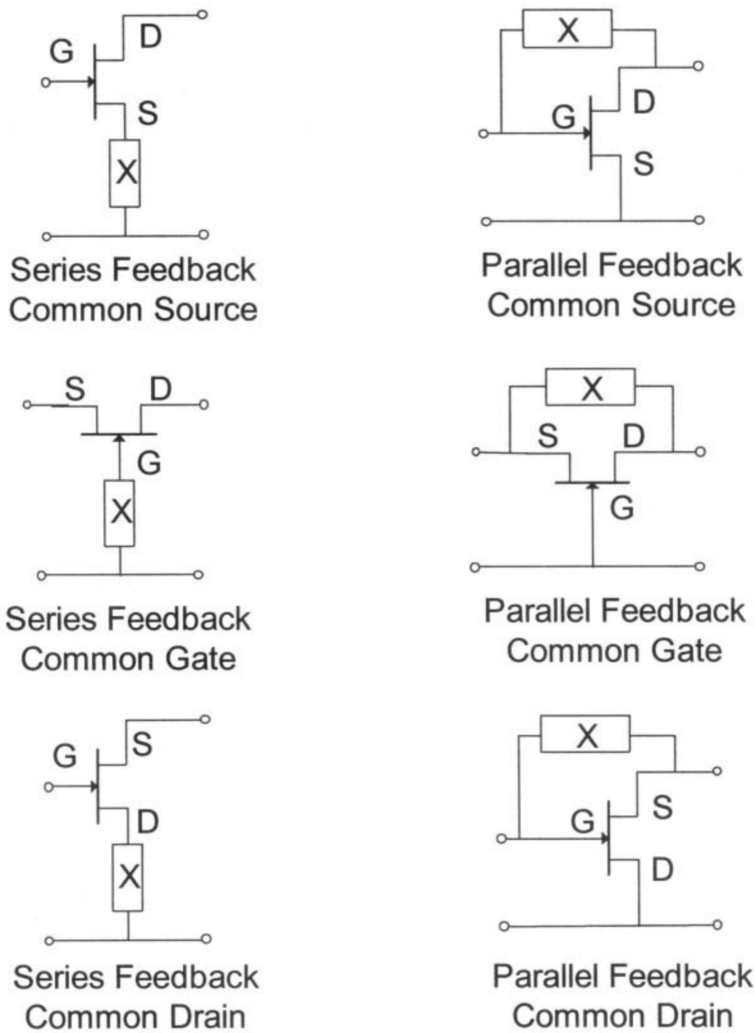

Figure 5.7. Six basic single YIG-tuned oscillator topologies

There are six basic single YIG-tuned oscillator topologies as shown in Figure 5.7, where 'X' represents the feedback element, the left side port is to be coupled to a YIG, and the right side port is to be connected to an output load. Common gate series feedback topology has recently become most widely used for single YIG-tuned Ku-band MESFET oscillators [108-110] for the following reasons [108]: The parallel feedback topologies are more susceptible than series feedback topologies to severe problems because of parasitics at Ku-band, and because they require dc blocks in the feedback area. The common gate topology doesn't require any dc block or RF short in the feedback circuit because the gate is run at 0 V dc, thereby further eliminating parasitics. The common gate structure of YIG-tuned Ku-band GaAs MESFET oscillator is shown in Figure 5.8.

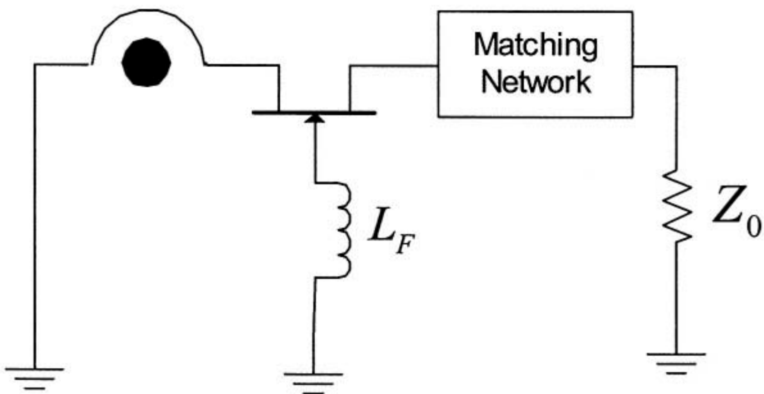

Figure 5.8. Common gate YIG-tuned GaAs MESFET oscillator

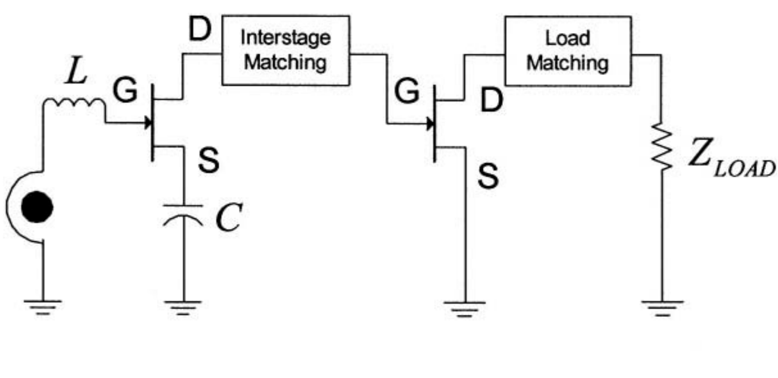

Figure 5.9. Common source YIG-tuned GaAs MESFET oscillator.

There also has been a YIG-tuned Ku-band GaAs MESFET oscillator using other topologies earlier. An 8 ~ 18 GHz FET YIG-tuned oscillator using capacitive source feedback was presented in 1976 [111]. In comparison with the common gate configuration in which a feedback inductance in the gate is used to control the frequency range of negative resistance, the common source configuration uses a feedback capacitance in the source as shown in Figure 5.9 [111]. There have been cases where both the source and the gate ports of a MESFET coupled to a common YIG resonator – as shown in Figure 5.10 [112] – and two YIG resonators – as shown in Figure 5.11 [113] – achieved 3.5 ~ 14 GHz and 2 ~ 20 GHz tuning ranges, respectively. In both cases, the coupling of the gate was used to increase negative resistance bandwidth and the coupling of the source was used for tuning of the oscillation frequency.

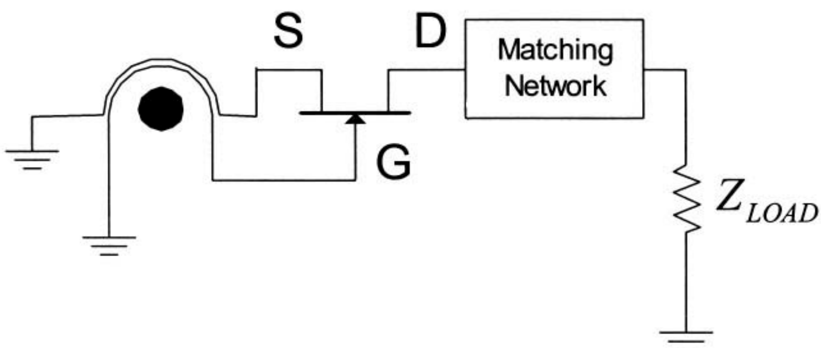

Figure 5.10. GaAs MESFET oscillator with single YIG tuning both gate and source.

GaAs MESFET YIG tuned oscillators are frequently used as a wideband signal source in sweep generators, spectrum analyzers, and electronic warfare applications because of their excellent linear tuning – ±32 MHz [108], low phase noise over wideband – below -90 dBc/Hz at 10 KHz offset, and small frequency drift with temperature – less than 18 MHz over -30 °C to +60 °C [109,110]. However, YIG tuned oscillators require a long time to tune, are bulky, much less efficient, and most importantly can only be realized in MIC form. Therefore, a YIG-tuned oscillator is not a suitable choice for GaAs MMIC Ku-band MESFET VCO designs.

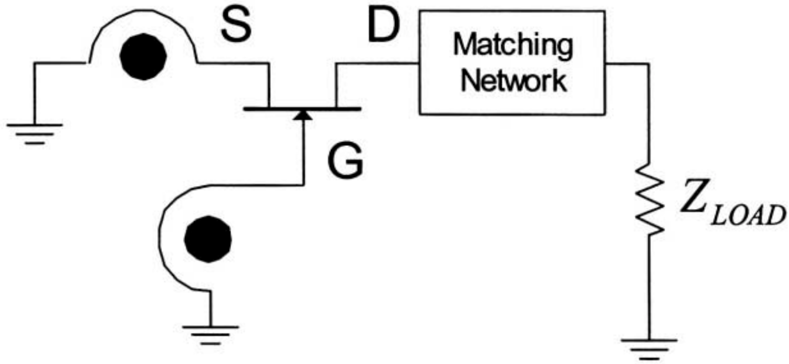

Figure 5.11. Two YIG-tuned GaAs MESFET oscillator

5.4.2 Varactor Tuned Oscillator

Varactors are commonly used for voltage controlled oscillators because of such advantages as faster switching time, small size, and ability to be monolithically integrated in GaAs MESFET technology. The term varactor is a shortened form of variable reactor. A varactor acts like a voltage-controlled capacitor when reverse biased. The applied reverse bias causes the depletion region to extend into a semiconductor active layer, which acts as a capacitor. The capacitance-voltage relationship for the Schottky barrier varactor is given by

$$C_j(V) = \frac{C_{jo}}{\left(1 - \frac{V}{V_b}\right)^{\gamma}} \tag{5.13}$$

where C_{jo} is the zero-bias junction capacitance, V is the applied voltage, V_b is the built-in potential of the diode, and γ is the diode junction parameter called as elastance. The γ is close to 1/2 for abrupt junction varactors, 1/3 for a linearly graded junction wherein the active layer doping increases linearly with distance from the junction, and between 1 and 2 for the hyperabrupt junction varactor in which the doping concentration decreases with distance from the junction. When a varactor is used with an inductor with its inductance L, the resonant frequency varies with voltage with the following relationship,

$$\omega_r = \frac{1}{(L \cdot C_{jo})^{1/2}} \left(1 - \frac{V}{V_b}\right)^{\gamma/2} \tag{5.14}$$

Equation (5.14) shows the nonlinearity between the resonant frequency and the tuning voltage. The nonlinearity can also be caused by the parasitic capacitance and decoupling capacitors in the resonator. A hyperabrupt junction varactor is frequently used to design VCOs because compared to abrupt and linearly graded junction varactors, it offers better linearity between the resonant frequency and the tuning voltage and a wider tuning range of the resonant frequency as shown in (5.14). The abrupt junction GaAs varactor is used when a higher Q varactor is needed because hyperabrupt junction varactors have a lower Q due to the higher series resistance that results from lighter doping of the undepleted part of the active layer. For integration in the GaAs FET-based MMIC, hyperabrupt junction varactors are rarely used because they require a thick epitaxial layer (> 1 μm) and a non-uniformly doped active layer whereas the GaAs FET-based MMIC requires a thin (< 0.05 μm), uniformly doped active layer on semi-insulating substrate [114,115].

There are two types of Schottky varactor diodes, which are the mesa and interdigitated planar Schottky varactor diode (IDSVD) types. The major advantages of a mesa type diode are a very simple equivalent circuit model, high Q factor, and minimal area requirement. An example of a mesa-type varactor diode for GaAs FET-based MMIC is shown in Figure 5.12 [116].

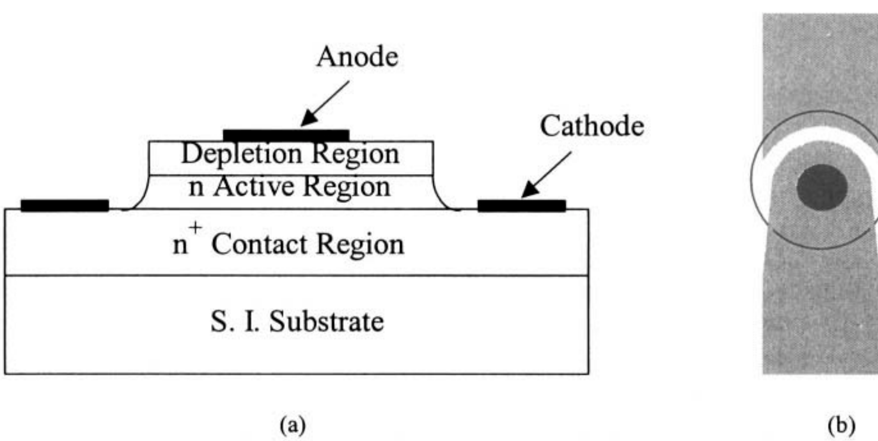

Figure 5.12. GaAs Monolithic mesa type Schottky varactor diode (a) Cross-sectional view (b) Layout

For mesa-type varactors shown in Figure 5.13, the current through the device has to spread laterally around the base of the mesa before flowing out of the cathode. This adds a resistive component, called spreading resistance, which is proportional to the anode area to periphery ratio [116]. The effect of spreading resistance can be reduced by using a finger structure as shown in Figure 5.14 [116].

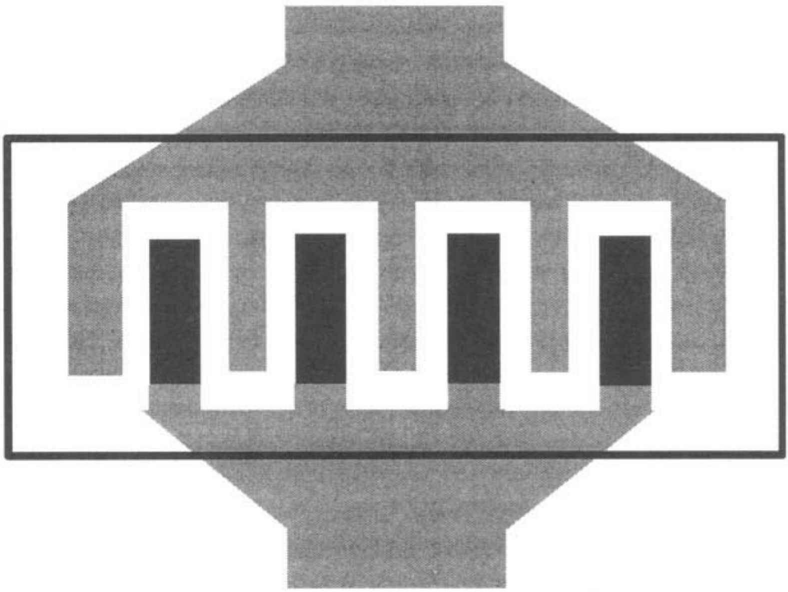

Figure 5.13. Interdigitated layout of mesa-type Schottky varactor diode

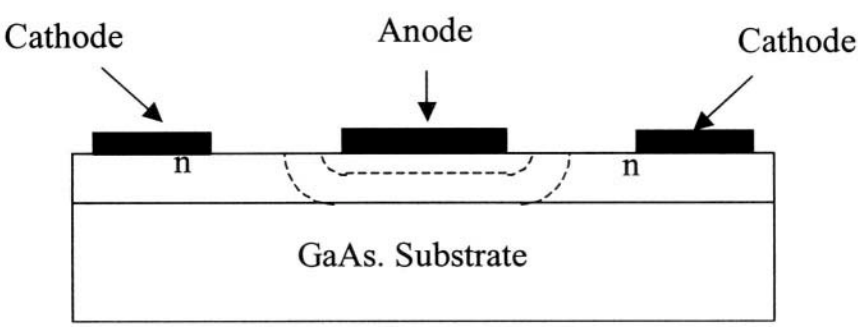

Figure 5.14. cross-sectional view of GaAs monolithic IDSVD type

The IDSVD can be made less expensive using the standard-implant MESFET process because it doesn't require air-bridges or additional layers. An example of IDSVD is shown in Figure 5.14 [114]. The IDSVD can also be realized by connecting the drain and source terminals of a MESFET [115,117,118].

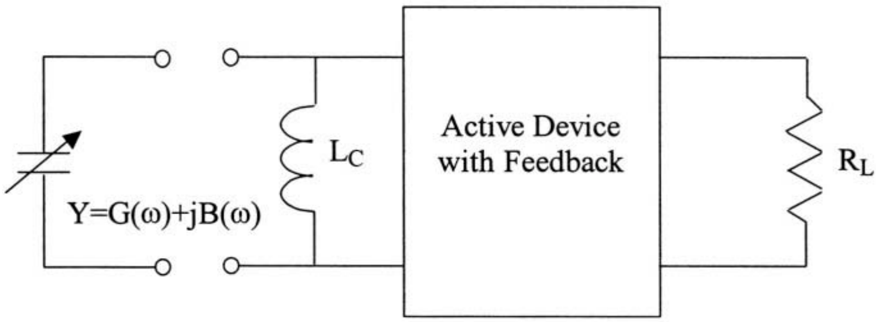

(a) General representation of transistor VCO

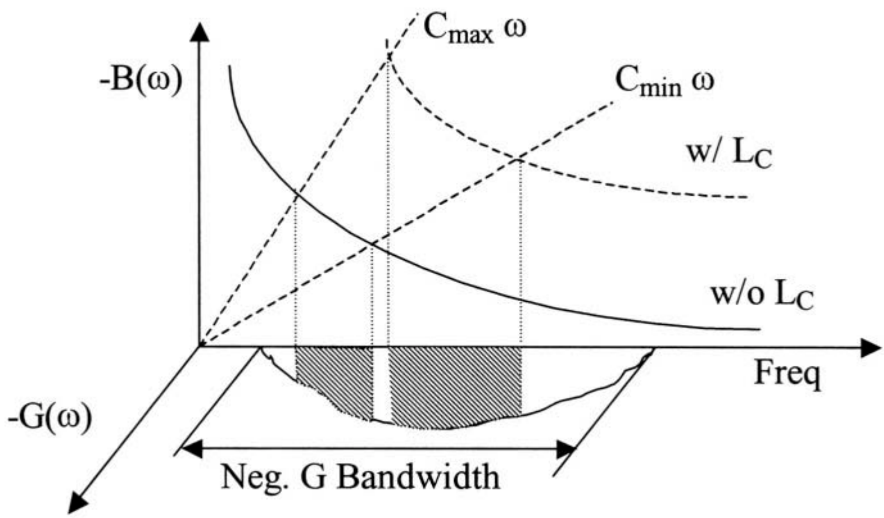

(b) Frequency limits of a varactor-tuned oscillator

Figure 5.15. Varactor-tuned oscillator

The tuning bandwidth of the varactor diode is limited by the susceptance ratio $C_{min}W_{max}/C_{max}W_{min}$ [102,104]. As can be seen from Figure 5.15, the frequency tuning bandwidth of a varactor controlled oscillator is limited at W_{min} and W_{max} at which

$$C_{\min} \cdot \omega_{\max} = -B(\omega_{\max}) \tag{5.15}$$

$$C_{\max} \cdot \omega_{\min} = -B(\omega_{\min}) \tag{5.16}$$

By dividng (5.14) by (5.15), it can be seen that for a given total capacitance ratio ($TCR = C_{max}/C_{min}$), tunable frequency range can increase if $B(\omega_{max})/B(\omega_{min})$ increases. The tuning bandwidth can also be increased by optimizing the value of L_c as shown in Figure 5.15.

GaAs Schottky barrier varactors generally have higher Q than the Si varactors because GaAs has higher electron mobility, which results in a lower resistivity than Si with the same doping level. However, the higher thermal resistance of GaAs devices causes longer frequency settling time because conduction occurs almost entirely as a result of thermal emission of electrons in the Schottky barrier diode.

A varactor controlled oscillator composed of a GaAs MESFET, a varactor diode, and an output port leading to the load is realizable in six basic topologies as shown in Figure 5.16 [119].

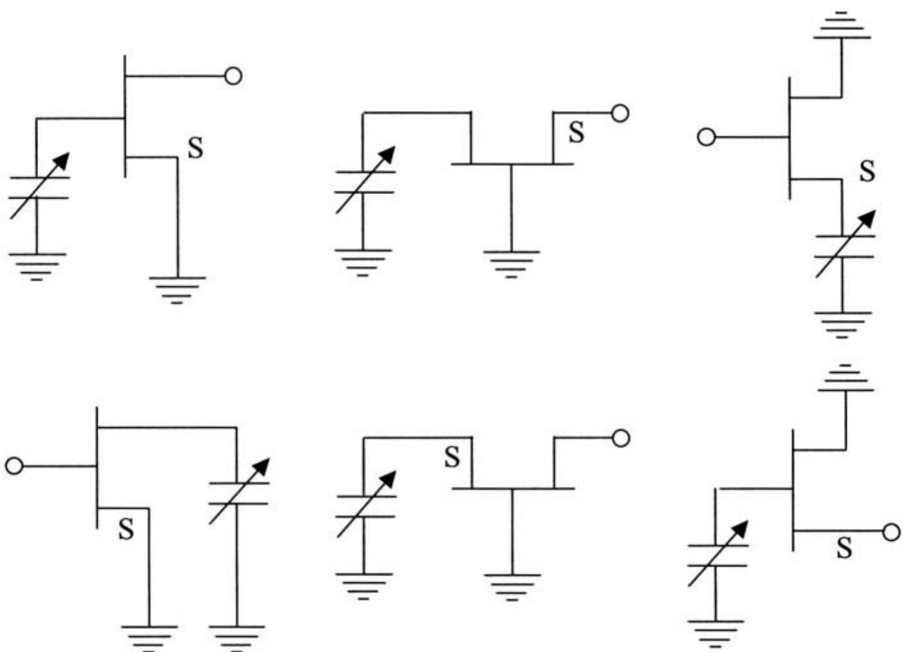

Figure 5.16. Six basic single varactor-tuned oscillator

The source-follower common-drain topology with a varactor diode at the gate is most widely used for GaAs MMIC Ku-band single varactor controlled oscillator designs because it offers a wide tuning range with small variable reactance change, a low pulling figure, and has intrinsic tendencies to instability with appropriate embedding elements because of the large value of internal feedback capacitance [115,119-121].

Multiple varactors are used for many GaAs MMIC Ku-band VCO designs [122,123]. The use of multiple varactors helps in increasing the frequency tuning range and in reducing the effects of constant capacitances because of the FET parasitics.

Varactor tuned oscillators present great advantages such as faster switching time, small size, and ability to be monolithically integrated in GaAs MESFET technology. The widest frequency tuning range reported for GaAs MMIC Ku-band VCO is 3 GHz [119] using a single varactor diode and entire Ku-band [124] using two varactor diodes. The spectral purity, the phase noise of GaAs MMIC Ku-band varactor controlled oscillators (< -95 dBc/Hz at 1 MHz offset [124]), and frequency stability (~ 200 ppm/°C -55 to 90 °C [124,125]) are generally not good enough for applications at Ku-band due to very low Q monolithic circuitry. However, if used with a phase locked loop (PLL) [118,119,121,126], a much better spectral purity and a phase noise of less than -80 dBc/Hz or less for 100 Hz ~10 MHz offset at 15 GHz can be obtained [121].

Tuning sensitivity describes the tuning frequency range as a function of the tuning voltage at the varactor input. The tuning sensitivity depends on the available capacity variation and is inversely proportional to the loaded Q of the resonator circuit.

5.4.3 Tunable Active Inductor Controlled Oscillator

An active inductor is an inductive transistor circuit. Using proper topologies, active inductors can be designed to have very stable, high-Q performance with large tunability and compact layout. This high-Q provides improved overall performance, including lower phase noise and more stable output frequency for VCOs [127]. The basic concepts for the design of active microwave inductor date back to the late 60's and early 70's [128-130]. However, the single inverted common collector topology didn't include independent electronic tuning of both the inductance and series resistance. More recently, an active inductor using a common source cascode FET with a feedback resistor as shown in Figure 5.17 has been reported [131].

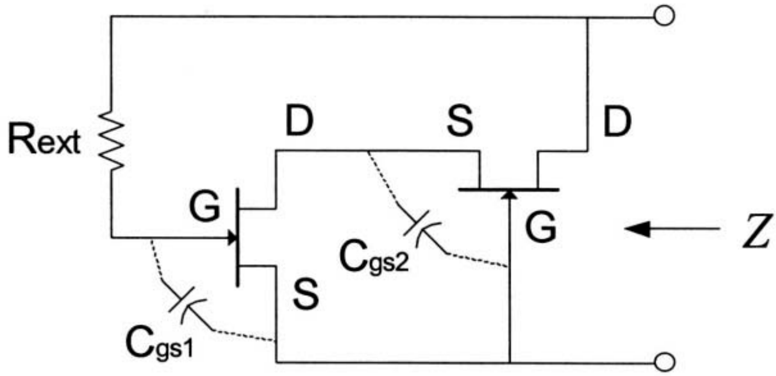

Figure 5.17. Active inductor using a common source cascode FET with a feedback resistor

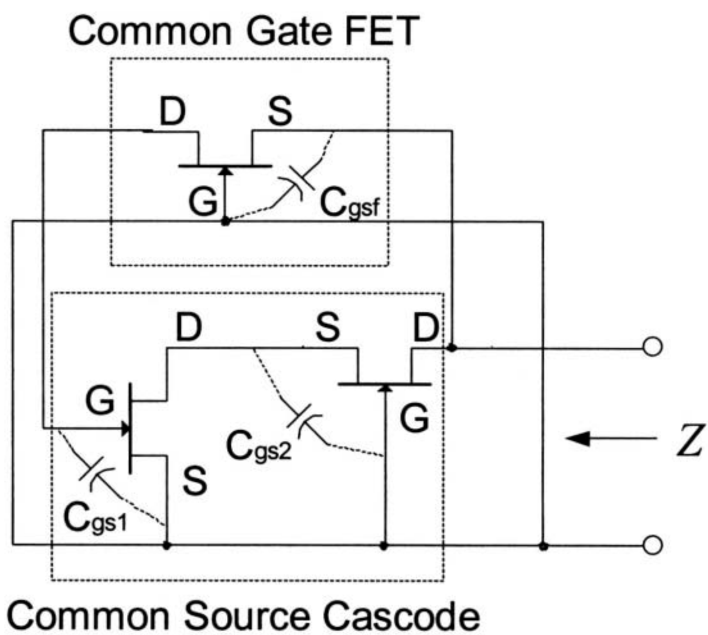

Figure 5.18. Active inductor using a common-source cascode FET with common-gate FET feedback

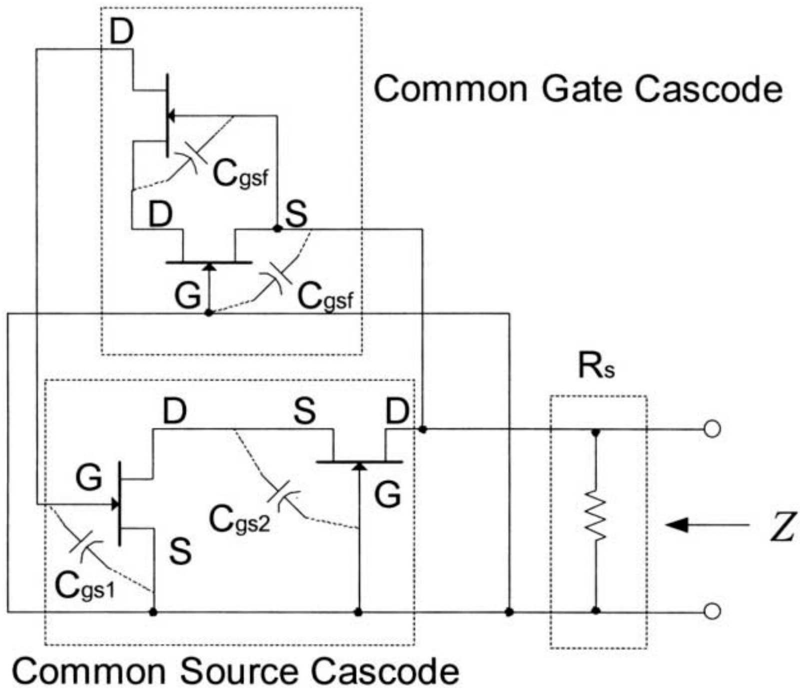

Figure 5.19. Active inductor using a common-source cascode FET with common-gate cascode FET feedback

This active inductor obtained inductances of 3.0 ± 0.4 nH at frequencies ranging up to 7.6 GHz. Later, a significant reduction in the series resistance of the active inductance was accomplished by use of a common-gate FET feedback as shown in Figure 5.18 and a common-gate cascode FET feedback as shown in Figure 5.19 [132]. Later topology showed it to have better Q of 65 at 8 GHz.

The idea of using a floating cold-FET as a varistor for inductance tuning of the lossy active inductor has been demonstrated with simple common-source cascode-FET with varistor feedback [133]. The Q-enhanced version of the active inductor is proposed by Alinikula *et al.* and shown in Figure 5.20 [134].

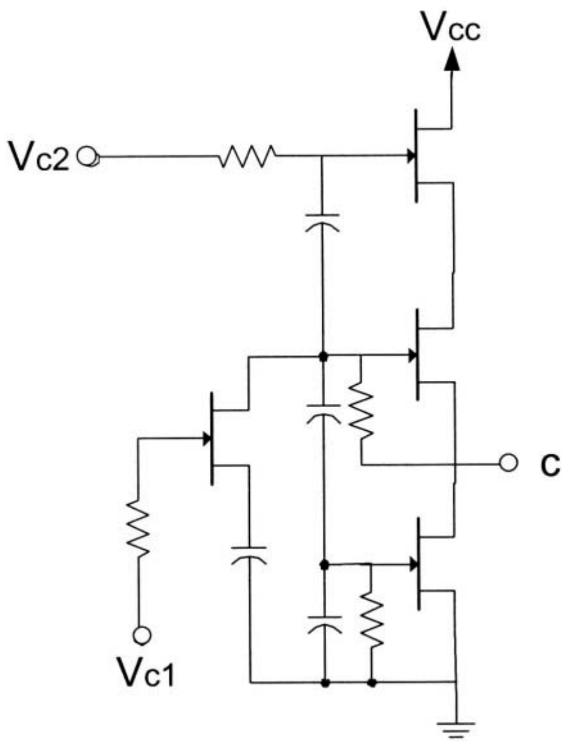

Figure 5.20. A Q-enhanced version of the active inductor

The feedback controlling resistance was achieved with a "cold" MESFET so that the Q-enhancement tuning is introduced for the circuit. The active resonator, which consists of Q-enhanced active inductor and metal-insulator-metal (MIM) capacitor, was designed and its simulated results show a frequency tuning range of a 500MHz (2.2 ~ 2.7 GHz) with a Q greater than 50 and a maximum Q of about 5,000; this is an impossible performance with a passive resonator that includes a varactor and a spiral inductor [134]. A TAI has recently been presented that allows both the inductance and series resistance to be varied across wide ranges [135]. The topology of this TAI is shown in Figure 5.21.

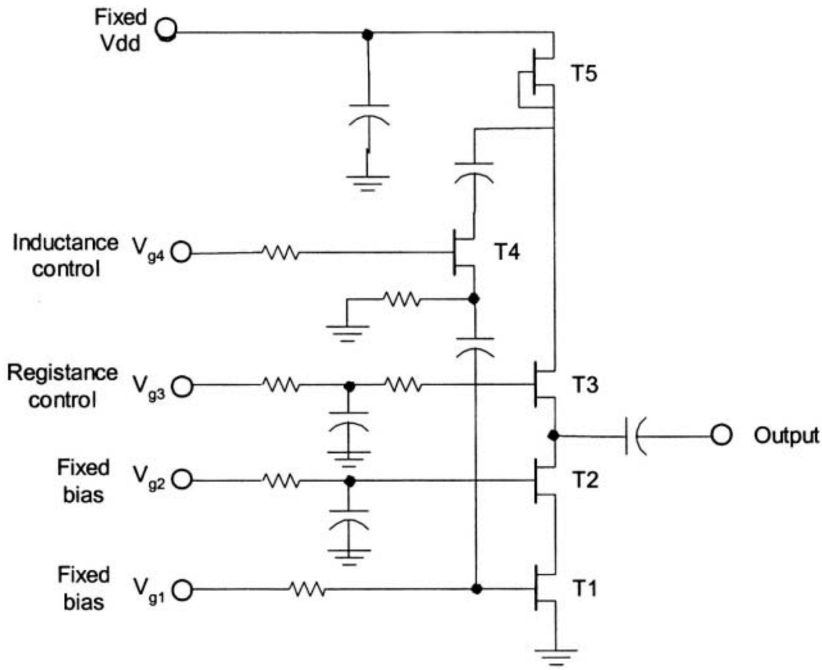

Figure 5.21. A tunable active inductor with variable inductance and series resistance.

The common-source cascode-FET arrangement has been used and is implemented with T_1 and T_2. The gate bias of T_3 effectively controls the level of series resistance. A cold-FET, T_4, is employed as a variable feedback resistor to control the value of inductance. The resistive load is implemented with an active load, T_5, instead of spiral load inductor to minimize the chip size. Large coupling capacitors are used for dc blocking purposes. Using this topology, TAI demonstrated measured performance of maximum Q-factor of more than 15,000 and inductance tuning range of 3.9 to 11.6 nH at 2 GHz.

Previously described approaches consumed too much power and required many bias pins. To minimize those problems, a low power TAI (LPTAI) design has been proposed in [136]. The schematic of this TAI is shown in Figure 5.22. The principle of this TAI is almost the same as one for an active gyrator [137]. This gyrator is realized by connecting an inverting amplifier to a non-inverting one in parallel and back-to-back. The common-gate cascode amplifier was used as the non-inverting amplifier because the commonly used common-gate amplifier has output impedance that is parallel connected C||R due to g_{ds}. To reduce the dc voltage drop, a common source amplifier is used as the inverting amplifier instead of a common source cascode one. R_{FB} and R_G are used to control the inductance and series loss. The series choke resistors (R_{SB}) towards parallel resistor chain (R_{1-5}) were used to reduce the number of bias pins. Power consumption was about one third of a conventional one with a wider range of tunability and a higher Q-factor[137].

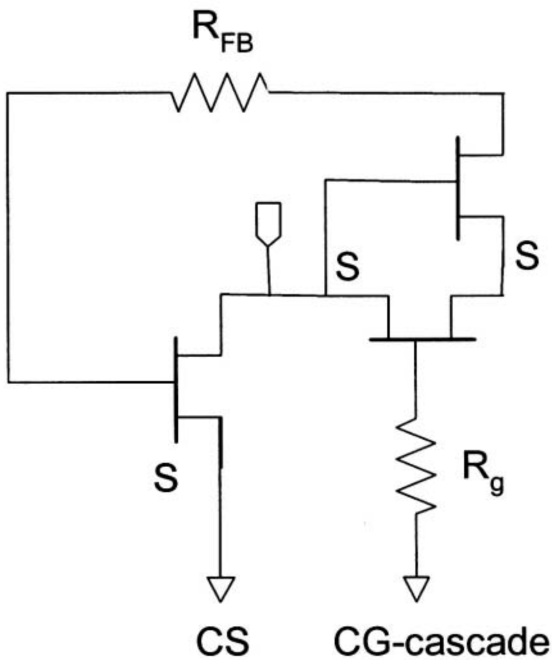

Figure 5.22. A low-power tunable active inductor

Because most of above topologies require stacking four or five FETs of the same size, low-voltage operation is difficult. The new TAI using a compact lossy active inductor composed of a common-source FET and a feedback resister in the feedback loop of a common-source cascode FET was presented in [138]. A newly proposed topology of active inductor is shown in Figure 5.23. Instead of using a resistor for R_f and a spiral inductor for L_f, a common-source FET with a resistive feedback that can be designed to be a lossy active inductor as shown in Figure 5.24 is used in the feedback loop. For simplified analysis, FET is assumed to be composed of transconductance

g_m, gate-source capacitance C_{gs}, and gate-drain capacitance C_{gd}. The proposed TAI's inductance and series resistance is [138]

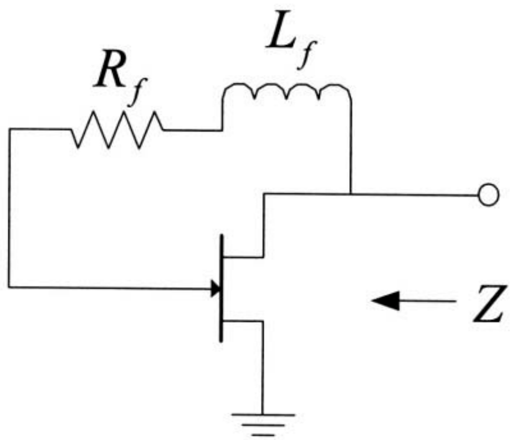

Figure 5.23. Active inductor – common source FET with a resistive and inductive feedback

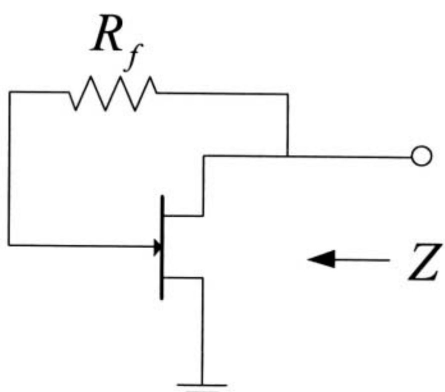

Figure 5.24. Active inductor – common source FET with a resistive feedback

$$R=\frac{\left(1-\omega^2/\omega_{r1}^{\ 2}\right)\left(1-\omega^2/\omega_{r2}^{\ 2}\right)/g_m+\left(\omega^2/\omega_{t2}^{\ 2}+\omega^2/\omega_{t1}\omega_f\right)R_f}{\left(1-\omega^2/\omega_{t2}\omega_f-\omega^2/\omega_{r2}^{\ 2}\right)^2+\left(\omega/\omega_{t2}+\omega/\omega_f-\omega^3/\omega_{r2}^{\ 2}\omega_{t2}\right)^2} \tag{5.17}$$

$$L=\frac{R_f}{\omega_{t2}}\frac{1-\omega^2/\omega_{t1}\omega_f-\left(1-\omega^2/\omega_{r1}^{\ 2}\right)\left(1-\omega^2/\omega_{r2}^{\ 2}\right)/g_mR_f}{\left(1-\omega^2/\omega_{t2}\omega_f-\omega^2/\omega_{r2}^{\ 2}\right)^2+\left(\omega/\omega_{t2}+\omega/\omega_f-\omega^3/\omega_{r2}^{\ 2}\omega_{t2}\right)^2} \tag{5.18}$$

where

$$\omega_{r1}=1/\sqrt{L_f\left(C_{gs}+C_{gd}\right)},\omega_{r2}=1/\sqrt{L_fC_{gd}},\omega_{t1}=g_m/\left(C_{gs}+C_{gd}\right),$$
$$\omega_{t2}=g_m/C_{gs},\omega_f=1/\left(R_fC_{gd}\right)$$

The full circuit diagram of the proposed TAI is shown in Figure 5.25 [138]. Capacitors C_a, C_b, and C_c are external gate-source capacitors for operating frequency tuning, and other capacitors are used for dc blocking. Instead of the common-source FET used in analysis, a common-source cascode FET (Q_3 and Q_4) was used. A cold FET was used instead of R_f for tuning purposes. The fabricated active inductor achieved more than 100 Q-factors with maximum value of 3,400 over the frequency bandwidth of 200 MHz, in the vicinity of 1.7 GHz. Tunable inductance range was 9.6 ~ 56 nH at 1.7 GHz.

A TAI controlled oscillator promises great advantages such as a high Q factor, wide runability, and the ability to be monolithically integrated in GaAs MESFET technology. However, a TAI consumes more dc power and requires more power supplies than varactors. Most GaAs MESFET TAI controlled oscillators have been designed around 2 GHz with a tuning range of about 35 % [134,136,137]. The best phase noise reported is -100 dBc/Hz at 1 MHz offset. The phase noise performance is relatively poor because of the bias drift [136] and noise generated by each FET, but because of high-Q better phase noise is expected with better optimized design [127]. No work has been done on TAI at Ku-band.

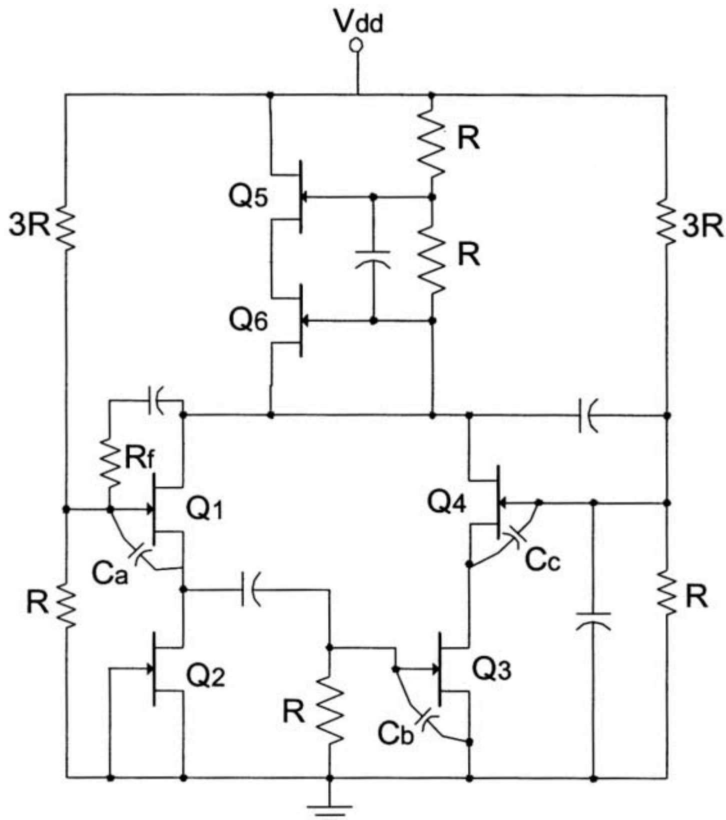

Figure 5.25. Active inductor – common source FET with a losy active inductor feedback

5.5 Ku-band GaAs MESFET VCO

Most transistor oscillators consist of a positive-feedback amplifier that has a resonator as an input termination. Selecting the oscillator circuit topology primarily involves selecting the type of amplifier; in turn the choice of amplifier depends heavily on the application of the oscillator.

There are two types of oscillators: relaxation and sinusoidal. Since applications for GaAs MMIC Ku-band MESFET VCO require low-noise pure sinusoid signals, only a sinusoidal oscillator will be discussed in this section.

For MESFET oscillators, the most widely used topology is common-gate, since a common-lead inductance increases the magnitude of the input- and output-reflection coefficient to a value well above unity. If these reflection coefficients are high, there will be a higher degree of freedom in selecting the load impedance and well-behaved operation will be easily obtained.

The analysis and design of wideband tunable oscillators are more complex than with fixed-frequency oscillators. The active elements of VCOs must be able to generate a negative resistance or a reflection coefficient greater than unity over the desired tuning range with suitable feedback. In order to obtain maximum negative resistance, the impedances connected to the terminals other than output should be low-loss reactive circuits. To realize a VCO, one of these reactances should be able to tune with voltage. In most cases, output loads are connected to the MESFET drain, and frequency tuning elements are placed in either or both of the other two terminals.

Various kinds of resonators can be used for oscillator design. For fixed frequency oscillators, the most widely used resonators are inductor-capacitor (LC) tuned circuits, cavity resonators, dielectric resonators (DR), and super conductive resonators. The LC tuned circuits have poor noise performance because of their low Q. The cavity resonator is bulky but has higher Q than the DR. The DR is smaller and lighter than the cavity resonator and has substantially high Q. The high temperature superconductors (HTS) usually operate at 77 °K and have very high Q even at microwave frequencies. For broadband tunable oscillator applications, LC-tuned circuits, cavity resonatosr, DRs, and HTS can't be used because they lack frequency tuning ability. YIG resonators, varactor diodes, and TAIs are suitable for VCO. YIG resonators have a very high Q of several thousands and a wide tuning range of several octaves [102] but also have slow tuning speed and high power dissipation. The varactor diode oscillator switched faster but has poor phase noise performance because of the low Q of the varactor diode. The TAI shows stable, high Q performance with large tunability and compact layout. However, their dc power consumption is high and the circuit requires many bias pins.

In designing the resonator and its tuning circuit, there is a direct trade-off between tuning range and frequency stability; more generally, the trade-off is between tuning range and phase noise. The contribution to phase noise and frequency stability from the resonator for a certain topology is dominated by the sensitivity of its impedance with respect to tuning voltage and the strength of coupling the tuning elements to the circuit. Since this sensitivity and strength of coupling determines the tuning range of VCO, an improvement in tuning range will result in degradation of phase noise and frequency stability because of the increased effects of its poor thermal stability and possible reduction of the resonator Q.

5.6 Ku-band AlGaAs/GaAs HBT VCO

The HBT offers the prospect of obtaining performance features similar to those of Si BJT translated to substantially higher frequencies. AlGaAs/GaAs HBT is a very attractive device for VCO designs for the following reasons. First, the vertical structure of the HBT eliminates the surface-state problems associated with GaAs MESFETs, resulting in superior phase noise characteristics (1/f corner frequency < 1 MHz) [139]. In other words, the main conduction path of HBT is through bulk material while that of FETs is along abrupt heterointerfaces and exposed surfaces where traps are abundant [140]. Second, this device can generate a wideband negative resistance because of its high conductance [139]. Lastly, its high breakdown voltage and current handling capability can lead to high output power in VCOs [141]. However, the AlGaAs/GaAs HBT process is more expensive than the GaAs MESFET process. Another drawback is that it is very difficult to construct both a varactor with a wide tuning range and a high f_t and f_{max} HBT on the same wafer using the same fabrication technology [142].

The first AlGaAs/GaAs HBT Ku-band oscillator whose phase noise was -60 dBc/Hz at 10 KHz offset, which is comparable to that of Si BJT oscillator and 20 dB less than that of a GaAs MESFET oscillator at the same frequency band [143], was reported in 1988. Improvement in the phase noise performance of Ku-band hybrid fundamental frequency AlGaAs/GaAs HBT oscillators was obtained to -65 dBc/Hz at 10 KHz offset [144,145].

The first monolithic Ku-band VCO using AlGaAs/GaAs HBT was reported in 1989 [141]. This VCO used integrated a p-n junction diode as the varactor for the frequency tuning element. Varactor diodes were fabricated by removing the emitter layer of the HBT structure and using the base-collector p-n junction diode in reverse bias. The SSB phase noise of this free running VCO was -55 dBc/Hz and -75 dBc/Hz at 10 KHz and 100 KHz offset, respectively, and a continuous tuning bandwidth of 2.3 GHz centered at 11.85 GHz with minimum power of 18 dBm. The better phase noise of -85 dBc/Hz at 100 KHz offset with 600 MHz tuning bandwidth was achieved in [142]. To obtain larger bandwidth, two external silicon varactors were used for a 7 ~ 15 GHz frequency tuning range with phase noise of -75 dBc/Hz at 100 KHz offset. A tunable active inductor has also been used for AlGaAs/GaAs HBT VCO designs for bandwidth of 1.19 GHz centered at 4.085 GHz with phase noise of -70 dBc/Hz at 100 KHz offset.

5.7 Conclusions

GaAs MESFET Ku-band VCO using three different types of frequency tuning scheme has been reviewed. GaAs MESFET YIG tuned oscillators offer excellent linear tuning, low phase noise over wideband, and small frequency drift with temperature. However, they require a long time to tune, are bulky, much less efficient, and most important can only be realized in MIC form. TAI controlled oscillators promise great advantages such as high Q factor, wide tunability, and ability to be monolithically integrated in GaAs MESFET technology. However, TAI has higher dc power consumption, requires more power supplies than varactors, and has a noise contribution from each FET on overall phase noise. Varactor tuned oscillators present great advantages such as faster switching time, small size, and the ability to be monolithically integrated in GaAs MESFET technology, but spectral purity, phase noise, and frequency stability of GaAs MMIC Ku-band varactor controlled oscillators are generally not good enough for applications at Ku-band due to very low Q monolithic circuitry. However, PLL can be used to improve the performance of such oscillators to the point that they can be used in Ku-band satellite communication applications. Therefore, varactor tuned oscillator is the most suitable approach for GaAs MMIC Ku-band MESFET VCO designs, but an improved tunable active inductor scheme at Ku-band might be an alternative approach.

Fully monolithic Ku-band VCO design employing AlGaAs/GaAs also has been discussed. AlGaAs/GaAs HBT has advantages over GaAs MESFET such as lower phase noise, ability to generate a wideband negative resistance, and a capability to generate higher output power. However, the AlGaAs/GaAs HBT process is more expensive and it is very difficult to construct both a varactor with a wide tuning range and a high f_t and f_{max} HBT on the same wafer using the same fabrication technology. Therefore, the choice of technology is largely matter of cost and the system requirements of the specific applications.

This page intentionally left blank

Chapter 6

Transmitter MMIC for Satellite Communication Applications

6.1 Introduction

The growing satellite communications markets have encouraged the use of MMICs in low noise block (LNB) units to reduce assembly time, component count, and cost with better performance. By integrating all the components into a single MMIC chip set, smaller and more cost-effective products can be achieved with higher performance. Also, integration into an MMIC chip set will eliminate interconnection losses and enable each component to be optimized for overall performance. GaAs MESFET processes are selected for Ku-band transmitter IC design because of its process maturity and relatively low cost devices. Even though its f_t is not high enough for Ku-band applications, it performs well with power amplifier and mixers with high linearity performance. In addition, a low phase noise VCO, that is comparable to that of GaAs HBT VCO, was implemented using reflection coefficient line analysis. GaAs MMIC up-converter block and the gain block are fabricated using the commercial 0.6-μm GaAs MESFET process. The gate-to-drain breakdown voltage is a 12 V minimum with a nominal value of 15 V. The active devices have f_t values of 20 GHz. This process can fabricate thick 3 layer interconnect metal, MIM capacitors, spiral inductors, and NiCr resistors.

6.2 Transmitter MMIC Design Criteria

In the design of the transmitter module, the main concern is to meet transmit power level and linearity, as well as to filter unwanted spurious signals. As shown in Figure 6.1, a LO buffer amplifier, a RF amplifier, a low phase noise VCO, and a dual-gate up mixer are integrated in a single chip. There are many benefits in integrating multiple RF functional blocks into a single IC. In other words, the size is reduced significantly over hybrid circuits and interconnection losses are minimized, enabling each component to be optimized for overall performance. A driver amplifier and a power amplifier are implemented in a different set of chips to apply the filtering network between the up-converter MMIC and to avoid the thermal effect on the up-converter MMIC. LO buffer and RF amplifier use the same topology since they require the same linearity performance in different frequency.

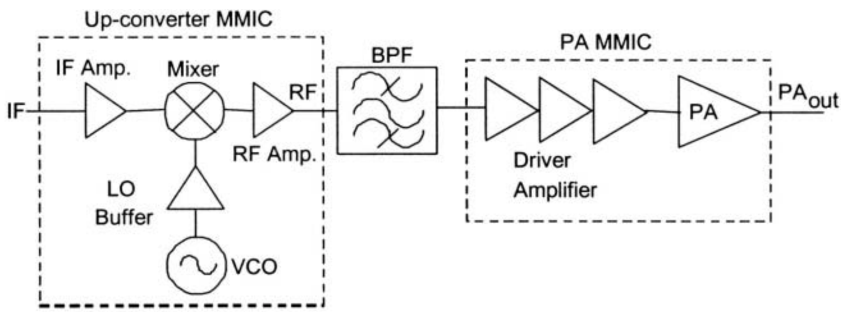

Figure 6.1. Block diagram of the monolithic Ku-band up-converter.

In the frequency up-converter, the low frequency input signal is fed into the IF port of the mixer. After mixing with the high frequency LO signal, the up-converted high frequency signal emerges from the RF port. For the Ku-band up-converter, the two input frequencies are very different. The IF signal is fixed in the L-band while the LO signal is in the Ku-band; they cannot be optimized simultaneously in both frequency bands. In the up-converter, the LO frequency is normally close to the output signal band so it is not easily rejected by the filtering network in the amplifier stage, while in a downconverter, the LO frequency is normally far away from the output signal band; therefore, it can be easily filtered. The primary design criteria for the up-converter are high IP3 and good spurious-response rejection. These are achieved through the use of the dual-gate FET mixer and high LO power provided by on-chip LO buffer amplifier. The LO buffer amplifier needs to provide a good match at the LO port. This helps to reduce conversion gain variations resulting from mismatches and also reduces the

LO input power requirement. Similarly, the RF amplifier at the output port of mixer amplifies the up-converted signal and provides a good output matching with the following BPF network. The up-converter MMIC was implemented with a dual-gate mixer in an unbalanced configuration operating over the 14 GHz to 14.5 GHz band. An output LTCC BPF provides spurious and LO suppression at the output port. The PA MMIC consists in multi-stage driver amplifier to have enough gain to drive the PA, and one stage power amplifier in Class A operation in order to have high linearity. An output power of more than 24 dBm will be achieved from the transmitter module over a 500 MHz RF bandwidth with an IF input power level of -15 dBm and a LO level of 15 dBm at 13 GHz.

6.3 Dual Gate Mixer

6.3.1 Mixer MMIC Design

A FET mixer topology was chosen because it offers lower noise and intermodulation products [42], as well as requiring less LO power than a diode mixer. The up-conversion mixer uses a dual-gate topology providing simplicity, lower distortion, and good LO-IF isolation because of the low capacitance between the gates. Another advantage of the dual-gate mixer is efficiency. Having conversion gain rather than loss eliminates the need for additional gain stages to compensate for the loss. Required LO power and overall dc power consumption are considerably lower than those of an amplifier. One disadvantage of the dual-gate mixer is the difficulty of achieving isolation of LO signal at the RF port. In this transmitter chain, isolation has been achieved through the use of a BPF at the RF port after the mixer. The dual-gate transistor is modeled as two single-gate transistors in series. The dual-gate device is biased so that the first FET of the cascode chain is biased in the linear region, while the second is biased in the saturated region. The IF signal drives the gate of the first FET, while the LO signal drives the second gate. The LO signal is generated by an integrated local oscillator and buffer amplifier to maintain stability from spurious oscillations over the required frequency band. A single-ended mixer cannot distinguish the image from the signal. The image suppression has been achieved with a BPF placed between RF amplifier and driver amplifier. The circuits were designed using large-signal simulation on a commercial microwave system/circuit design CAD tool. The harmonic balance (HB) technique has been employed to simulate the entire up-converter MMIC.

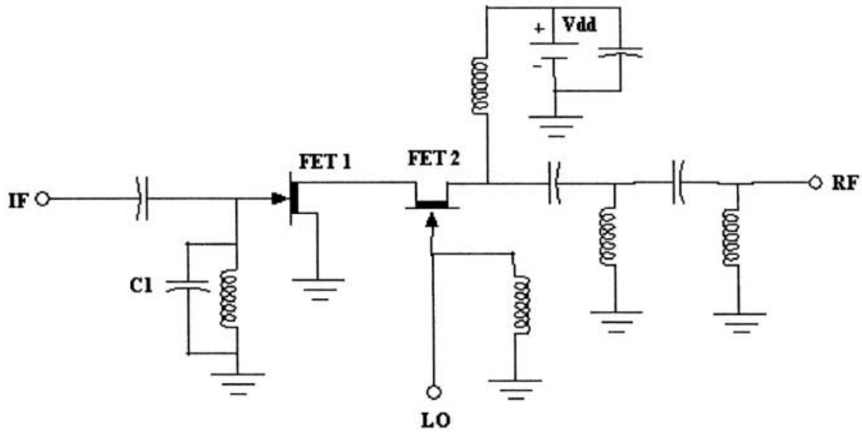

Figure 6.2. Schematic diagram of the dual-gate mixer.

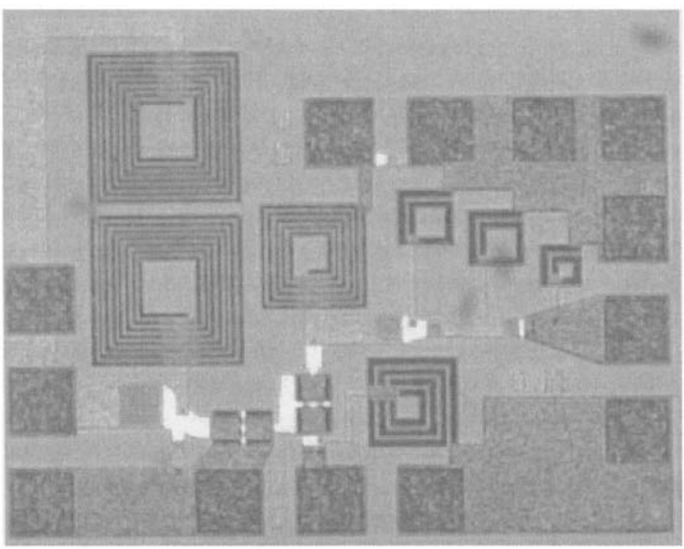

Figure 6.3. Photograph of the fabricated dual gate mixer.

A schematic of a dual-gate FET mixer is shown in Figure 6.2. Since the IF signal is applied to the gate of FET 1 and the LO signal is applied to the gate of FET 2, the mixing occurs by varying the transconductance between V_{gs} and I_d [146]. The bypass capacitor, C_1, is used to improve LO-IF isolation. For simplicity of the biasing circuitry, a single-bias supply scheme is used without the gate bias, and the mixed RF signal is generated at the drain of FET 2 with a drain bias of 4 Volts. Because of their compact design, spiral inductors and MIM capacitors are used for the IF, LO, and RF matching circuits instead of transmission lines.

The entire occupies 32×29 mil^2 die area, as shown in Figure 6.3. The absence of via holes simplifies the process and augments the MMIC chip yields.

6.3.2 Measured Performance

Measurements were made on-wafer using a coplanar probe station and a spectrum analyzer. The conversion gain and IP3 at the output RF frequency (14 GHz) are 2 dB at a LO power of 15 dBm, as shown in Figure 6.4. The two-tone intermodulation products were measured with two equal amplitude input signals separated by a 10 MHz and a 13 GHz LO signal. The third-order intermodulation product (IM3) level is about -40 dBc, and the IP3 at the output is 15 dBm. The output power at the 1dB gain compression point has been measured to be about 2 dBm at the desired frequency band. Figure 6.5 and Figure 6.6 show the flat conversion gain performance across an IF frequency between 0.7 GHz to 1.5 GHz and LO frequency between 12 GHz to 15 GHz, respectively.

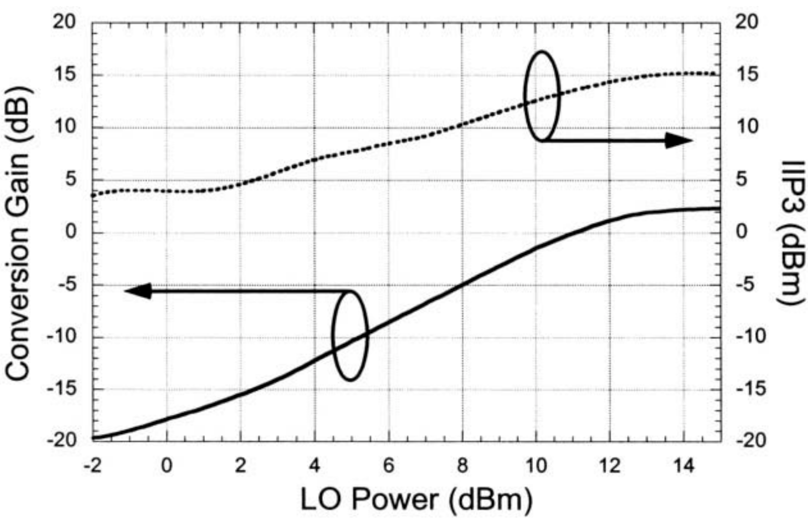

Figure 6.4. Measured conversion gain and IIP3 performance versus LO power.

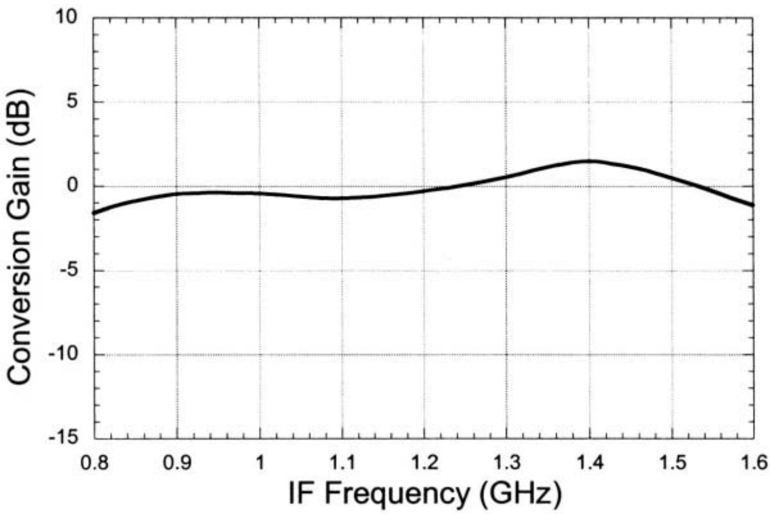

Figure 6.5. Measured conversion gain performance versus IF frequency with LO power of 15 dBm.

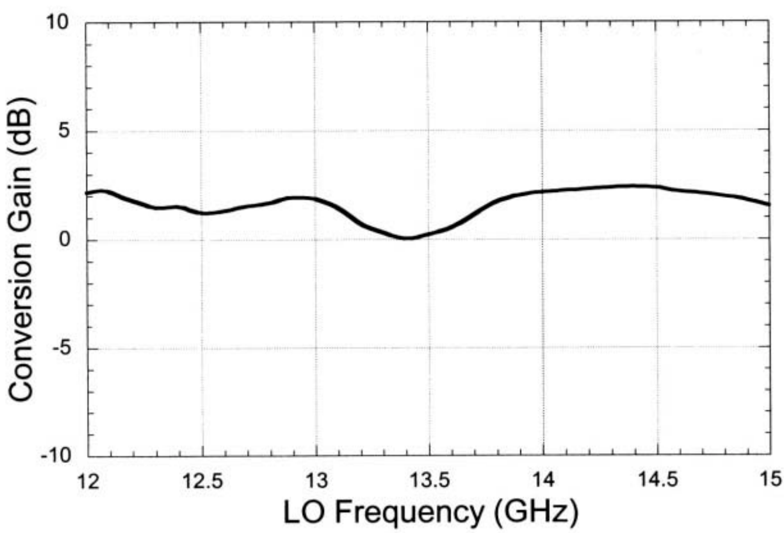

Figure 6.6. Measured conversion gain performance versus LO frequency with LO power of 15 dBm.

Figure 6.7 shows the LO to IF isolation performance by varying the LO frequency. The LO to IF isolation of better than 30 dB over the entire band was obtained. Figure 6.8 shows a LO to RF isolation of 10 dB at a LO frequency of 13 GHz. To reject the LO feed-through signal at the output, the BPF will be inserted between the RF amplifier and driver amplifier. Figure 6.9 shows the RF-IF isolation performance with a varying IF frequency. Because of the high pass network at the mixer output, isolation of better than 30 dB can be achieved. Table 6.1 summarizes the measured performance of dual-gate mixer.

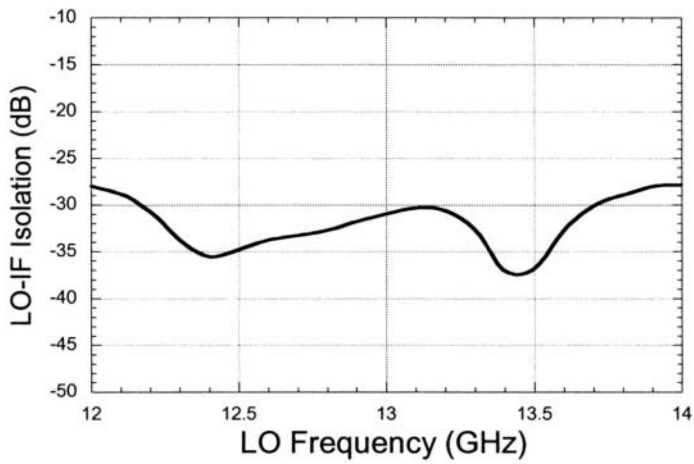

Figure 6.7. Measured LO-IF isolation versus LO frequency.

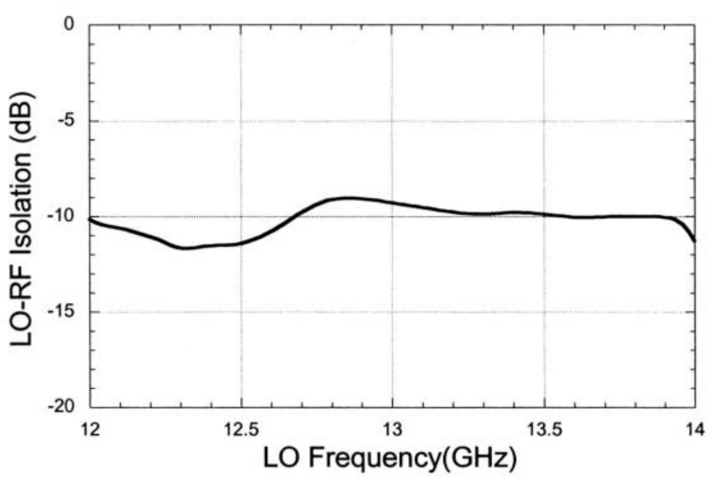

(a)

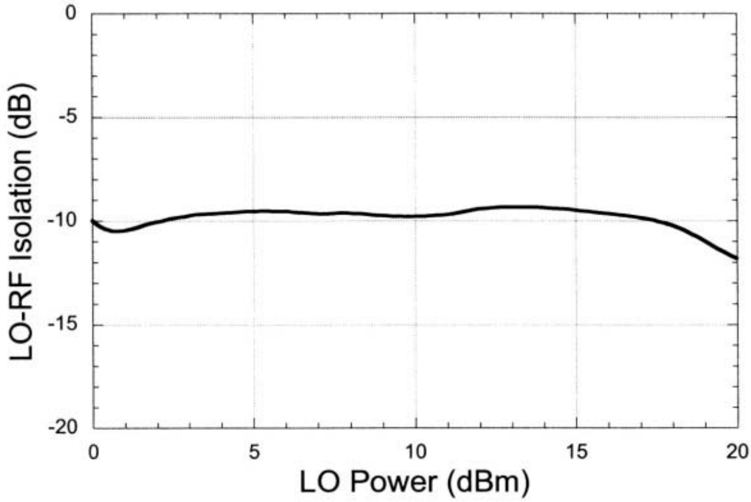

(b)

Figure 6.8. Measured LO-RF isolation versus (a) LO frequency, (b) LO power.

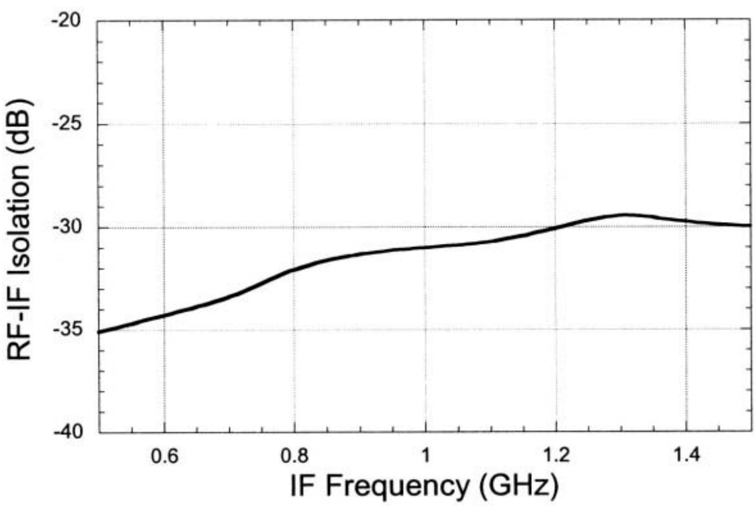

Figure 6.9. Measured RF-IF isolation versus IF frequency.

Table 6.1. Summary of mixer measured performance.

Specifications	Measured Performance
Conversion Gain (dB)	2
IIP3 (dBm)	15
LO-RF Isolation (dB)	> 10
LO-IF Isolation (dB)	> 30
RF-IF Isolation (dB)	> 30

6.4 Voltage Controlled Oscillator

6.4.1 VCO MMIC Design

A common-gate configuration is used to generate strong negative resistance by inductive feedback.

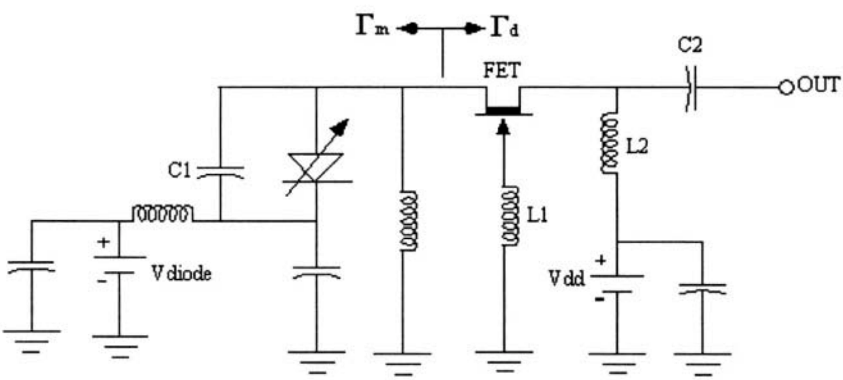

Figure 6.10. Schematic of the VCO circuit.

As shown in Figure 6.10, the resonator of the VCO consists of a spiral inductor, MIM capacitors, and a varactor diode, which is used for frequency tuning. Although a much wider tuning bandwidth can be obtained by placing the varactor on the gate path, the varactor is incorporated in the resonator on the source path to reduce its noise contribution to the VCO [147]. In addition, an MIM capacitor is placed in parallel with a small varactor to reduce its loading effects on the resonator Q. To eliminate undesirable low-frequency oscillations, a LC network is also incorporated as a high pass filter on the output path. Reflection coefficient line analysis is used to optimize the resonator load impedance for frequency stability and noise performance. The gate load is critical in determining the conditions of oscillation.

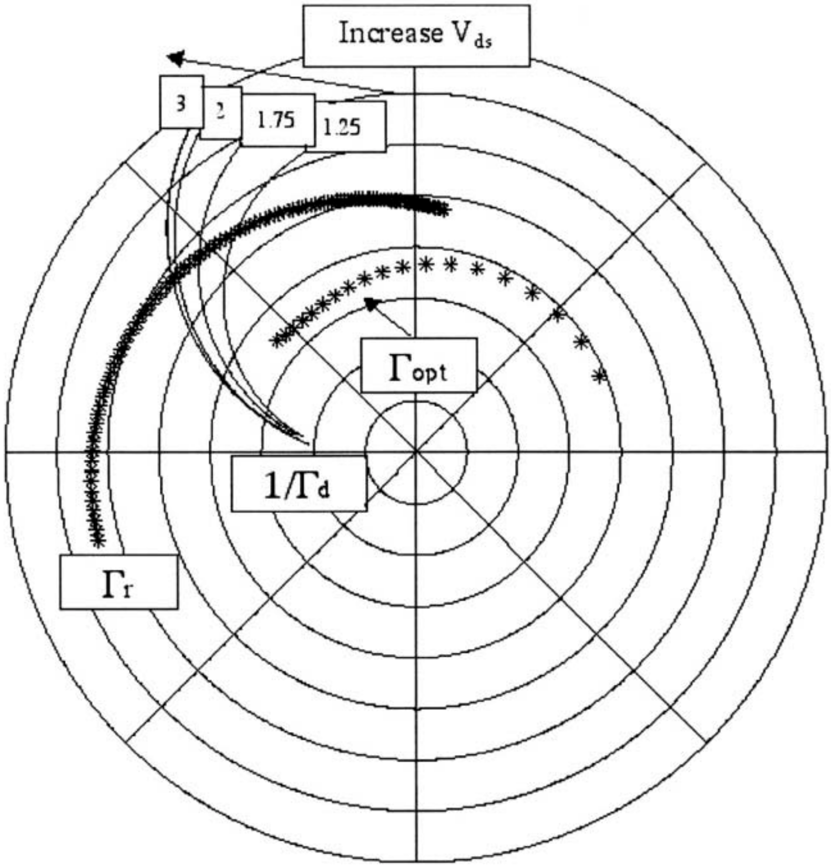

Figure 6.11. Reflection coefficient line of VCO and its phase noise performance.

Figure 6.11 shows the reflection coefficient lines of the resonator and the device at various drain-bias conditions. The crossover point implies the operating frequency of the oscillator, and the angle between two lines indicates the Q-factor [148]. As the drain voltage increases, the angle approaches 90 degrees, where Q is at a maximum. Increasing the drain voltage also reduces the phase noise by extending the depletion region in the channel to the drain side and consequently reducing the sensitivity of the oscillator to the gate-source voltage [149]. The noise parameters of the device are measured to determine the optimum matching point for the resonator. To further improve phase noise performance, the load impedance of the resonator is carefully designed to provide a perpendicular bisector for the reflection coefficient lines and to match near the Γ_{opt} point. High Q spiral inductors are implemented using 6-μm thick double-stacked metal.

For an accurate inductor model, a commercial method-of-moments (MoM) simulator is used, and transmission line effects in the layout are considered. This MMIC also includes pads for on-wafer testing and shunt capacitors on the bias pads to minimize parasitic effects of the dc probes. The VCO is using a depletion mode FET. The circuit occupies a 0.66×0.92 mm^2 die area, as shown in Figure 6.12.

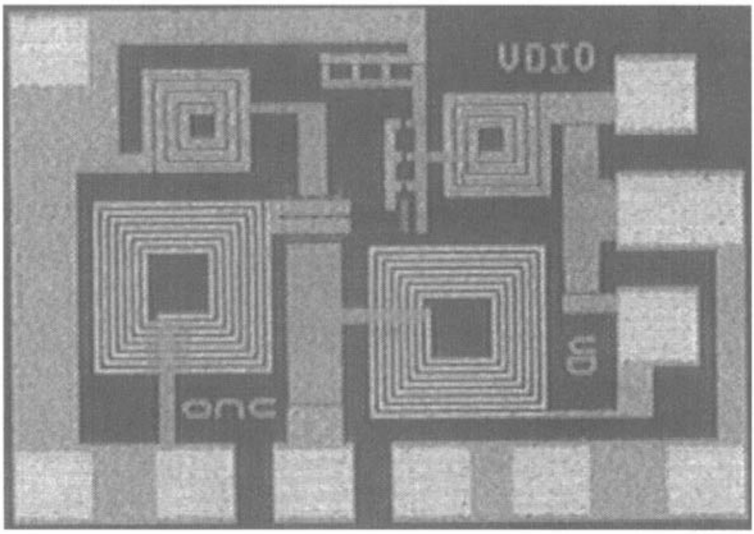

Figure 6.12. Photograph of the fabricated VCO MMIC.

6.4.2 Measured Performance

The oscillation frequency, output power, frequency tuning range, harmonics, and phase noise of the designed VCO has been measured on-wafer using a SUMMIT 9000 Cascade probe station, a Agilent 8563E spectrum analyzer and two HP3620A power supplies. The Agilent 8563E spectrum analyzer has low enough noise floors (i.e., <–102 dBm with a resolution bandwidth of 10 KHz) to measure the phase noise of many commercial local oscillators, and it has the ability to correct the measured power spectrum automatically and display the resulting phase noise [150]. Single-side band phase noise was measured as the relative spectral density of the noise sidebands for a given offset frequency from the carrier.

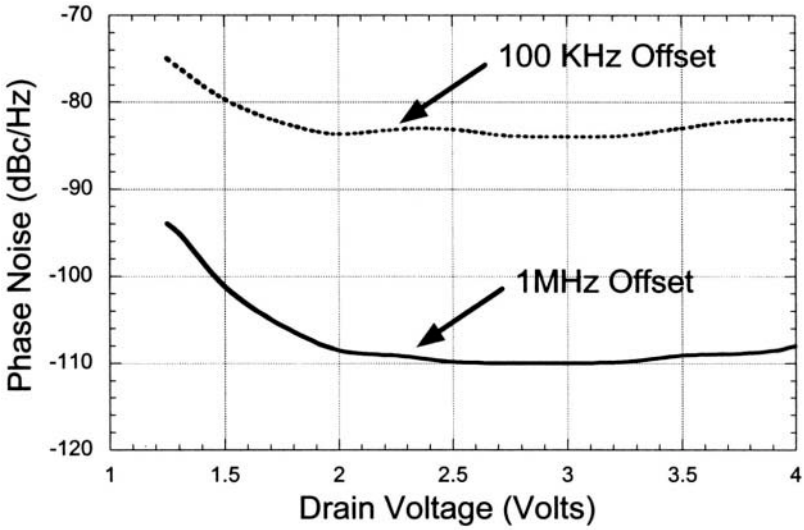

Figure 6.13. Phase noise as a function of drain bias.

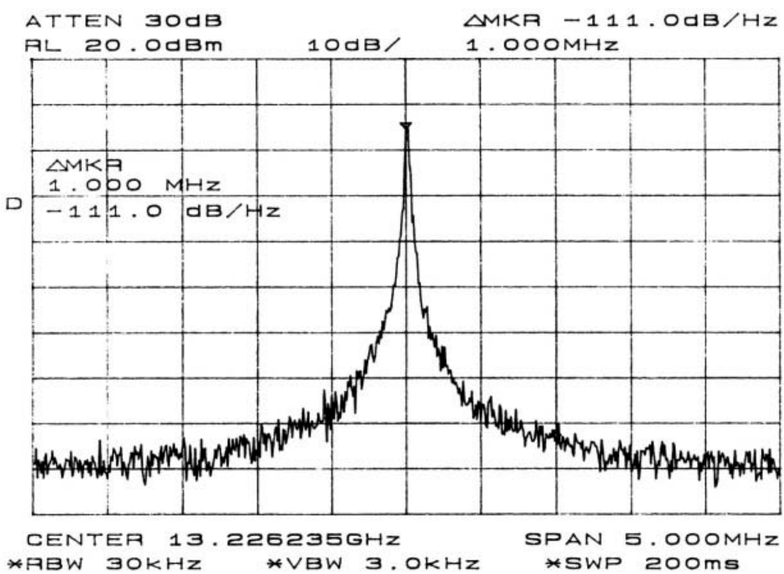

Figure 6.14. Output frequency spectrum of the VCO over a 5MHz span.

Figure 6.13 plots the VCO phase noise at offsets of 100 KHz and 1 MHz as a function of drain bias. A phase noise improvement of 9 dB at 100 KHz offset was achieved as the drain voltage increased to 3.25 V.

Figure 6.14 shows the signal spectrum of the VCO over a 5 MHz span, resulting in a phase noise of -111 dBc/Hz at a 1 MHz offset. Second harmonic suppression of 40 dB or more was observed across the entire power and frequency range, and no parasitic oscillations were detected, as shown in Figure 6.15.

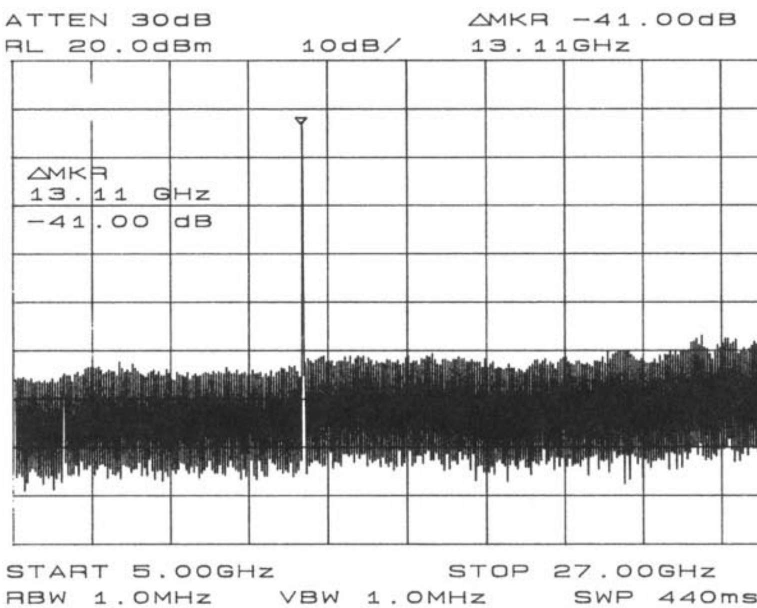

Figure 6.15. Harmonic measurement result of the VCO.

Figure 6.16 shows the dependence of oscillation frequency and output power level on the drain voltage. A maximum output power of 9.5 dBm was measured, and a power control level of 12 dB was obtained by varying the drain voltage from 1.5 to 4 V. The frequency pulling occurs at a drain voltage of less than 1.5 V and can be reduced by using a buffer amplifier. Figure 6.17 shows the measured frequency and output power level as a function of the varactor voltage. A frequency tuning range of 550 MHz, ranging from 12.8 GHz to 13.25 GHz, with uniform phase noise performance was achieved over a tuning voltage range of -1 to +3 V. These characteristics have been achieved without any buffer amplifiers. Table 6.2 summarizes the measured performance of VCO MMIC.

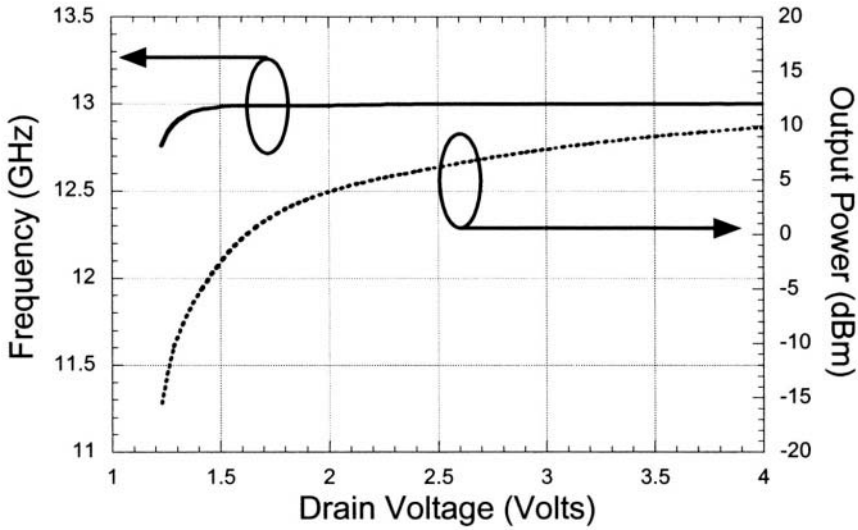

Figure 6.16. Measured frequency and output power as a function of drain bias.

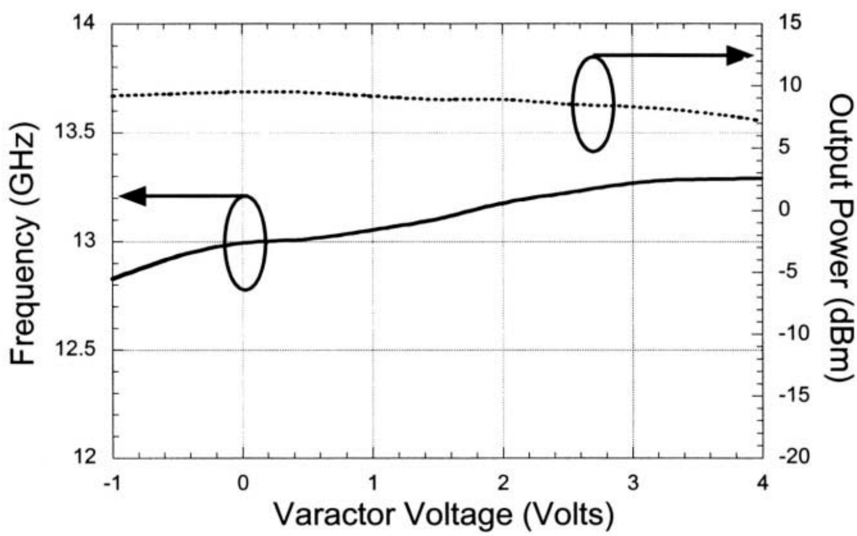

Figure 6.17. Measured frequency and output power as a function of varactor control voltage.

Table 6.2. Summary of VCO measured performance.

Specifications	Measured Performance
Center frequency (GHz)	13
Maximum output power (dBm)	9.5
Frequency tuning range (MHz)	550
Output power control level (dB)	12
Phase noise (dBc/Hz)	-85 dBc/Hz @ 100 KHz offset -110 dBc/Hz @ 1 MHz offset
Harmonics (dBc)	40

6.4.3 LO Buffer Amplifier MMIC

The buffer amplifier was designed to facilitate better output matching and desensitize the VCO to the external load impedance. It is essentially responsible for providing an unconditionally stable operation for the up-converter, both in the presence and absence of a LO signal. Because the mixers do not have a good wideband match, the LO buffer amplifier is needed to provide a good match at the LO port.

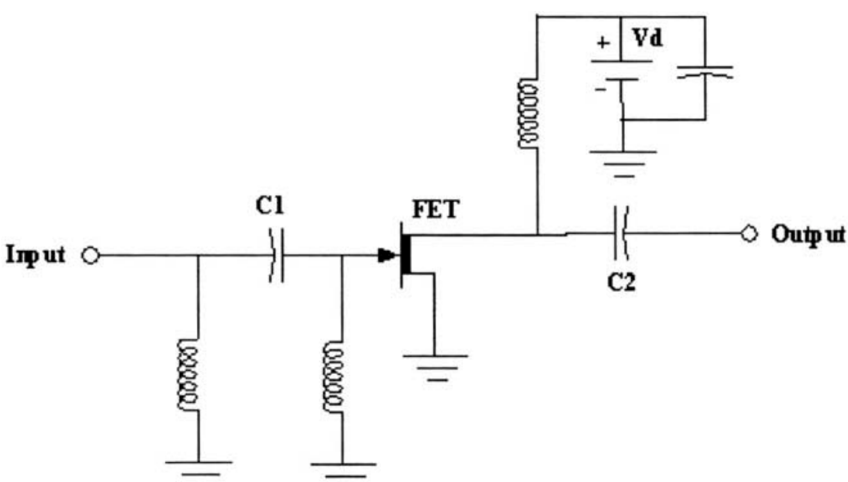

Figure 6.18. Schematic diagram of the LO buffer amplifier.

It has been designed to deliver the required drive power (about 15 dBm) to the mixer. A 500 μm FET was chosen to achieve the specification. The LO amplifier uses a single stage common source amplifier topology incorporating reactive matching. It provides 7 dB of gain and return loss of better than 14 dB at 13 GHz as shown in Figure 6.19. Output 1-dB compression point of 18 dBm was achieved with the input power of 12 dBm as shown in Figure 6.20. This buffer amplifier was designed to operate at a zero gate bias to reduce the number of power supplies.

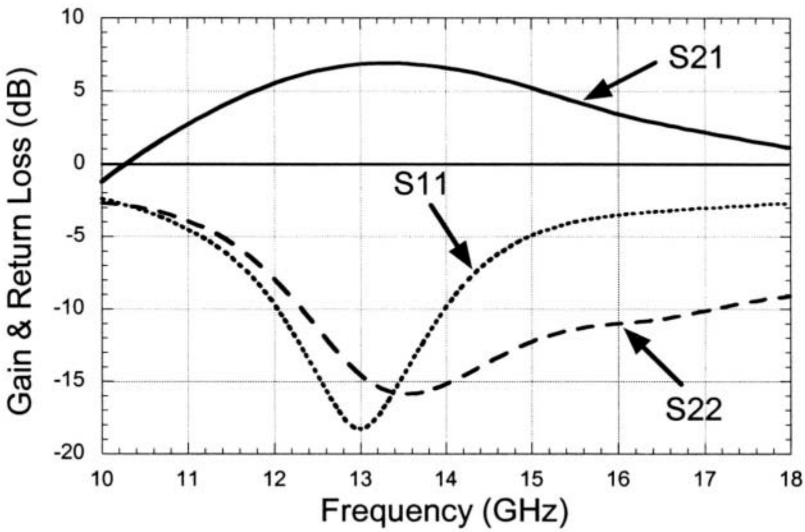

Figure 6.19. Measured gain and return loss of the LO buffer amplifier.

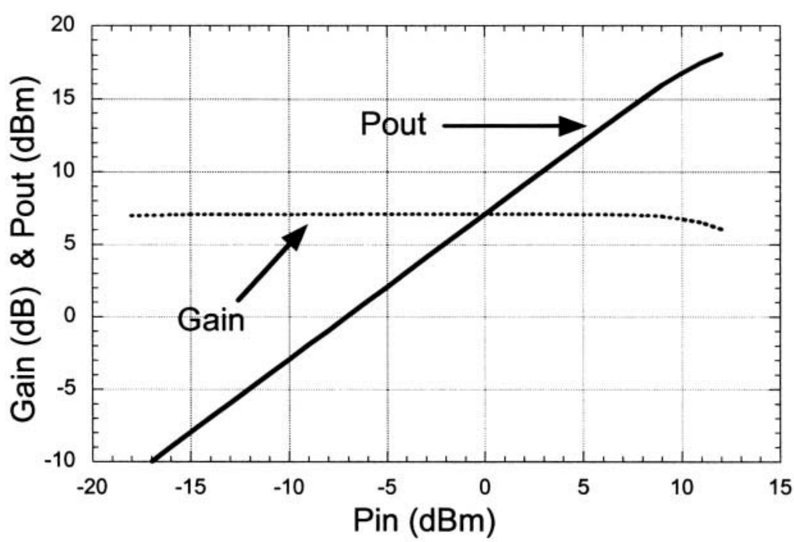

Figure 6.20. Measured gain and 1 dB compression point of the LO buffer.

Figure 6.18 shows the schematic diagram of a buffer amplifier. The gain and return loss performances are shown in Figure 6.19. The size of the entire amplifier is only 24 × 22 $mils^2$, as shown in Figure 6.21. The amplifier requires a 3 V bias and draws 80 mA current. Table 6.3 summarizes the measured performance of LO buffer amplifier MMIC.

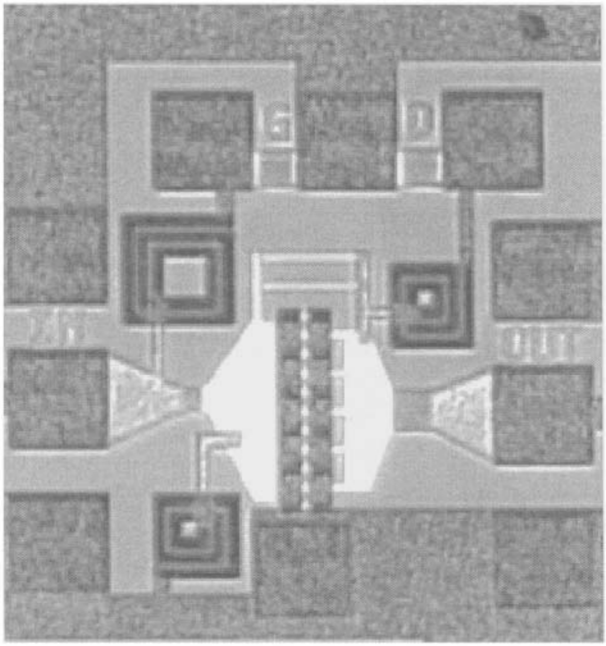

Figure 6.21. Photograph of the fabricated LO buffer amplifier.

Table 6.3. Summary of Buffer Amplifier Measured performance.

Specifications	Measured Performance
Gain (dB)	7
Return Loss (dB)	> 14
1dB compression point (dBm)	18
Power consumption (mW)	240

6.5 IF Amplifier MMIC and RF Amplifier MMIC

The IF amplifier was designed to increase the gain of the dual gate mixer and have a low noise figure for the entire up-converter as well as to provide better input matching to the IF port of the mixer. Reactive matching was used to have a good noise figure while sacrificing the broadband input match. It occupies the die area of 30×26 mils^2, as shown in Figure 6.22.

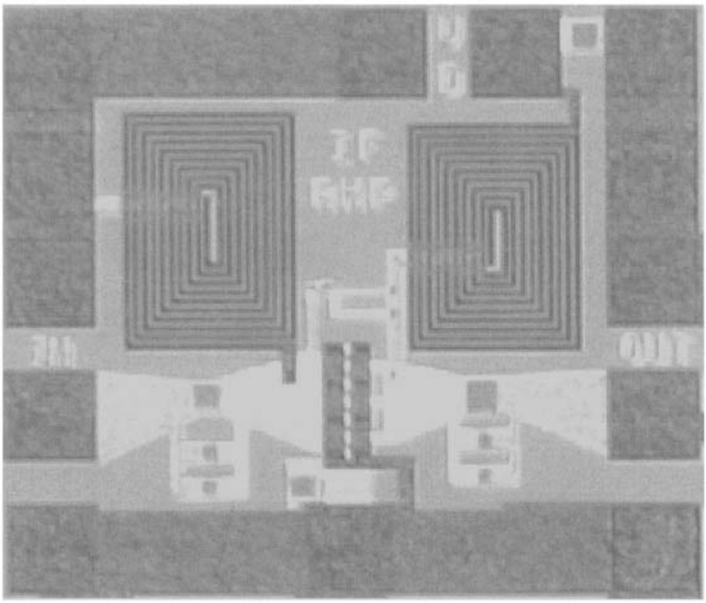

Figure 6.22. Photograph of the fabricated IF amplifier.

Experimental data shows a more than 10 dB gain, 3 to 4 dB noise figure and IIP3 of 5 dBm between 600 MHz and 1200 MHz. It shows the wide band output match (S22 < -10 dB) that can provide wide matching with the IF port of the dual gate mixer. Figure 6.23 shows the measured gain and return loss performance from 0.1 to 5 GHz. It draws 80 mA current with a 2 V drain bias operation. Table 6.4 summarizes the measured performance of IF amplifier MMIC.

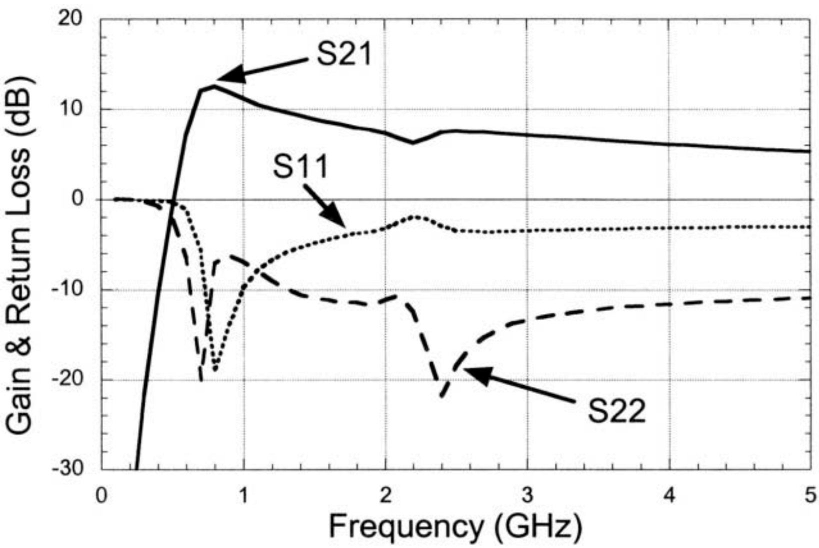

Figure 6.23. Measured gain and return loss of the IF amplifier.

Table 6.4. Summary of IF amplifier measured performance.

Specifications	Measured Performance
Gain (dB)	> 10
Return Loss (dB)	> 14
1dB compression point (dBm)	5
Power consumption (mW)	160

The output power of the up-converter has to be sufficient to overcome the loss of a bandpass filter while maintaining the desired output power of the entire module. The RF amplifier with a measured gain of 5 dB and 1-dB compression point of 16 dBm was implemented to increase the conversion gain of the entire up-converter MMIC, and provides a good output matching with the following BPF network.

The RF amplifier uses the single stage common source topology incorporating reactive matching. A self-bias scheme was used in conjunction with this topology to simplify the biasing circuitry. The amplifier requires a 3 V bias and draws 80 mA current. The size of the circuit is only 23×22 mils^2, as shown in Figure 6.24. The RF amplifier is used to boost the upper side band (USB) output power and also contains a high pass filter network in its input matching network to reduce the level of IF signal from the dual gate mixer. Figure 6.25 shows the measured gain and return loss performance from 10 to 18 GHz. Output 1-dB compression point of 16 dBm was achieved as shown in Figure 6.26. Table 6.5 summarizes the measured performance of RF amplifier MMIC.

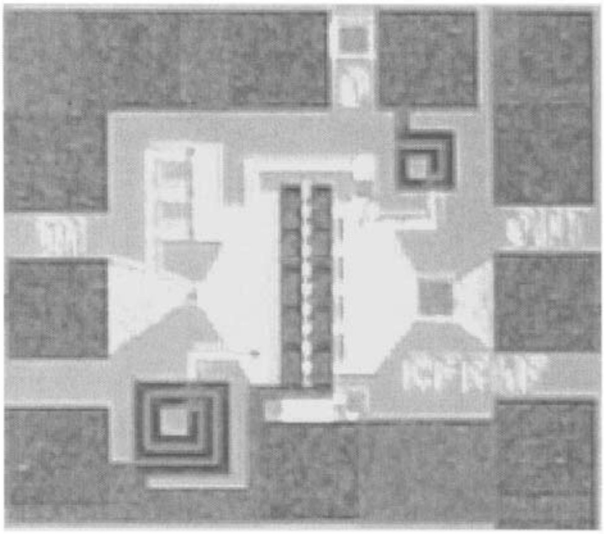

Figure 6.24. Photograph of the fabricated RF amplifier.

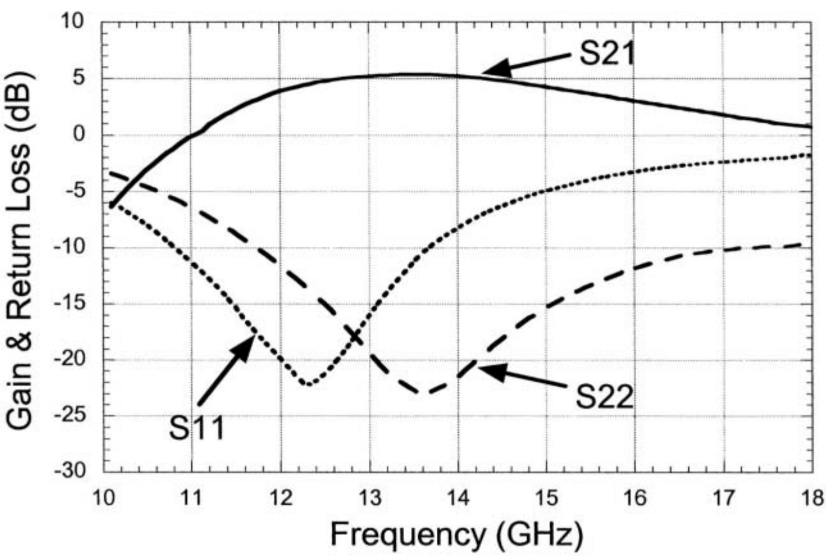

Figure 6.25. Measured gain and return loss of the RF amplifier.

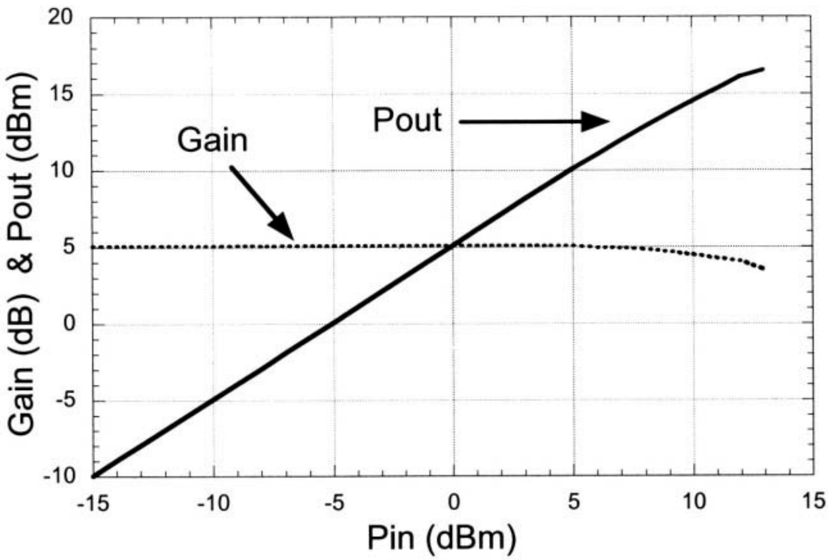

Figure 6.26. Measured gain and 1 dB compression point of the RF amplifier.

Table 6.5. Summary of RF amplifier measured performance.

Specifications	Measured Performance
Gain (dB)	5
Return Loss (dB)	> 14
1dB compression point (dBm)	16
Power consumption (mW)	240

6.6 Driver Amplifier MMIC

6.6.1 Driver Amplifier Design

The driver amplifier specification was derived to maximize the performance of the entire transmitter chain. The gain of the driver amplifier had to be sufficient to overcome the loss of a BPF and to drive the power amplifier into saturation from 14 to 14.5 GHz. The output power level of the entire transmitter was determined to be more than 24 dBm. The gain requirement for driver amplifier was determined from the input IF power level, the up-conversion gain from up-converter MMIC and the associated losses of the bonding wire and the BPF. The anticipated minimum input power level available to the driver amplifier is -5 dBm, because the minimum output power from the up-converter is 0 dBm and the associated losses are expected to be about 5 dB including 3dB insertion loss of BPF, 2dB loss of bonding wire at 14 GHz. Therefore, the driver amplifier required a minimum gain of 25 dB to produce the 20 dBm output power. To meet the specification and to allow for process variations, the five-stage amplifier was designed to produce more than 25 dB of small signal gain from 14 GHz to 14.5 GHz. The amplifier was realized with five 600 μm × 0.6 μm FETs. A common source topology and single bias supply scheme were used to simplify the biasing circuitry.

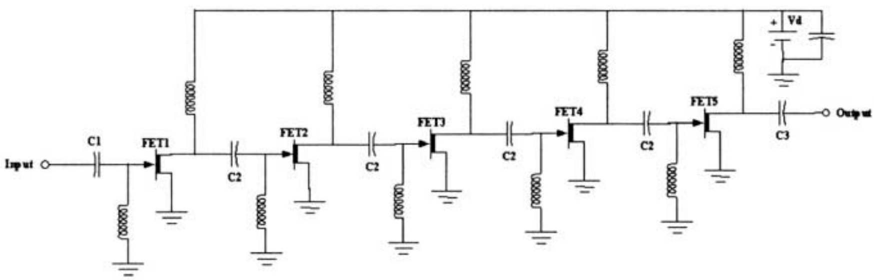

Figure 6.27. Schematic diagram of the five-stage driver amplifier.

Figure 6.27 shows the schematic diagram of the driver amplifier. The five devices were reactively matched with feedback resistance for unconditional stability. The interstage dc blocks were realized by MIM capacitors.

Three kind of matching circuits can be used in the transmitter chain. They are LC matching, active matching, and resistive matching. The LC matching has lower noise and a higher Q and filtering performance. However, LC matching takes more die area than the other matching circuits, especially at lower frequencies. Both active matching and resistive matching have wideband performance. However, active matching needs extra dc current and resistive matching is lossy. These considerations, plus the system specifications and the die area limitation, requires a compromise. LC matching was used at the input and output of the driver amplifier because the transmitter has a higher frequency, and LC matching also plays a role in filtering. A full chip MMIC layout simulation, taking into account the distributed effects of metal interconnects, was successfully done in the design. On-wafer microwave measurement was carried out for circuit characterization. The size of the entire amplifier is 26 × 63 mils^2 and this incorporates all dc blocking and bypassing capacitors on-chip as shown in

Figure 6.28. In this circuit, the self-biasing network was inserted to change the gate-bias point for better gain performance.

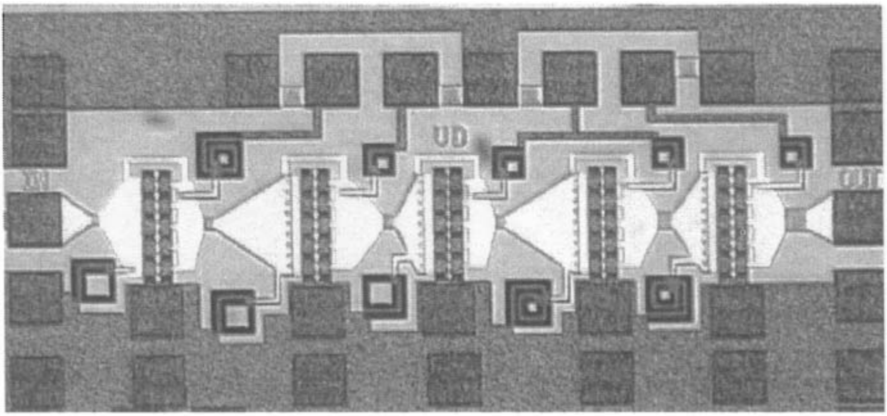

Figure 6.28. Photograph of the fabricated five stage driver amplifier.

6.6.2 Measured Performance

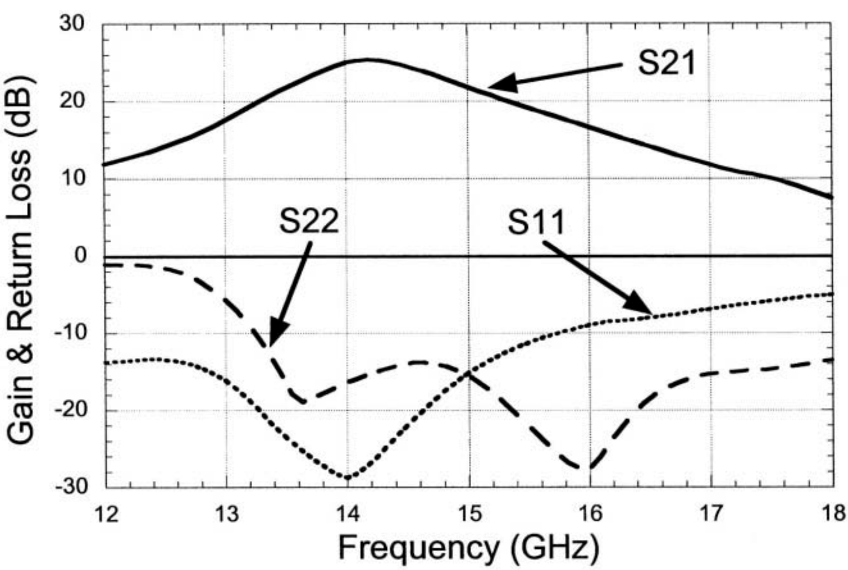

Figure 6.29. Measured gain and return loss of the five-stage drive amplifier.

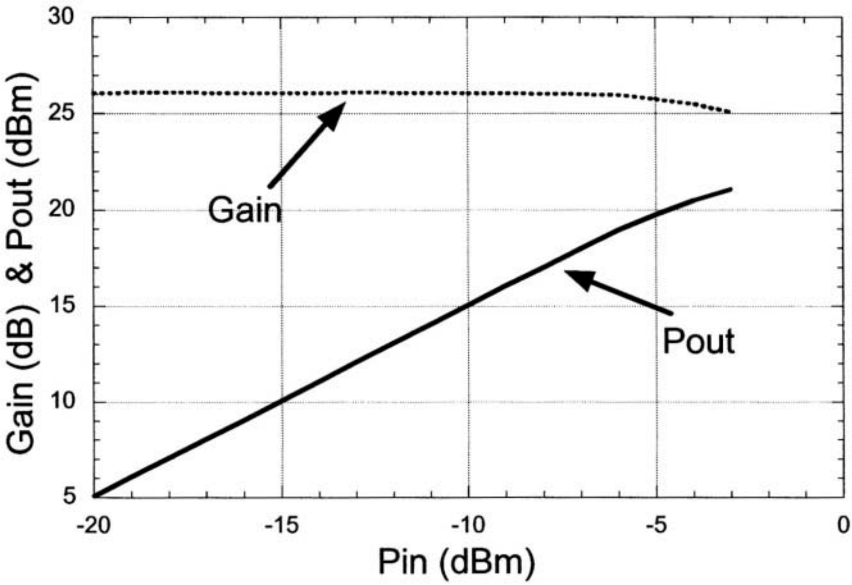

Figure 6.30. Measured gain and 1 dB compression point of the drive amplifier.

Figure 6.29 shows the gain and return loss performance of the driver amplifier. The resulting amplifier exhibited 26 dB of small-signal gain while drawing 300 mA from 4 V supply. When driven with -6 dBm, the amplifier provides 20 dBm output power. Measurements show a return loss of greater than 15 dB over the entire frequency band. Measurement shows that its 1-dB compression point is 21 dBm across the required frequency range as shown in Figure 6.30. Table 6.6 summarizes the measured performance of driver amplifier MMIC.

Table 6.6. Summary of driver amplifier measured performance.

Specifications	Measured Performance
Gain (dB)	26
Return Loss (dB)	> 13
1dB compression point (dBm)	21
Power consumption (mW)	1200

6.7 Power Amplifier Design

6.7.1 Power Amplifier Design Principles

PA is the primary power consumer in the transmitter unit. Thus, the major design issue is how efficiently the PA can convert dc input power to RF output power. Another important characteristic of a PA is linearity; the input-output relation must be linear to preserve signal integrity. A primary consideration in the design of the PA involves tradeoffs of efficiency and linearity. There have been a lot of different architectures in which a PA could be implemented. The number of different types of classes of PA is too numerous to list, and they range from entirely linear to entirely non-linear as well as from quite simple to inordinately complex. The choice in system and corresponding modulation method defines the RF waveform and directly affects the linearity requirements of the PA. For highly linear applications, efficiency may be sacrificed. Modulation methods that have high peak-to-average ratio must have great linearity. Often, this is at the expense of efficiency. On the other hand, there are modulation techniques that result in more constant envelope signals, allowing the PA to operate in saturation so that higher efficiency can be achieved.

In the satellite communication service that uses a QPSK modulation scheme, the linearity issue is more important than efficiency in order to avoid spectral regrowth and to preserve modulation accuracy. Therefore, only linear classes of PA, where the output amplitude and phase are linearly related to the input amplitude and phase, will be reviewed.

6.7.2 Linear Power Amplifier Review [151]

Three main classes of linear amplifier are A, AB, and B, with class A generally being the most linear and least efficient of the three. A Class A power amplifier is the simplest and most basic form of power amplifier. In Class A operation, the transistor is in the active region for the entire input cycle, and thus is always conducting current. As such, the device maintains the same gain approximately throughput the entire region. The problem with Class A structures, however, is their inherently poor efficiency. The device, since it is on at all times, its constantly carrying current, and that current represents a continuous loss of power in the device. As a result, Class A tends to be used only in those situations where either the linearity requirements are so stringent as to necessitate an entirely linear output stage, or in those situations in which the power consumption of the amplifier is less of an issue.

A Class B amplifier is one in which the operating point is at one or another of the extremes of its characteristics so that the quiscent power is small. The quiscent current or quiescent voltage of a Class B stage is approximately zero, and hence if the excitation is sinusoidal, then amplification takes place for only one-half of a cycle. Class B operation is significantly more efficient than Class A for use in linear power amplifiers, while still providing useful levels of linearity. A common implementation of a Class B design is in a push-pull fashion, where two power devices each operate half of the time in an alternating fashion.

Class AB is a compromise between the two extremes of Class A and Class B operation. The output signal of this type of amplifier is zero for part of the signal, but less than one-half of the input sinusoidal signal. The distortion added by a Class AB amplifier is consequently greater than that of a Class A stage, but less than that of a Class B stage. Conversely its efficiency will be less than that of a Class B stage and greater than that of a Class A stage.

There are several factors that go into the class of PA, most of which depend on the communications system for which the PA is being designed. As stated in Chapter 3, in this transmitter module design, the PA must have output power of more than 24 dBm. It must also be able to meet the frequency domain transmission spectral masks. In these considerations, the issue of meeting the transmission spectral masks plays an important role in determining the class of PA to use. While nonlinear PA have great efficiency, their nonlinearity can cause the output signal to spread out due to intermodulation products. Especially if there is a lot of phase noise in the local oscillator that will cause spreading of the input to the PA, and this spreading of the output can cause the above restrictions to be violated. Moreover, a key point of the transmission spectral masks is that during the PA turn-on-time, the transmitted signal must still meet the spectral mask, which can be difficult for a nonlinear PA. As a result, a nominally linear class of PA was chosen to be used in this design so as to avoid some of the problems caused by PA nonlinearity. Since this was really the first attempt at designing and building a PA at Ku-band with 0.6-μm GaAs MESFET process, a more cautious route was chosen that would make it easier to meet the spectral mask requirements.

6.7.3 Power Amplifier Design

Class A power amplifier was designed using a 0.6-μm GaAs MESFET device. The circuit was designed and simulated using HB analysis. A Triquint own model-3 (TOM3) large signal MESFET model was used for the simulations. To accurately model the high-frequency parasitics, the spiral inductors were incorporated using the EM simulation data [152]. The PA has a single ended one-stage common source topology. Figure 6.31 shows the schematic diagram of class-A power amplifier. The device size is 1.5 mm, as shown in Figure 6.32.

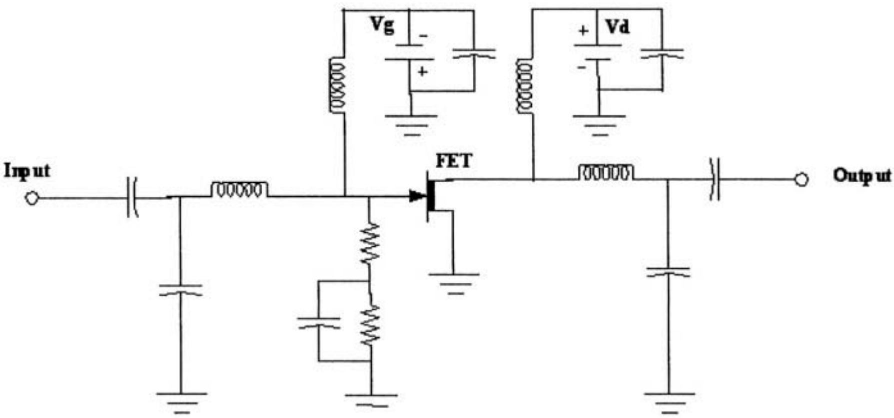

Figure 6.31. Schematic diagram of the one-stage class-A PA.

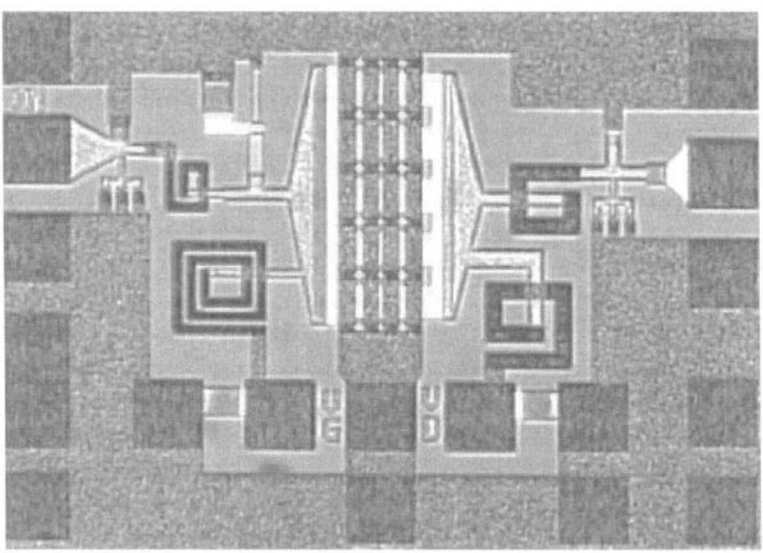

Figure 6.32. Photograph of the fabricated one stage class A PA.

6.7.4 Measured Performance

Figure 6.33 shows the measured small signal gain of 6dB and return loss of better than 10 dB at transmitted frequency band.

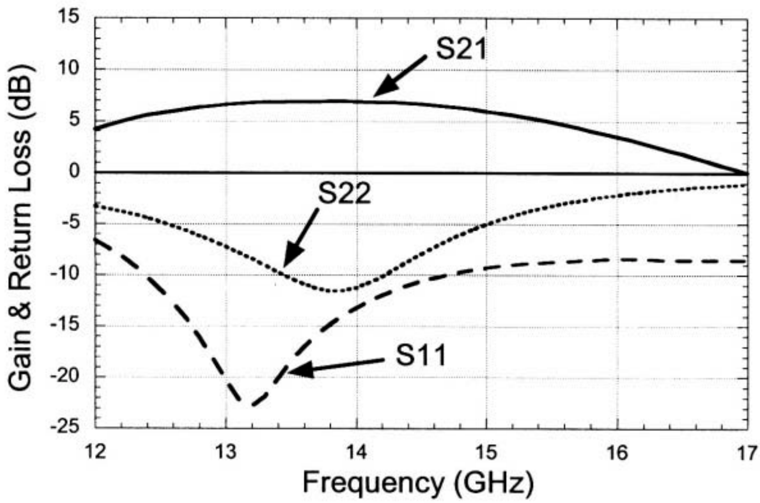

Figure 6.33. Measured gain and return loss of PA.

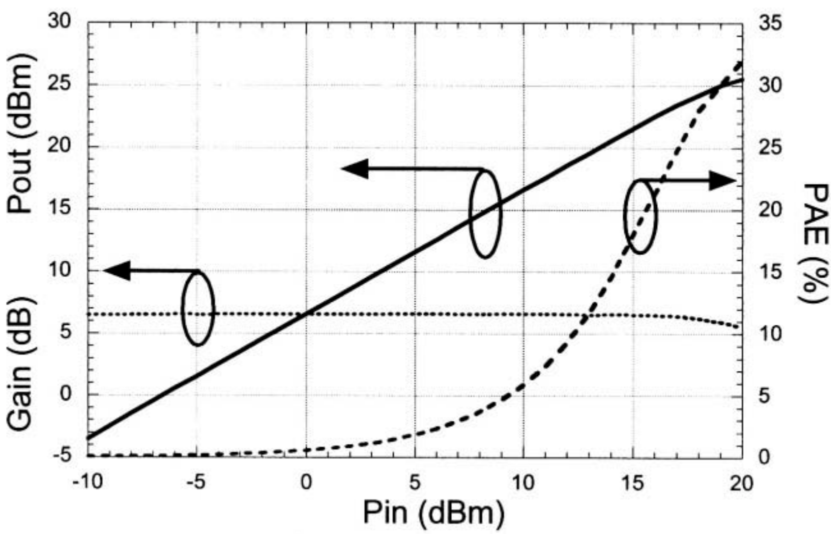

Figure 6.34. Measured gain, output power, and efficiency of PA.

The power amplifier exhibits 6 dB of power gain, 33 % of power added efficiency (PAE), and 26 dBm of output power, as indicated in Figure 6.34. The measured small signal performance of the power amplifier also shows good agreement with the simulation results. The 5 V is applied with 200 mA drain current. Lumped elements were used to realize the matching network. Each lumped element was modeled by the electro-magnetic (EM) simulation data. Table 6.7 summarizes the measured performance of power amplifier MMIC.

Table 6.7. Summary of power amplifier measured performance.

Specifications	Measured Performance
Gain (dB)	6
Return Loss (dB)	> 10
1dB compression point (dBm)	26
PAE (%)	33
Power consumption (mW)	1200

6.8 Conclusions

Transmitter MMICs have been fabricated in the commercial 0.6 μm GaAs MESFET process. Figure 6.35 shows the implemented MMIC chip sets. Up-converter MMIC and PA MMIC occupy the die area of 62 mil × 87 mil, 33 mil × 106 mil, respectively. The absence of via holes simplifies the process and augments the MMIC chip yields.

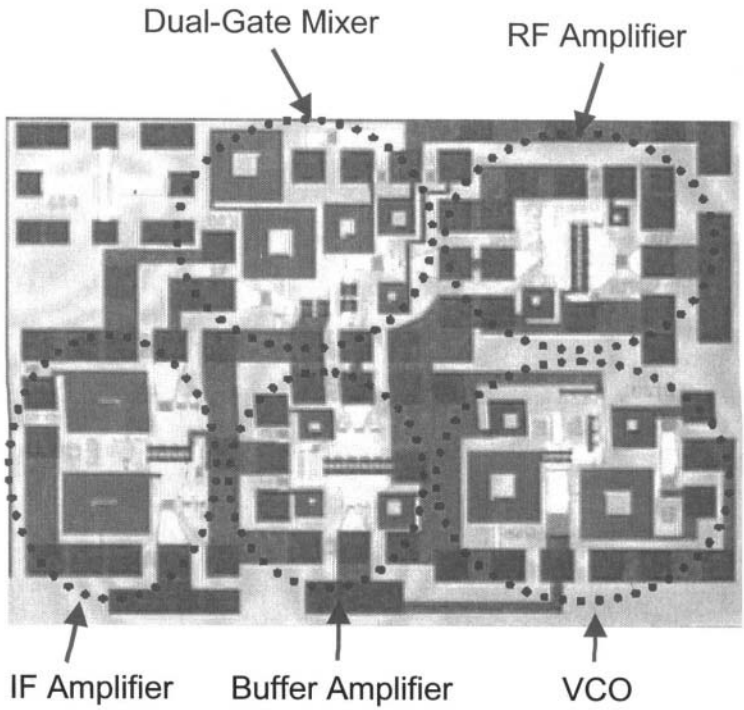

(a)

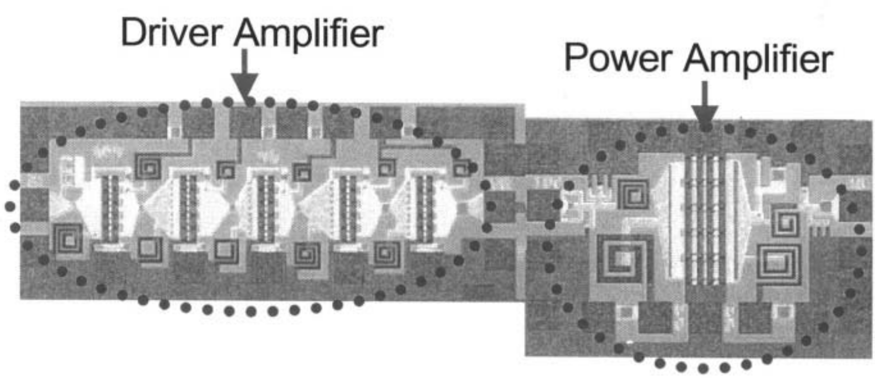

(b)

Figure 6.35. Photograph of the implemented MMIC chip sets (a) Up-converter MMIC, (b) Power amplifier MMIC.

Chapter 7

Transmitter Module Design

7.1 Introduction

The system was designed in modular form, consisting of two MMIC chips, an up-converter MMIC and a power amplifier MMIC, and a coupled strip line BPF. Two MMIC chips are mounted on the LTCC substrate, where a coupled-line BPF is embedded. The LTCC is composed of 20 layers of Dupont 951 fired ceramic. However, only 10 layers are the part of this transmitter module. Other layers were used for different purpose. Each layer of the structure is 4.4 mil thick. The 7 mil thick MMICs are mounted and wire bonded on the board incorporating with an embedded strip line BPF.

7.2 Strip Line Band Pass Filter

7.2.1 Strip Line Filter Design Principles

There are three configurations showing band pass filter response [153] that can be obtained from a pair of coupled strip lines by terminating two of the four ports in either open or short circuits, or connecting the ends of the lines together. Figure 7.1 shows single sections of the three possible coupled line BPFs. In most cases, it is necessary to cascade several segments of the filter in order to obtain the required performance such as bandwidth and insertion loss. Only when the input and output of a single segment are placed at the opposite side of the strips, any number of segments can be cascaded. But, in case of Figure 7.1 (c), only two segments can be cascaded because the input and output of a single segment are placed at the same end. In addition, it is easier to fabricate filter segments in form of open circuits rather than short circuits. Therefore, Figure 7.1(b) is chosen for band pass filter implementation for its inherent configurations.

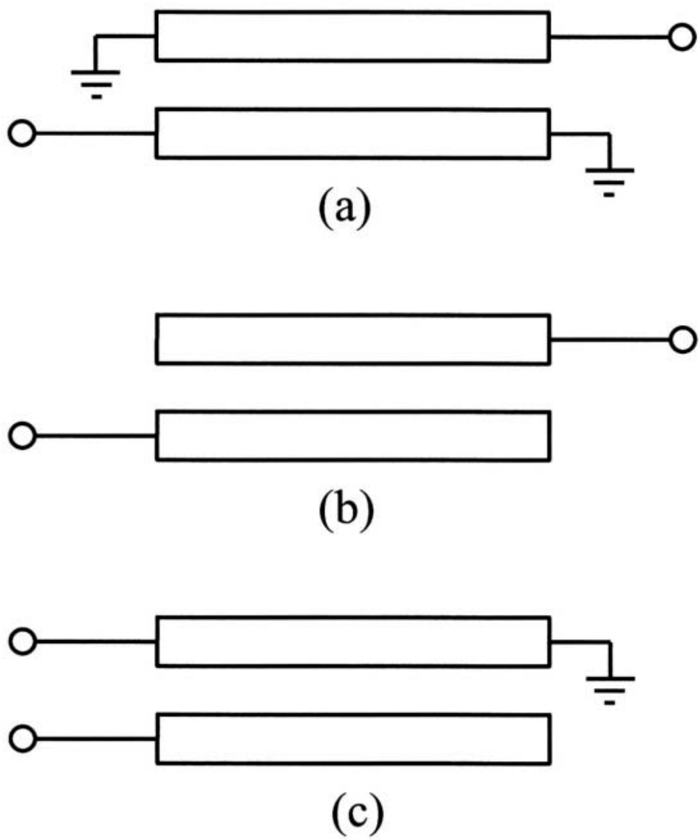

Figure 7.1. Coupled line configuration.

The image impedance of the coupled strip line filters differs from the characteristic impedance of an isolated strip [153]. Therefore, it is necessary to connect the filter strips with the coupled strips having different widths in order to reduce the loss resulting from mismatch at the terminals. The filter was designed by following the general design procedure outlined in [154,155]. The cross section of coupled strip line filter is shown in Figure 7.2.

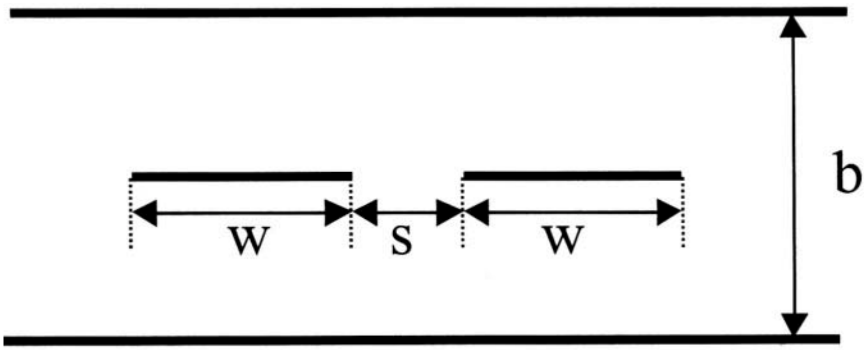

Figure 7.2. Coupled strip line cross sections.

The parameters for the coupled strip line dimension were obtained by using the Eq. 5.1, Eq. 5.4, and the graph of the Z_{0e} and Z_{0o} as a function of w/b and s/b as shown in [155].

$$Z_{0e} = \frac{30\pi}{\sqrt{\varepsilon_r}} \frac{K(k_e^{'})}{K(k_e)} ohms \qquad (7.1)$$

where Z_{0e} is the even-mode characteristic impedance measured from one strip to ground, K is the complete elliptic integral of the first kind, ε_r is the relative dielectric constant of the material filling the cross section.

$$k_e = \tanh(\frac{\pi}{2}\frac{w}{b}) \cdot \tanh(\frac{\pi}{2}\frac{w+s}{b}) \qquad (7.2)$$

$$k_e^{'} = \sqrt{1-k_e^{2}} \qquad (7.3)$$

For the odd mode, the characteristic impedance from one strip to ground is

$$Z_{0o} = \frac{30\pi}{\sqrt{\varepsilon_r}} \frac{K(k_o^{'})}{K(k_o)} ohms \qquad (7.4)$$

where

$$k_o = \tanh(\frac{\pi}{2}\frac{w}{b}) \cdot \coth(\frac{\pi}{2}\frac{w+s}{b}) \quad (7.5)$$

$$k_o' = \sqrt{1-k_o^2} \quad (7.6)$$

The nature of the dependence of Z_{0e} and Z_{0o} on w/b and s/b is illustrated in [155]. Commercial microwave design CAD tools have a function that automatically calculates the coupled line dimensions such as w, s, 1 with given Z_{0e} and Z_{0o}.

7.2.2 LTCC-based Strip Line Filter Design

In the transmitter module, three stage folded edge coupled strip line filters are needed to suppress the LO signal at 13 GHz, as well as the harmonics and spurious signals. This filter is designed by using commercial microwave design tool and a MoM EM simulator [152].

Figure 7.3 shows the schematic diagram of folded edge coupled strip line band pass filter structure.

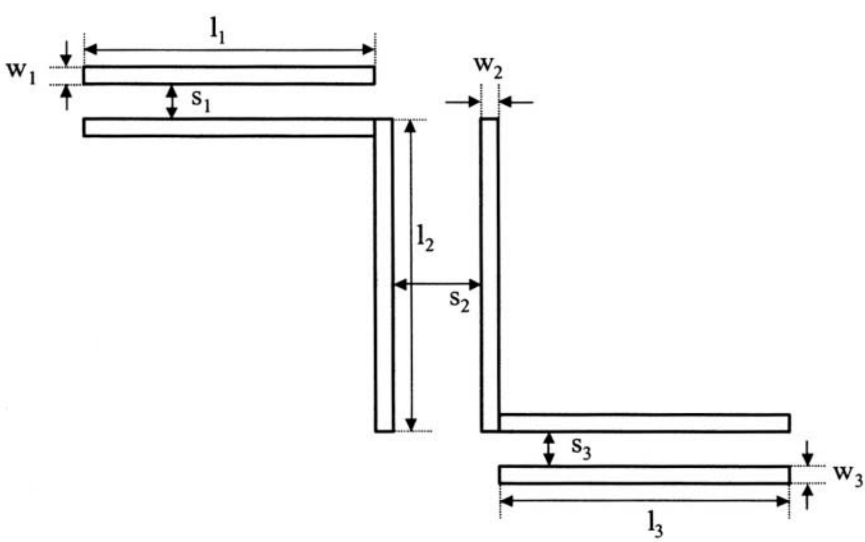

Figure 7.3. Schematic diagram of folded edge-coupled strip line filter.

Eight filters were fabricated; all have the same dimensions for the w_1, w_2, w_3 and s_1, s_3 strips as well as l_2 strips, but have different dimensions for l_1, l_3 and s_2. Table 5.1 summarizes the comparison between the eight filters, including the measured performance in terms of the center frequency f_c, insertion and return losses at f_c, LO rejection performance at 13 GHz, and 3dB bandwidth. These filters were designed by incorporating a MoM EM simulator [152].

Table 5.1. Summary of measured performance of the fabricated LTCC coupled strip line filter.

	Dimension		Center Freq. (GHz)	Insertion Loss (dB)	Return Loss (dB)	LO Rejection (dB)	3dB BW (GHz)
	L_1, L_3	S_2					
A	66	16	14.527	-3.27	-29.61	-19.71	1.1
B	68	16	14.329	-3.06	-27.82	-18.15	1.1
C	69	16	14.229	-3.14	-21.91	-17.05	1.1
D	70	16	14.130	-3.12	-18.97	-16.15	1.1
E	68	18	14.225	-3.01	-20.34	-18.05	1.0

From the summary in Table 5.1, it is obvious that the center frequency f_c depends on l_1, l_3. by noting the variation for f_c of 400 MHz among the five filters. The role of s, spacing between coupled lines affects the bandwidth and Q of the filter. Also w, width of the coupled line, affects the center frequency. From the system point of view, Filter E is selected for module implementation because it meets well all the specifications. It exhibits a maximum of 3 dB insertion loss, a minimum of 20 dB return loss and an attenuation of 18 dB at 13 GHz LO frequency, and a minimum attenuation of 28 dB at 12 GHz image frequency. Also it has the best gain flatness between 13.9 to 14.4 GHz.

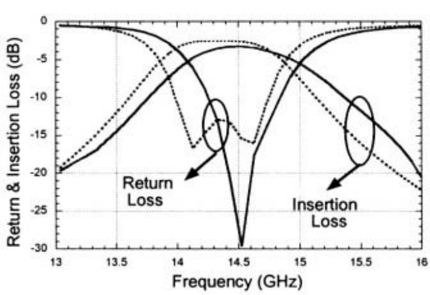

(a)

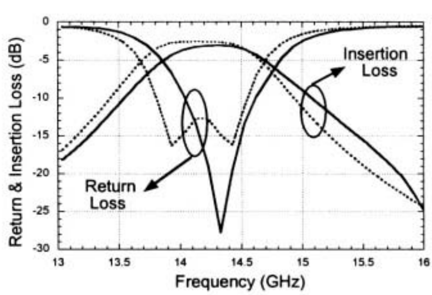

(b)

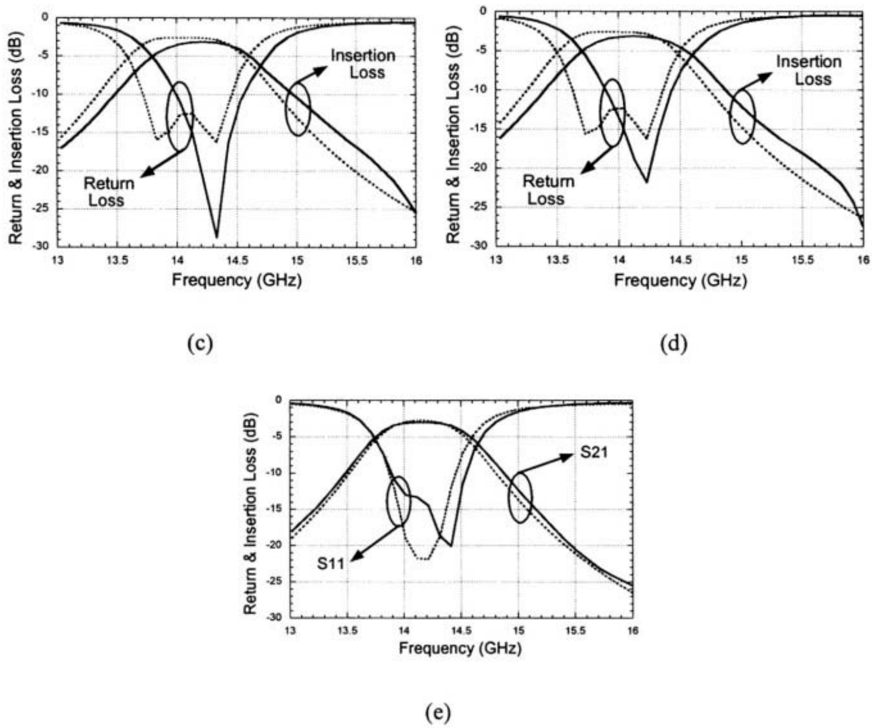

Figure 7.4. Performance comparison of coupled strip line BPFs between measurement (solid line) and simulations (dashed line) (a) Filter A, (b) Filter B, (c) Filter C, (d) Filter D, (e) Filter E

As it is observed from Figure 7.4, the measurement shows a slightly higher center frequency than simulation results. This can be explained by investigating the actual layout and implementation. In real implementation, via connecting the strip line to coplanar waveguide (CPW) is placed on the coupled line with 8 mil apart from the edge of strips because of the design rule for via process. This via location on strips reduced the actual length of the coupled strip line length by 5 to 10 mils. Therefore, the center frequency is expected to increase by the amount of the reduced strip line length. Meanwhile, because of its folded structure, additional coupling between two neighboring segments is expected and results in more parasitic capacitance between them. So this additional coupling can compensate for the increasing effects on center frequency for some amount, which overall is slightly higher than the MoM simulation results. The mismatch between CPW and strip line transition through via interconnects potentially causes the discrepancy between measurement and simulation. Also the coupled strip line filter was designed to have two resonant modes in order to meet bandwidth specifications. However, it turns out that the resulting return loss has only one resonant mode. It is potentially caused because the transition between strip line and CPW is not perfect and gives rise to unknown propagation that has another resonant mode such a situation could combine the two resonant mode into one mode as shown in Figure 7.4. Figure 7.5 shows the layout of the designed coupled strip line filter with folded edge structure that is showing the coupled line trace embedded 4 layers below from the top layer. CPW pad for on-wafer measurement along with via transition from strip line to CPW is also shown in Figure 7.5.

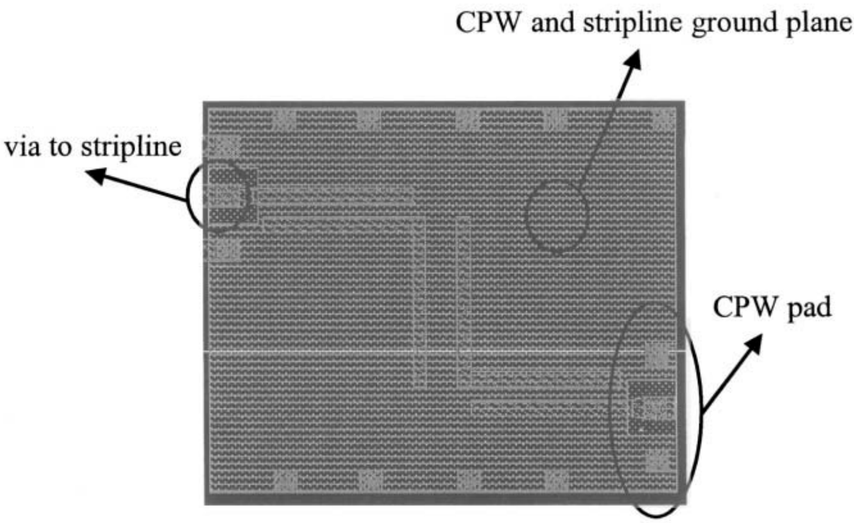

Figure 7.5. Top view of layout of the LTCC folded edge-coupled line filter with CPW pads and via to the strip line.

The BPF for the transmitter module was implemented in a coupled line filter topology on a multi-layer LTCC substrate to suppress the LO signal at 13 GHz and image signal at 12 GHz as well as suppress the harmonics and spurious signals. The number of coupled line segments depends on the filter order needed to meet the bandwidth specifications. Figure 7.6. shows the implemented LTCC-based three segment folded edge coupled line filter, where the middle segment was deployed perpendicular to the first and third segments for compactness. It has a compact size of 5.5mm × 3.8 mm × 0.7 mm with the CPW pads and 3.8 mm × 2.4 mm × 0.7 mm without the measurement pads.

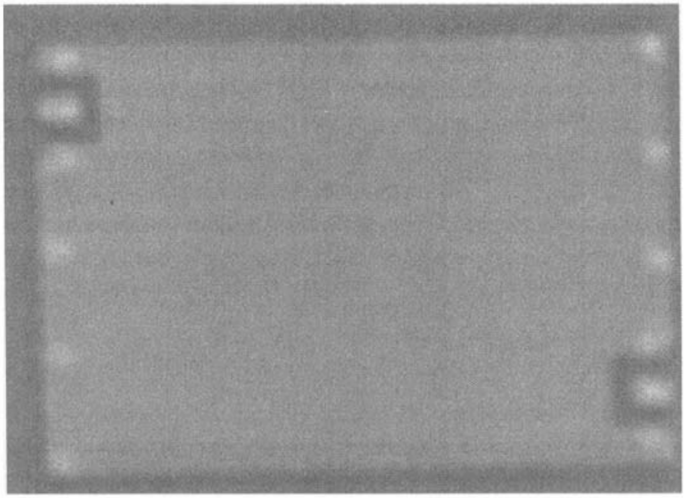

Figure 7.6. Photograph of implemented LTCC folded edge-coupled line filter.

An on-board integrated ceramic filter offers an alternative implementation to an on-chip active filtering, with trade-offs in terms of size, loss performance, power consumption and dynamic range. One of the advantages of this configuration is that it can be integrated on the substrate where the MMIC module is mounted without any assembly efforts. The LTCC process uses screen printing as well as low-loss stacked via processes and high conductivity metalization useful for high frequency applications. The substrate material is the 3.7 mil thick 951 stackable ceramic tape from Dupont. The metalization of the buried layers is a 7 μm thick silver alloy and the surface metalization is a 7 μm wire bondable electroplated gold. A familiar implementation of the distributed filter uses cascaded edge-connected quarter wavelength coupled-lines [154]. The Conventional version of such a filter cascades the coupled line segments laterally on a single layer circuit board. Implementation of the filter in a strip line topology is desirable because it allows component placement on the surface layer to be in the same location as the filter is the x-y direction. This would have been impossible if the filter were implemented in microstrip configuration. The two strip line ground planes are physically connected by vias. To allow on wafer characterization using air coplanar probes, the input and output have to be on the same layer that requires a good strip line to CPW transition that exhibits additional parasitic mechanisms.

The actual input and output are connected to the RF amplifier and driver amplifier, respectively, from an MMIC transmitter chip sets via wire bonds. The three coupled-line filter segments are located 4 layers away from the top and bottom strip line ground plane. Figure 7.7 depicts a cross-section of the LTCC tape stack-up, showing the eight layers used to create a strip line environment. This is a balanced strip line topology in which the coupled line segments are sandwiched by two ground planes at an equal distance of 14.8 mils (four tape layers) as shown in Figure 7.7.

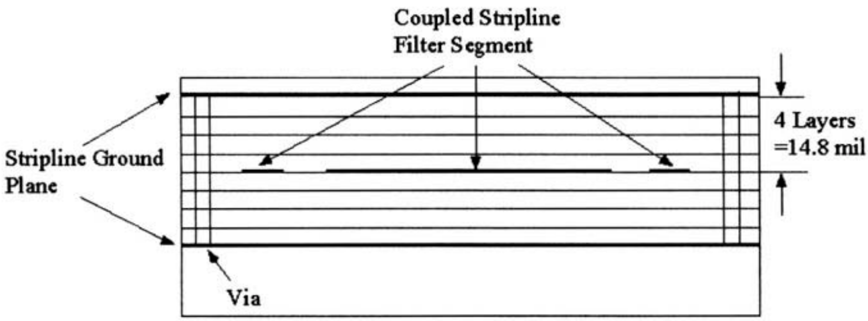

Figure 7.7. Cross-sectional view of a folded edge-coupled line filter.

The first and third segments of the selected filter E have dimensions of coupled line length, width, and gap of 68, 7, and 6 mils, respectively. The second segment has dimensions of 80, 6, and 18 mils, respectively. The coupled line segments were deployed in z-coordinator instead of in a straight-line fashion to minimize space. In this design, for the on wafer characterization using air coplanar probes, the input and output are connected to the top layer using via process.

7.2.3 Measured Performance

Figure 7.8 shows the measured insertion loss and return loss of the filter E from frequency range of 10 to 20 GHz. This filter exhibits a maximum insertion loss of 3 dB from 14.0 to 14.5 GHz with the corresponding return loss as high as 20 dB at 14.5 GHz. For a double conversion VSAT scheme where the IF frequency is at 1 GHz, the filter rejection at the image frequency of 12 GHz and at the LO frequency of 13 GHz is about 28 dB, 20 dB, respectively. An improved return loss is expected by adding a 50-ohm strip line segment as an interface, connected by a tapered line segment to the input and the output of the filter to allow for a better impedance match. Table 5.2 summarized the performance of the measured coupled strip line filter E used for transmitter module implementation.

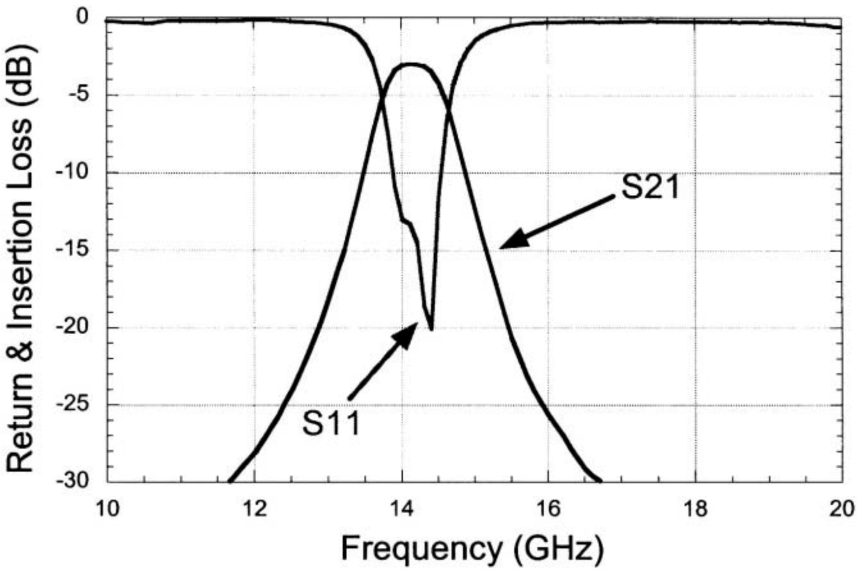

Figure 7.8. Measurement result of Ku-band filter.

Table 5.1. Summary of coupled strip line filter measured performance.

Specifications	Measured Performance
Center Frequency (GHz)	14
Insertion Loss (dB)	3
Return Loss (dB)	20
3-dB bandwidth (MHz)	1000
Q	26

7.3 Module Design

A photograph of a implemented LTCC 951 coupon including four different completed transmitter modules and eight different test structures for coupled strip line BPF is shown in Figure 7.9. The two MMICs were wirebonded on the multi-layer LTCC substrate.

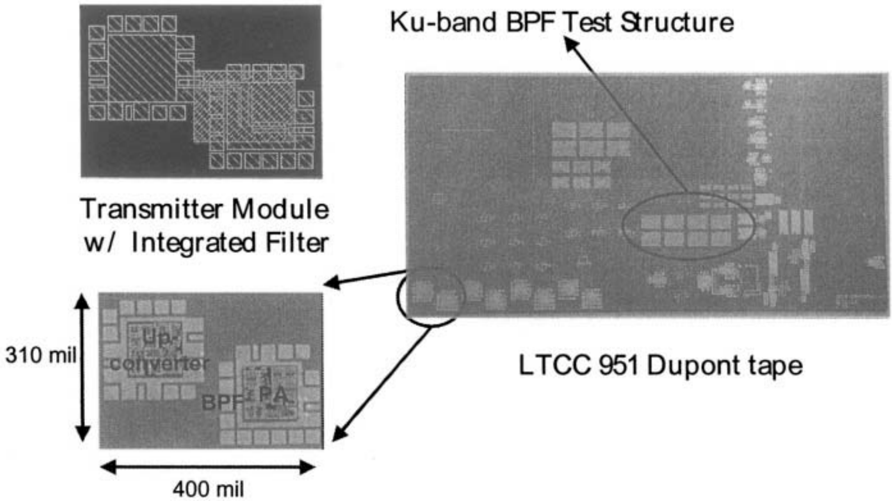

Figure 7.9. Photograph of the implemented LTCC coupon including four transmitter modules and eight test structures for BPF.

Figure 7.10 depicts the three-dimensional exploded view of the LTCC module in which the MMIC chips were wire-bonded on the surface. This module occupies a compact area of $400 \times 310 \times 35.2$ mil^3 as shown in Figure 7.9. The length of the wirebond is approximately 40 mils. The estimated loss of 40 mils ball crescent bond wires incorporated in the module at 14 GHz is 2 dB [156]. The filter ground planes were properly connected to the ground pads on the surface layers that are wire-bonded to the ground pads on the MMICs. Also as shown in Figure 7.10, the filter input was transitioned to the CPW line wire-bonded to the output of the RF amplifier while the output transition to CPW was wire-bonded to the input of the driver amplifier. Such configuration where the filter is integrated between the mixer and PA was chosen to eliminate the mixer harmonics and thereby improve the linearity of the transmitter. The transition to CPW also enables separate measurement of the filter.

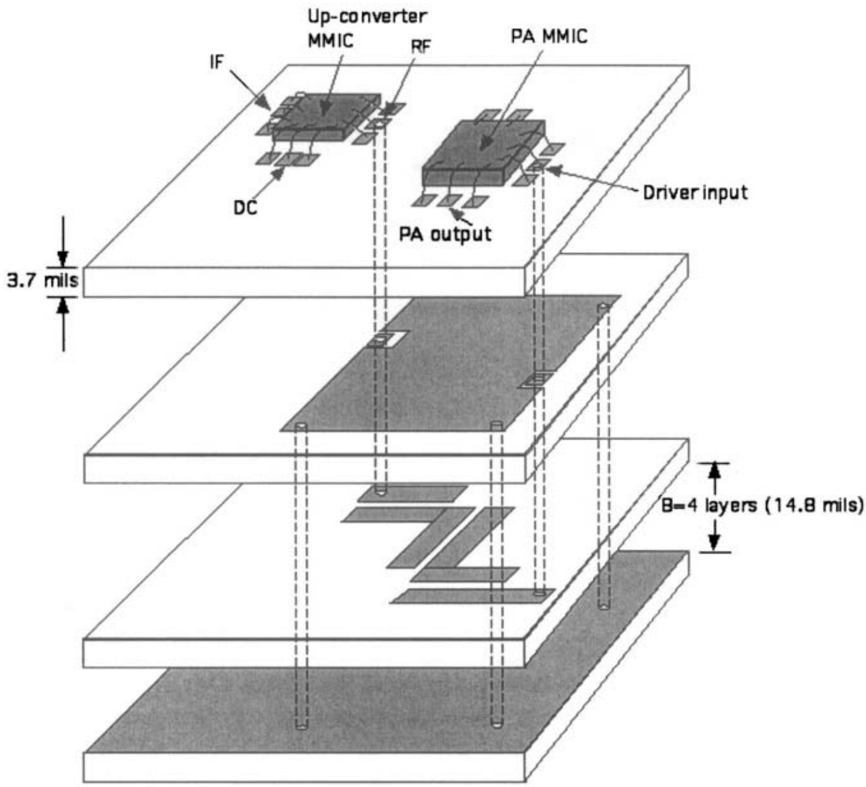

Figure 7.10. Exploded diagram of the transmitter module.

7.4 Module Measurement Results

Figure 7.11 shows the double conversion transmitter block diagram and output spectrum at the output of each block. The LO and image signal is attenuated after the BPF in the transmitter chain. Figure 7.12 shows the measured overall system gain performance with filter characteristics. The entire transmitter chain exhibits a total conversion gain of 41 dB and output power of 26 dBm incorporating the filter and wirebond losses from 14 GHz to 14.5 GHz and LO rejection of 20 dBc as well as image rejection of more than 40 dBc. Measurements were made on-wafer using a coplanar probe station, a network analyzer and a spectrum analyzer.

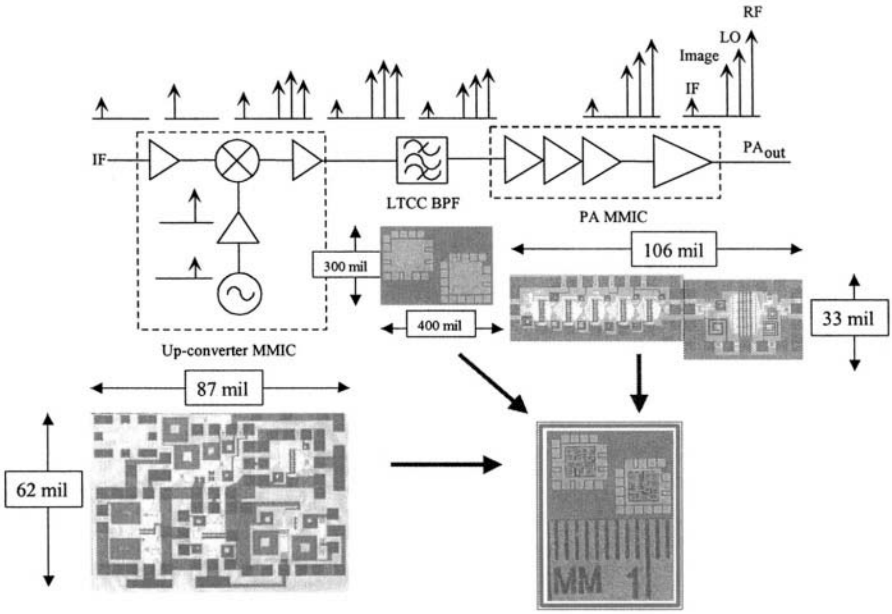

Figure 7.11. Double conversion transmitter block diagram with output spectrum at each block.

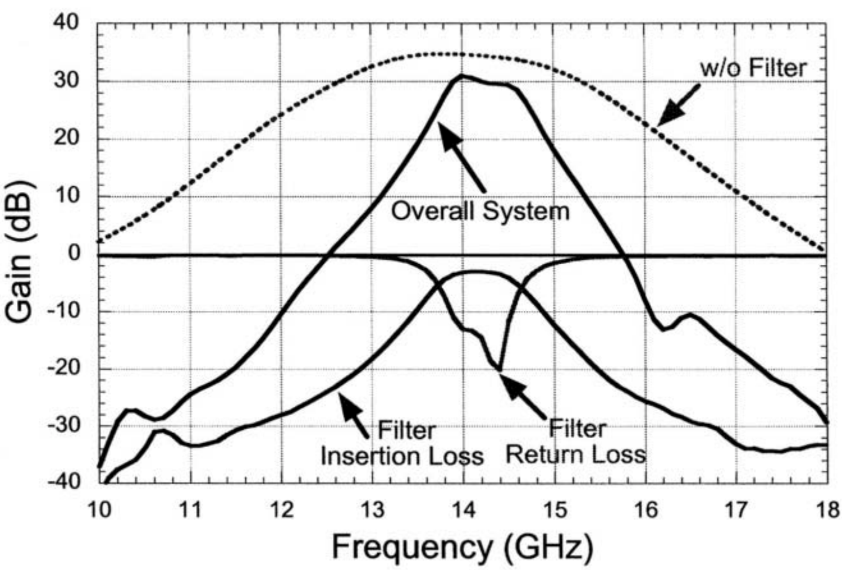

Figure 7.12. Overall system gain performance with filter characteristics.

Figure 7.13 shows the output spectrum of up-converter for a data rate of 4 Mbps and 16 Mbps, respectively. The operability for Ku-band application requires an output power of more than 24 dBm [22]. Spectrum mask for Ku-band system [22] requires relative power spectrum levels of -9, -16 , -26 dB at 0.3R , 0.35R , 0.5R frequency offsets from the center frequency, where R is defined as the bit rate entering the modulator. Measurement results of the chipset indicate that the output spectrum of the developed module fits well within the specified spectrum mask for the data rates of 64, 128, 192, and up to 32 Mbps as shown in Figure 7.14, making it suitable for satellite outdoor units. ACPR analysis has been performed to estimate the power leakage between adjacent channels due to RF front-end nonlinearities. There are 6 channels within the 210 MHz band as per DBS standard [22], hence the adjacent channels are taken to be 41 MHz apart from each other. Measured performance of chipset indicated an ACPR of 42 dB for the transmitter module with a data rate of 32 Mbps as shown in Figure 7.15.

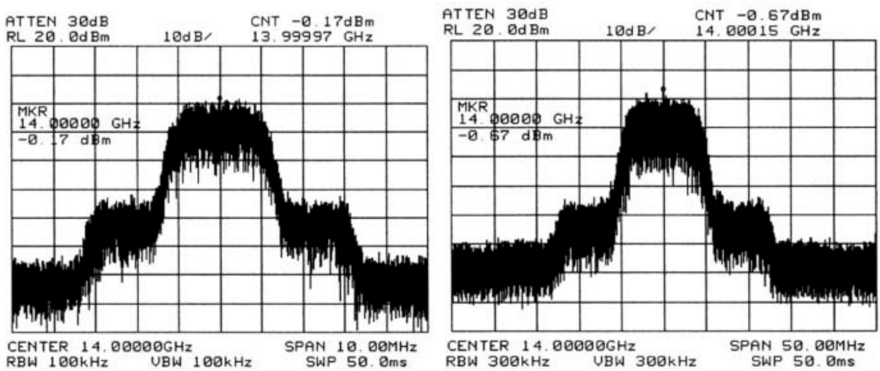

(a) (b)

Figure 7.13. Output power spectrum from up-converter with QPSK modulation (a) 4 Mbps QPSK Modulation, (b) 16 Mbps QPSK Modulation

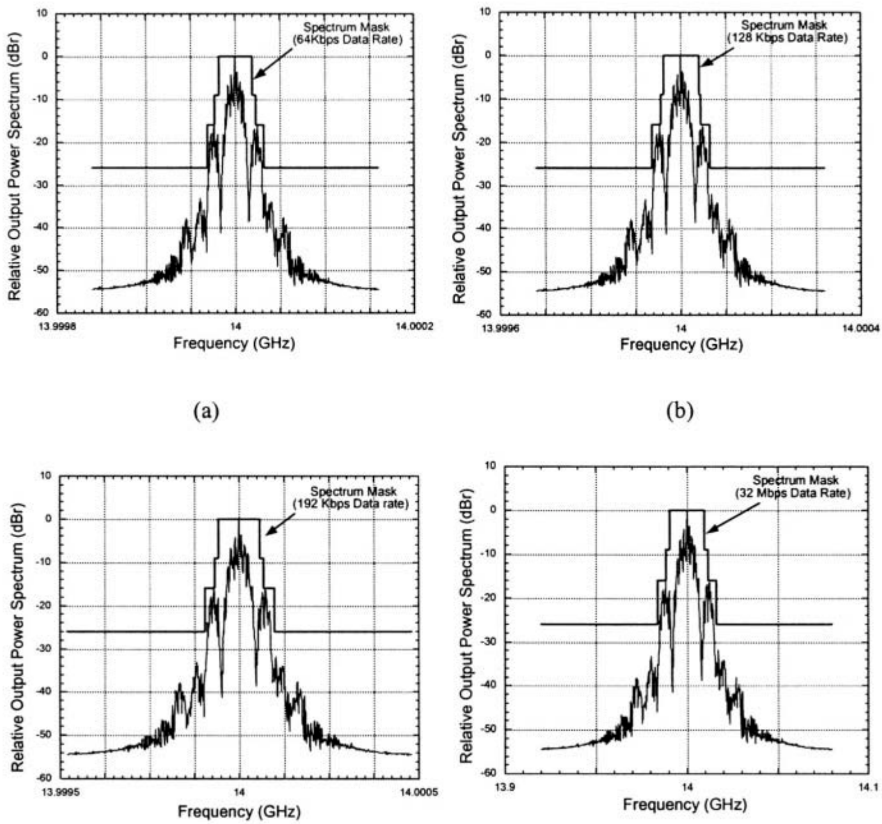

(a) (b) (c) (d)

Figure 7.14. Output power spectrum with the spectrum mask (a) 64 Kbps (b) 128 Kbps (c) 192 Kbps (d) 32 Mbps

Figure 7.16 shows the measured system level diagram and 1-dB power compression performance of the entire transmitter chain based on the measurement of each transmitter blocks. These results demonstrate good agreement with the system simulation results from the developed transmitter system model described in Chapter 3.

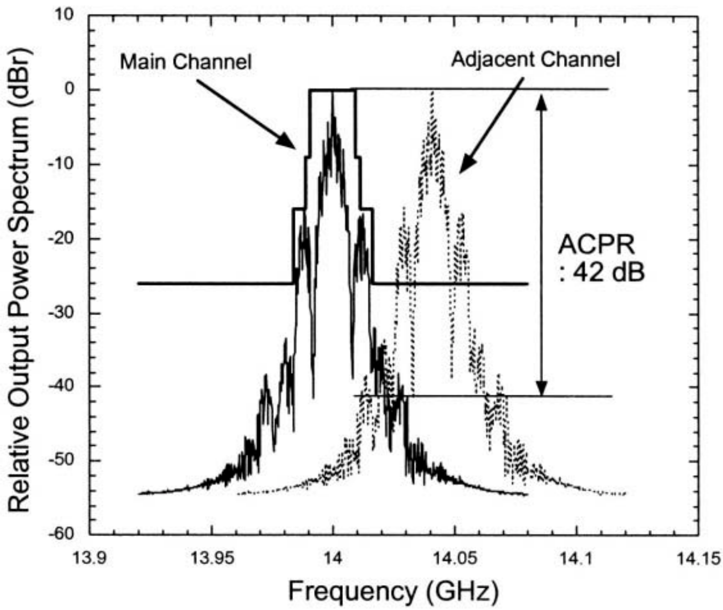

Figure 7.15. ACPR with 32 Mbps data rate.

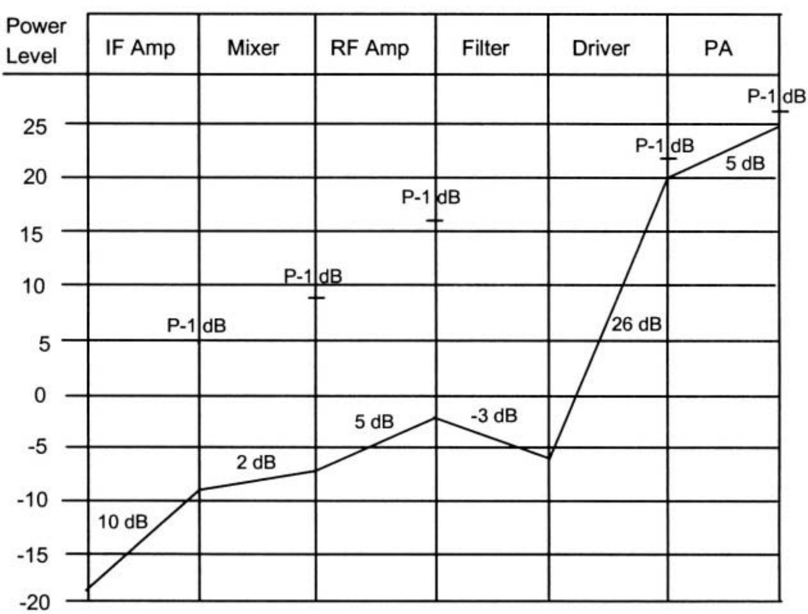

Figure 7.16. Measured link budget and power compression performance.

7.5 Conclusion

This book has presented the first demonstration of a compact LTCC-based transmitter module with functional MMICs, which consist of VCO-mixer and PA implemented in a commercial GaAs MESFET technology. The up-converter MMIC demonstrated the conversion gain of 15 dB and IIP3 of 15 dBm. The PA MMIC exhibits the total gain of 31 dB and 1-dB compressed output power of 26 dBm. The compact module was made possible by embedding the filter and thereby reducing the size of the area required by 40 % compared to such a module implemented on a typical alumina substrate. The integrated strip line filter inserted between the mixer and the PA demonstrates a low insertion loss of 3 dB from 14 to 14.5 GHz. The transmitter module exhibits the total conversion gain of 41 dB and output power of 26 dBm incorporating wirebond and filter losses. Measured performance of the chipsets indicates that the output power spectral density at various data rates conforms to the spectral mask specification, thereby proving the applicability of the developed transmitter module in the Ku-band satellite communication standard. This ultra-compact module is an attractive solution for low-cost Ku-band satellite outdoor units.

This page intentionally left blank

Chapter 8

Conclusion

This book presented a Ku-band transmitter behavioral system model development and the first demonstration of a compact LTCC-based transmitter module to reduce cost and complexity with functional MMICs that consist of a VCO-mixer and a PA implemented in a commercial GaAs MESFET technology.

An accurate Ku-band transmitter system simulation model has been developed with a commercial CAD tool. The system model provides an efficient way to design and to implement the transmitter module for satellite communication application. The developed simulation model can be used to study the transmitter topologies for a satellite communication system, to determine the critical design criteria for each building block in order to enhance overall system performance, and to anticipate the overall system performance accurately prior to the actual system development. This model has been verified with physical transmitter output spectrum and overall transmitted gain measurements.

An ultra-compact transmitter module, incorporated with functional MMICs and an embedded BPF, has been developed in a commercial GaAs MESFET and LTCC technologies. The two MMICs were wirebonded on the multi-layer LTCC substrates, where a coupled strip line BPF is embedded. The LTCC module is composed of 10 layers of Dupont 951 fired ceramic. This module occupies a compact area of $400 \times 300 \times 35.2$ mil^3.

The up-converter MMIC demonstrated the conversion gain of 15 dB and IIP3 of 15 dBm. The PA MMIC exhibits the total gain of 31 dB and 1-dB compressed output power of 26 dBm. The compact module was made possible by embedding the filter and thereby reducing the size of the area required by 40 % compared to such a module implemented on a typical alumina substrate as shown in Figure 8.1.

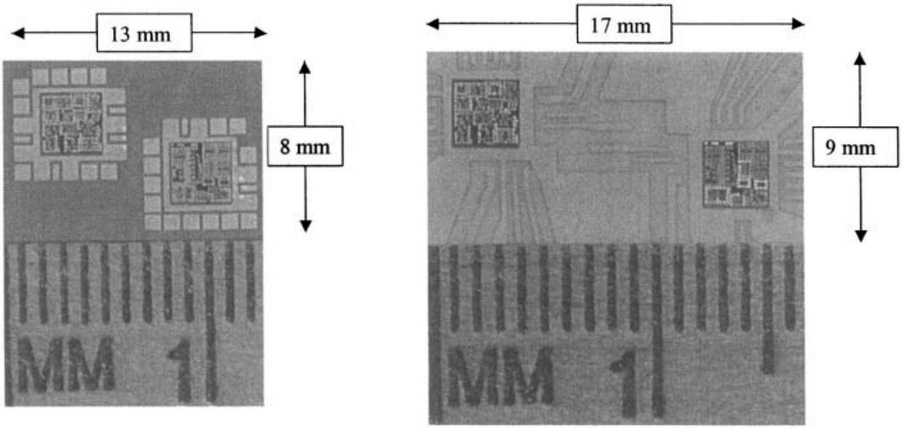

Figure 8.1. Comparison of LTCC module vs. typical alumina module.

The integrated strip line filter inserted between the mixer and the PA demonstrates a low insertion loss of 3 dB. The transmitter module exhibits the total conversion gain of 41 dB and output power of 26 dBm incorporating wirebond and filter losses. Table 6.1 summarizes the overall transmitter performance. Measured performance of the MMIC chipsets indicate that the output power spectral density at various data rates conforms to the spectral mask specification, thereby proving the applicability of the developed transmitter module in the Ku-band satellite communication standard. This ultra-compact module is an attractive solution for low-cost Ku-band satellite outdoor units.

Table 8.1. Transmitter module system performance at 14 GHz, with a LO (13 GHz) power of 7 dBm and an IF (1GHz) power of -15 dBm.

Specifications	Measured Performance
Up-conversion Gain (dB)	41
Output P1dB (dBm)	26
3dB Bandwidth (MHz)	600
LO Rejection (dB)	13
Image Rejection (dB)	40
Data Rates (Mbps)	32
ACPR (dB)	42

Bibliography

[1] http://www.comsoc.org/socstr/techcom/ssc.

[2] B. R. Elber, *Introduction to Satellite Communication*, Artech House, Boston, 1999.

[3] B. G. Evans, *Satellite Communication Systems*, Institute of Electrical Engineers, London, 1999.

[4] M. A. Sturza, and F. Ghazvinian, "The Teledesic Satellite System," *Telesystems Conference Proceedings*, pp. 123 -126, 1994.

[5] J. V. Evans, "Proposed U.S. Global Satellite Systems Operating at Ka-Band," *IEEE Aerospace Conference*, vol. 4, pp. 525-537, 1998.

[6] J. B. Shealy, and et al., "A 2 Watt Ku-band Linear Transmit Module for VSAT Applications," *IEEE MTT-S Digest,* vol. 2, pp. 1055-1058, 1999.

[7] Ge Zhiqiang, "A Downsized and Integrated C-band Transceiver for VSAT," *1995 IEEE Microwave and Optoelectronics Conference*, vol. 1, pp. 33-36, 1995.

[8] W. Simon, R. Kulke, A. Wien, M. Rittweger, L. Wolff, A. Girard, and J.-P. Bertinet, "Interconnects and Transitions in Multilayer LTCC Multichip Modules for 24 GHz ISM-band Applications," *2000 IEEE MTT-S International Digest*, vol.2, pp. 1047-1050, Boston, MA.

[9] K. Fujii, Y. Hara, Y. Shibuya, T. Sakai, and Y. Takano, "Highly Integrated T/R Module for Active Phased Array Antennas," *1998 IEEE RFIC Digest*, pp. 77-80, Baltimore, MD.

[10] J. W. Gipprich, L. E. Dickens, and J. A. Faulkner, "Power Amplifier Yields 10 Watts over 8-14 GHz Using GaAs MMICs in an LTCC Serial Combiner/Divider Network," *1993 IEEE MTT-S International Digest*, vol. 3, pp. 1369-1372, Atlanta, GA.

[11] A. Sutono, J. Laskar, and W. R. Smith, "Development of Three Dimensional Integrated Bluetooth Image Reject Filter," *IEEE MTT-S International Digest*, vol.1, pp. 339-342, Boston, MA, June 2000.

[12] J. A. Lester, M. Ahmadi, S. Peratoner, J. Hathaway, D. Garske, P. D. Chow, "Low Cost Miniaturized EHF SATCOM Transceiver Featuring HEMT MMICs and LTCC Multilayer Packaging," *IEEE Microwave and Millimeter-Wave Monolithic Circuits Symposium Digest*, pp. 35–38, 1995.

[13] C.-H. Lee, A. Sutono, S. Han, and J. Laskar, "A Compact LTCC Ku-Band Transmitter Module with Integrated Filter for Satellite Communication Applications," *IEEE MTT-S International Microwave Symposium*, vol. 2, pp. 945-948, Phoenix, AZ, June 2001.

[14] M. C. Comparini, M. Feudale, and A. Suriani, "MMICs for Commercial Satellite Applications," *27th European Microwave Conference and Exhibition*, vol. 2, pp. 1198-1206, 1998.

[15] A. Bellaouar, "RF Transmitter Architectures for Integrated Wireless Transceivers," *The Eleventh International Conference on Microelectronics*, pp. 25–30, 2000.

[16] Behzad Razavi, *RF Microelectronics*, Prentice Hall, NJ, 1998.

[17] J. B. Shealy, and et al., "GaAs MMIC Frequency Upconverters for Satellite Applications," *IEE Colloquium on Recent Advances in Microwave Sub-Systems for Space and Satellite Applications*, pp. 2/1-2/5, 1993.

[18] A. Sabban, A. Shapir, and D. Behar, "A Ka-band Compact Integrated Transmitter for VSAT Satellite Communication Ground

Terminal," *27th European Microwave Conference and Exhibition,* vol. 2, pp. 671 -675.

[19] S. B. Cohn, "An Overview of Transceiver Structures for Advanced Wireless Personal Communication Systems (PCS)," *Proceedings on IEEE Asia Pacific Conference on Circuits and Systems*, pp. 255 - 262, Nov. 1996.

[20] T. Yamawaki, and et al., "A 2.7-V GSM RF transceiver IC," *IEEE Journal of Solid State Circuits,* vol. 32, pp. 2089 -2096, Dec. 1997.

[21] J. C. Rudell, O. Jia-Jiunn, and et al., "Recent Developments in High Integration Multi-Standard CMOS Transceivers for Personal Communication Systems," *Proceedings of 1998 International Symposium on Low Power Electronics and Design*, pp. 149-154, 1998.

[22] INTELSAT Earth Station Standards (IESS) Document IESS-208.

[23] Thomas H. Lee, *The Design of CMOS Radio-Frequency Integrated Circuits*, Cambridge University Press, 1998.

[24] Lawrence E. Larson, *RF and Microwave Circuit Design for Wireless Communications*, Artech House, 1996.

[25] George D. Vendelin, Anthony M. Pavio, and Ulrich L. Rohde, *Microwave Circuit Design using Linear and Nonlinear Techniques*, Johns Wiley & Sons, 1990.

[26] Kevin W. Kobayashi, Liem T. Tran, Mike Lammert, Tom R. Block, Aaron K. Oki, and Dwight C. Streit, "A Novel 12-24GHz Broadband HBT Distributed Active Balanced Mixer," *IEEE Radio Frequency Integrated Circuits Symposium*, pp. 75-78, 1997.

[27] Dennis A. Kruger, "Monolithic Dual-Quadrature Mixer Using GaAs FETs," *Microwave Journal*, pp. 201-206, September 1990.

[28] R. Plana, and L. Escotte, "Noise Properties of Microwave Heterojunction Bipolar Transistors," *Proc. 21st International Conference on Microelectronics*, vol. 1, pp. 215-222, Sep. 1997.

[29] Van De Roer, *Microwave Electronic Devices*, Chapman & Hall 1994.

[30] D.L. Harame, and et al., "A 200 mm SiGe HBT Technology for Wireless and Mixed Signal Applications," *International Electron Devices Meeting, Technical Digest*, pp. 437-440, 1994.

[31] K. Strohm, and et al., "Si/SiGe MMICs," *IEEE Trans. on Microwave Theory and Techniques*, vol. 43, no. 4, April 1995.

[32] L. Treitinger, and et al., "Silicon Technologies for RF Integrated Circuits," *IEEE Eurocomm, Information Systems for Enhanced Public Safety and Security*, pp. 398-399, 2000.

[33] M. Case, S. A. Maas, L. Larson, D. Rensch, D. Harame, and B. Meyesrson, "An X-band Monolithic Active Mixer in Si-Ge HBT Technology," *IEEE MTT-S International Microwave Symposium*, pp. 655-658, 1996.

[34] Michael Case, "SiGe MMICs and Flip-chip MICs for Low-cost Microwave Systems," *IEEE Radio Frequency Integrated Circuits Symposium*, pp. 117-120, 1997.

[35] A. Schuppen, H. Dietrich, S. Gerlach, H. Hohnemann, J. Arndt, U. Seiler, R. Gotzfried, U. Erben, and H. Schumacher, "SiGe Technology and Components for Mobile Communication Systems," *Proc. of the Bipolar/BiCMOS Circuits and Technology*, pp. 130-133, 1996.

[36] O. Kurita, and K. Morita, "Microwave MESFET Mixer," *IEEE Trans. on Microwave Theory and Techniques*, vol. 24, pp. 361-366, Jun. 1976.

[37] S. A. Mass, "Design and Performance of a 45GHz HEMT Mixer," *IEEE Trans. on Microwave Theory and Techniques*, vol. 34, pp. 799-803, 1986.

[38] S. Weiner, and et al., "2 to 8GHz Double Balanced MESFET Mixer with 30dBm Input 3rd Order Intercept," *IEEE MTT-S International Microwave Symposium*, pp. 1097-1100, 1988.

[39] T. H. Chen, K. W. Chang, S. B. T. Bui, L. C. T. Liu and S. Pak, "A Double Balanced 3-18GHz Resistive HEMT Monolithic Mixer," *IEEE Microwave and Millimeter-Wave Monolithic Circuits Symposium*, pp. 167-170, 1992.

[40] C. S. Wu, C. K. Pao, W. Tau, H. Kanber, M. Hu, S. X. Bar, A. Kurdoghlian, Z. Bardai, D. Bosch, C. Seashore, and M. Gawronski, "Pseudomorphic HEMT Manufacturing Technology for Multifunctional Ka-band MMIC Applications," *IEEE Transactions on Microwave Theory and Techniques*, vol. 43, No. 2, pp. 257-266, Feb. 1995.

[41] I. D. Robertson, *MMIC Design*, Institute of Electrical Engineers, UK, 1995.

[42] Stephen A. Maas, *Nonlinear Microwave Circuits*, Artech House, 1988.

[43] John A. Eisenberg, Jeffrey S. Paneli, and Weiming Ou, "Slotline and Coplanar Waveguide Team to Realize a Novel MMIC Double Balanced Mixer," *Microwave Journal*, pp.123-131, September 1992.

[44] S. A. Maas, and K. W. Chang, "A Broadband, Planar, Doubly Balanced Monolithic Ka-band Diode Mixer," *IEEE Microwave and Millimeter-Wave monolithic circuits symposium*, 1993.

[45] Y. I. Ryu, K. W. Kobayashi, and A. K. Oki, "A Monolithic Broadband Doubly Balanced EHF HBT Star Mixer with Novel Microstrip Baluns", IEEE MTT-S International microwave Symposium, *IEEE MTT-S International Digest*, vol. 1, pp. 119-122, 1995.

[46] Stephen A. Maas, *Microwave Mixers*, Artech house 1993.

[47] Hwann-Kaeo Chiou, and Hao-Hsiung Lin, "A Miniature MMIC Double Doubly Balanced Mixer Using Lumped Dual Balun for High Dynamic Receiver Application," *IEEE Microwave and Guided Wave Letters*, vol. 7, No. 8, pp.227-229, Aug. 1997.

[48] Reza Majidi-Ahy, Cliff Nishimoto, Jeff Russell, Weiming Ou, Steve Bandy, and George Zdasiuk, "23-40 GHz InP HEMT MMIC Distributed Mixer," *IEEE Microwave and Millimeter-Wave monolithic Circuits Symposium*, pp. 201-204, 1992.

[49] P. Bura, and R. Dikshit, "FET Mixer with the Drain LO Injection," *IEEE Electron Letter*, vol. 12, no. 20, pp. 536, Sep. 1976.

[50] M. Madihian, L. Desclos, K. Maruhashi, K. Onda, and M. Kuzuhara, "A K-band Monolithic CPW Upconverter Utilizing a Source Mixing Concept," *IEEE MTT-S International Microwave Symposium*, pp. 127-130, 1995.

[51] J. Michael Golio, *Microwave MESFETs & HEMTs*, Artech House, 1991.

[52] R.A. Pucel, D. Masse, and R. Bera, "Performance of GaAs MESFET mixers at X-band," *IEEE Transactions on Microwave Theory and Techniques*, vol. 24, pp. 351, Jun. 1976.

[53] C.C. Penalosa, and C. Aichison, "Analysis and Design of Ka-band MESFET Gate Mixer," *IEEE Transactions on Microwave Theory and Techniques*, vol. 35, pp. 643, Jul. 1987.

[54] G. Tomassetti, "An Unusual Microwave Mixer," *Proc. European Microwave Conference*, pp. 754, 1986.

[55] V. Brady, T. Hsu, R, Reeves, and M. Vermeulen, "Development of a Monolithic FET Single Side Band Upconverter and Image Reject Downconverter", *IEEE GaAs IC Symposium Digest*, pp. 189-192, Oct. 1989.

[56] W. R. Brinlee, A. M. Pavio, C. L. Goldsmith, and W. J. Thompson, "A Monolithic Multifunction EW Broadband Receiver Converter," *IEEE GaAs IC Symposium Digest*, pp. 207-210, Oct. 1993.

[57] T. Hirota, and M. Muraguchi, "A K-band Frequency Upconverters Using Reduced Size Couplers and Dividers," *IEEE GaAs IC Symposium Digest*, pp. 53-56, Oct. 1991.

[58] A. Minakawa, and T. Hirota, "An Extremely Small 26GHz Monolithic Image-Rejection Mixer without DC Power Consumption," *IEEE Transactions on Microwave Theory and Techniques*, vol. 41, pp. 1634-1637, Sep. 1993.

[59] R. Michels, P. Wallace, R. Goyal, N. Scheinberg, and M. Patel, "A High-Performance, Minimized X-band Active Mixer for DBS Receiver Application with On-Chip IF Noise Filter," *IEEE Transactions on Microwave Theory and Techniques*, vol. 38, no. 9, pp. 1249-1251, Sep. 1990.

[60] Howard Fundem, Sanjay Moghe, and Greg Dietz, "A Highly Integrated Wideband Millimeter-Wave MMIC Converter Using 0.25-um p-HEMT Technology," *IEEE Journal of Solid-State Circuits*, vol. 28, no. 10, pp. 1001-1004, Oct. 1993.

[61] A. Y. Umeda, C. T. Matsuno, A. K. Oki, G. S. Dow, K. W. Kobayashi, D. K. Umemoto, and M. E. Kim, "A Monolithic GaAs HBT Upconverter," *IEEE Microwave and Millimeter-Wave monolithic Circuits Symposium*, pp.77-80, 1990.

[62] H. Yang, K. W. Angel, and K. N. Fry, "A Single-Chip K-band Receiver," *IEEE GaAs IC Symposium*, pp. 57-60, 1991.

[63] C. Licqurish, M. J. Howes, and C. M. Snowden, "Dual-gate FET Modeling," *IEE Colloquium on Microwave Devices, Fundamentals and Applications*, pp. 2/1-2/7, 1998.

[64] C. Tsironis, R. meierer, and R. Stahlmann, "Dual-Gate Mixers," *IEEE Transactions on Microwave Theory and Techniques,* vol. 32, no. 3, pp. 248-255, Mar. 1984.

[65] C. Tsironis, and R. Meierer, "Microwave Wide-Band Model of GaAs Dual Gate MESFETs Dual-Gate Mixers," *IEEE Transactions on Microwave Theory and Techniques,* vol. 32, no. 3, pp. 243-251, Mar. 1982.

[66] A. M. Pavio and R. H. Halladay, "A Distributed Double-Balanced Dual-Gate FET Mixer," *IEEE GaAs IC Symposium,* pp. 177-180, 1998.

[67] Kevin W. Kobayashi, Robert Kasody, and Aaron K. Oki, "A 5-10GHz Octave-Band AlGaAs/GaAs HBT Down-Converter MMIC," *IEEE GaAs IC Symposium*, pp. 249-252, 1995.

[68] Klas Yhland, Niklas Roesman, and Herbert H. G. Zirath, "Novel Single Device Balanced Resistive HEMT Mixers," *IEEE Transactions on Microwave Theory and Techniques*, vol. 43, no. 12, pp. 2863-2867, Dec. 1995.

[69] Yoshihiro Konishi, "GaAs Devices and the MIC Applications in Satellite Broadcasting," *IEEE Microwave and Millimeter-Wave Monolithic Circuits Symposium*, pp. 1-6, 1990.

[70] S. A. Mass, "A GaAs MESFET Mixer with Very Low Intermodulation," *IEEE Transactions on Microwave Theory and Techniques*, vol. 35, pp. 425-429, 1987.

[71] T. H. Chen, K. W. Chang, S. B. T. Bui, L. C. T. Liu, G. S. Dow, and S. Pak, "Broadband Single- and Double-Balanced Resistive HEMT Mixers," *IEEE Transactions on Microwave Theory and Techniques*, vol. 43, no. 3, pp. 477-484 Mar. 1995.

[72] H. Zirath, C.-Y. Chi, N. Rorsman, C. Karlsson, and R. Weikle, "A 40GHz Integrated Quasi Optical Slot HFET Mixer," *IEEE Transactions on Microwave Theory and Techniques*, vol. 42, pp. 2492-2497, 1994.

[73] Kevin W. Kobayashi, Liem T. Tran, Stacey Bui, Aaron K. Oki, Dwight C. Streit, and Mark Rosen, "InAlAs/InGaAs HBT X-Band Double-Balanced Upconverter," *IEEE Journal of Solid-State Circuits*, vol. 29, no. 10, pp. 1238-1243, Oct. 1994.

[74] Kevin W. Kobayashi, "A Novel HBT Active Transformer Balanced Schottky Diode Mixer," *IEEE MTT-S International Microwave Symposium*, pp. 947-950, 1996.

[75] A. P. Freundorfer and C. Falt, "A Ka-band GaInP/GaAs HBT Double Balanced Upconverter Mixer Using Lumped Element Balun," *IEEE MTT-S International Microwave Symposium*, pp. 963-966, 1996.

[76] I. D. Robertson and A. H. Aghavami, "A Compact X-band Monolithic Balanced FET Mixer," *IEEE/ESTEC European GaAs Applications Symposium Digest*, Apr., 1992.

[77] Ma. L. de la fuente, J. Portilla, J. P. Pascual, and E. Artel, "Low-Noise Ku-band MMIC Balanced p-HEMT Upconverter," *IEEE Journal of Solid-State Circuits*, vol. 34, no. 2, pp. 259-263, Feb. 1999.

[78] D. L. Ingram, L. Sjogren, J. Kraus, M. Nshimoto, M. Siddiqui, S. Sang, K. Cha, M. Huang, and R. Lai, "A Highly Integrated Multi-Functional Chip Set for Low Cost Ka-band Transceiver," *IEEE Radio Frequency Integrated Circuits Symposium*, pp. 227-230, 1998.

[79] S. Hori, and et al., "GaAs Monolithic MIC's for Direct Broadcast Satellite Receivers," *IEEE Transactions on Microwave Theory and Techniques*, vol. 31, no. 12, pp. 1089-1096, 1983.

[80] H. Honjo, and et al., "X-band Low-Noise GaAs Monolithic Frequency Converter," *IEEE Transactions on Microwave Theory and Techniques*, vol. 33, no. 11, pp. 1231-1235, 1985.

[81] E. M. Bastida, and et al., "Air Bridge Gate FET for GaAs Monolithic Circuits," *IEEE Transactions on Microwave Theory and Techniques*, vol. 33, no. 12, pp. 1585-1590, 1985.

[82] N. Ayaki, and et al., "A 12GHz-Band Monolithic HEMT MMIC Low-Noise Amplifier," *IEEE GaAs IC Symposium*, pp. 101-104, 1988.

[83] T. Mekata, and et al., "Very Small BS Converter Module," *IEICE Technical Reports*, MW89-26, 1989.

[84] Nobuo Shiga, Takeshi Sekiguchi, Shigeru Nakajima, Kenji Otobe, Nobuhiro Kuwata, Ken-ichiro Matsuzaki, and Hideki Hayashi, "MMIC Family for DBS Down-Converter with Pulse-Doped GaAs MESFETs," *IEEE Journal of Solid-State Circuits*, vol. 27, no. 10, pp. 1413-1420, Oct. 1992.

[85] Bernard A. Xavier, and Colin S. Aitchison, "The Measured and Predicted Noise Figure of a GaAs Heterojunction Bipolar Transistor Mixer," *IEEE Radio Frequency Integrated Circuits Symposium*, pp. 135-138 1997.

[86] B.A. Xavier, and C.S. Aitchison, "Simulation & Modeling of a HBT Mixer," *IEEE MTT-S International Microwave Symposium*, pp. 333-336, 1992.

[87] A. P. Freundorfer, "A Ka-band GaInP/GaAs HBT Double Balanced Downconverter Mixer Using Lumped Element Balun," *IEEE Antenna and Propagation Society International Symposium*, vol. 1, pp. 578-581, 1997.

[88] Kevin W. Kobayashi, Robert Kasody, Aaron K. Oki, and Dwight C. Streit, "A 5-10GHz Octave-Band AlGaAs/GaAs HBT-Schottky Diode Down-Converter MMIC," *IEEE Journal of Solid State Circuits*, vol. 31, no. 10, pp. 1412-1418, Oct. 1996.

[89] K. W. Kobayashi, R. Kasody, A. K. Oki, G. S. Dow, B. Allen, and D. C. Streit, "A Double-double Balanced HBT Schottky Diode Broadband Mixer at X-Band," *IEEE GaAs IC Symposium*, pp. 315-318, 1994.

[90] W. Durr, U. Erben, A. Schuppen, H. Dietrich, and H. Schumacher, "Low-Power Low-Noise Active Mixers for 5.7 and 11.2 GHz Using Commercially Available SiGe HBT MMIC Technology," *IEEE Electronics Letters*, pp. 1994-1996, vol. 34, no. 21, Oct. 1998.

[91] P. Weger, G. Schultes, L. Treitinger, E. Bertagnolli, and K. Ehinger, "Gilbert Multiplier as an Active Mixer with Conversion Gain bandwidth of up to 17GHz," *IEEE Electronics Letters*, vol. 27, pp. 570-571, 1991.

[92] Jack Glenn, Michael Case, David Harame, Bernard Meyerson, and Roger Poisson, "12 GHz Gilbert Mixers using a Manufacturable Si/SiGe Epitaxial-Base Bipolar Technology," *IEEE Proceedings of Bipolar/BiCMOS Circuits and Technology Meeting*, pp. 186-189, 1995.

[93] Virender Sadhir, David Williams, and Inder Bahl, "MMIC Process Fabricates Low-Loss GaAs Downconverter, " *Microwave & RF*, pp. 134-140, March 1992.

[94] R. Goyal, *High-Frequency Analog Integrated Circuit Design*, John Wiley and Sons, 1995.

[95] I. Bahl, and P. Bhartia, *Microwave Solid State Circuit Design*, John Wiley and Sons, New York, 1988

[96] D. B. Lesson, "A Simple Model of Feedback Oscillator Noise Spectrum," *Proceedings of the IEEE*, vol. 54, pp. 329-330, February 1966.

[97] G. D. Venderlin, A. M. Pavio, and U. L. Rohde, *Microwave Circuit Design Using Linear and Nonlinear Techniques*, New York, Wiley, 1990.

[98] M. Prigent, and J. Obregon, "Phase Noise Reduction in FET Oscillators by Low-Frequency Loading and Feedback Circuitry Optimization," *IEEE Transactions on Microwave Theory and Techniques*, vol. MTT-35, pp. 349-352, March 1987.

[99] X. Zhang, D. Sturzebecher, and A. S. Daryoush, "Comparison of the Phase Noise Performance of HEMT and HBT based Oscillators," *IEEE MTT-S International Microwave Symposium,* vol. 1, pp. 697-700, 1995.

[100] Randall W. Rhea, *Oscillator Design and Computer Simulation*, NJ, Prentice Hall, 1990.

[101] J. Obregon, and A. P. S. Khanna, "Exact deviation of the non-linear negative resistance oscillator pulling figure," *IEEE Transactions on Microwave Theory and Techniques*, vol. 30, pp. 1109-1111, July 1982.

[102] Robert Soares, *GaAs MESFET Circuit Design*, Boston, Artech House, 1988.

[103] C. Ansorge, "Bipolar Transistor Ku-band Oscillators with Low Phase-Noise," *IEEE MTT-S International Microwave Symposium Digest*, pp. 91-94, 1986.

[104] A. P. S. Khanna, "Fast-Settling, Low Noise Ku-Band Fundamental Bipolar VCO," *IEEE MTT-S International Microwave Symposium Digest*, pp. 579-581, 1987.

[105] D. A. Boyd, "Low Phase Noise X/Ku-Band VCO," *IEEE MTT-S International Microwave Symposium Digest*, pp. 587-590, 1987.

[106] N. K. Osbrink, "YIG-Tuned Oscillator Fundamentals," *Microwave Systems News*, pp. 207-225, March 1983.

[107] P. Olliver, "Microwave YIG-Tuned Oscillator," *IEEE Journal of Solid-State Circuits*, pp. 54-60, February, 1972.

[108] J. C. Papp, and Y. Koyano, "An 8-18 GHz YIG-Tuned FET Oscillator," *IEEE Transactions on Microwave Theory and Techniques*, vol. 28, pp. 762-767, July, 1980.

[109] Y. Mizunuma, T. Ohgihara, H. Nakano, T. Okamoto, M. Kubota, and Y. Murakami, "X- and Ku-Band YIG-Film Tuned Low Noise Oscillators," *IEEE MTT-S International Microwave Symposium Digest*, pp. 161-164, 1989.

[110] Y. Mizunuma, Y. Murakami, H. Nakano, T. Ohgihara, and T. Okamoto, "A 13 GHz YIG Film Tuned Oscillator for VSAT Applications," *IEEE Transactions on Microwave Theory and Techniques,* vol. 36, pp. 1885-1889, December 1988.

[111] R. Oyafuso, "An 8-18 GHz FET YIG Tuned Oscillator," *IEEE MTT-S International Microwave Symposium Digest*, pp. 183-184, 1979.

[112] Y. Le Tron, S. Barvet, and J. Obregon, "Multioctave FET Oscillators Double Tuned by a Single YIG," *ISSCC Digest of Technical Papers*, pp. 162-163, 1979.

[113] J. Obregon, Y. Le Tron, R. Funk, and S. Barvet, "Decade Bandwidth FET Functions," *IEEE MTT-S International Microwave Symposium Digest*, pp. 141-142, 1981.

[114] B. N. Scott, and G. E. Brehm, "Monolithic Voltage Controlled Oscillator for X- and Ku-Bands," *IEEE Transactions on Microwave Theory and Techniques*, vol. 30, pp. 2172-2177, December 1982.

[115] T. Ohira, M. Muraguchi, T. Hirota, K. Osafune, and M. Ino, "Dual-Chip GaAs Monolithic Integration Ku-Band Phase-Locked-Loop Microwave Synthesizer," *IEEE Transactions on Microwave Theory and Techniques*, vol. 30, pp. 1204-1209, September 1990.

[116] M. G. McDermott, C. N. Sweeney, M. Benedek, J. J. Borelli, G. Dawe, and L. Raffaelli, "Integration of High-Q GaAs Varactor Diodes and 0.25-um GaAs MESFETs for Multifunction Millimeter-

Wave Monolithic Circuit Applications," *IEEE Transactions on Microwave Theory and Techniques*, vol. 38, pp. 1183-1990, September 1990.

[117] M. Muraguchi, and K. Ohwada, "A Ku-Band GaAs Monolithic Voltage Controlled Oscillator," *Transaction on IEICE*, vol. 70, no. 4, pp. 261-263, April 1987.

[118] T. Ohira, M. Muraguchi, T. Hirota, K. Osafune, and M. Ino, "A Ku-Band MMIC PLL Synthesizer," *IEEE MTT-S International Microwave Symposium Digest*, *pp.* 1047-1050, 1989.

[119] T. Ohira, T. Hiraoka, and H. Kato, "MMIC 14-GHz VCO and Frequency Divider for Low-Noise Local Oscillators," *IEEE Transactions on Microwave Theory and Techniques*, vol. 35, pp. 657-662, July, 1987.

[120] J. M. Bunting, C. M. Snowden, M. J. Howes, S. Flynn, G. King, "The Design and Realization of a Fully Monolithic GaAs VCO," *IEE Colloquium on 'Electronically Tunable Microwave Oscillators'*, no. 02, pp. 4/1-4, 1987.

[121] T. Ohira, H. Kato, K. Araki, and F. Ishitsuka, "A Compact Full MMIC Module for Ku-Band Phase-Locked Oscillators," *IEEE Transactions on Microwave Theory and Techniques*, vol. 35, pp. 723-727, April 1989.

[122] E. Reese Jr. and J. M. Beall, "Optimized X & Ku Band GaAs MMIC Varactor Tuned FET Oscillators," *IEEE MTT-S International Microwave Symposium Digest*, pp. 487-490, 1988.

[123] P. J. McNally, T. Smith, F. R. Phelleps, and K. Hogan, "Ku- and K-Band GaAs MMIC Varactor-Tuned FET Oscillators using MEV Ion-Implanted Buried-Layer Back Contacts," *IEEE MTT-S International Microwave Symposium Digest*, pp. 107-110, 1990.

[124] E. Reese Jr., and J. M. Beall, "Optimized X & Ku Band GaAs MMIC Varactor Tuned FET Oscillators," *IEEE MTT-S International Microwave Symposium Digest*, pp. 487-490, 1988.

[125] M. Camiade, and A. Bert, "Wide Tuning Bandwidth Ku-Band Varactor FET Oscillators," *Conference Proceedings - European Microwave Conference*, pp. 413-418, 1985.

[126] A. Dupuis, J. Hausner, and P. Russer, "Hybrid Integrated Ku-Band VCO," *Conference Proceedings - European Microwave Conference*, no. 19, pp. 1009-1014, 1989.

[127] P. Alinikula, R. Kaunisto, and K. Stadius, "Integrating Active Resonators for Wireless Applications," *Microwave Journal,* vol. 38, pp. 106-113, January 1995.

[128] D. K. Adams, and R. Y. C. Ho, "Active Filters for UHF and Microwave Frequencies," *IEEE Transactions on Microwave Theory and Techniques*, vol. 17, pp. 662-670, September 1969.

[129] R. V. Snyder, and D. L. Bozarth, " Analysis and Design of a Microwave Transistor Active Filter," *IEEE Transactions on Microwave Theory and Techniques*, vol. 18, pp. 2-9, January 1970.

[130] E. Fliegler, "Operating Criteria for Active Microwave Inductors," *IEEE Transactions on Microwave Theory and Techniques*, vol. 19, pp. 89-91, January 1971.

[131] S. Hara, T. Tokumitsu, T. Tanaka, and M. Aikawa, "Broad-Band Monolithic Microwave Active Inductor and Its Application to Miniaturized Wide-Band Amplifiers," *IEEE Transactions on Microwave Theory and Techniques*, vol. 36, pp. 1920-1924, December 1988.

[132] S. Hara, T. Tokumitsu, and M. Aikawa, "Lossless Broad-Band Monolithic Microwave Active Inductors," *IEEE Transactions on Microwave Theory and Techniques*, vol. 37, pp. 1979-1984, December 1989.

[133] E. M. Bastida, G. P. Donzelli, and L. Scopelliti, "GaAs Monolithic Microwave Integrated Circuits Using Broadband Tunable Active Inductors," *Conference Proceedings - European Microwave Conference*, *pp.* 1282-1287, 1989.

[134] P. Alinikula, R. Kaunisto, and K. Stadius, "Monolithic Active Resonators For Wireless Applications," *IEEE MTT-S International Microwave Symposium Digest*, pp. 1151-1154, 1994.

[135] S. Lucynszyn, and D. Robertson, "Monolithic Narrow-Band Filter Using Ultrahigh-Q Tunable Active Inductors," *IEEE Transactions on Microwave Theory and Techniques*, vol. 42, pp. 2617-2622, December 1994.

[136] J. Ko, and K. Lee, "Low Power, Tunable Active Inductor and Its Applications to Monolithic VCO and BPF," *IEEE MTT-S International Microwave Symposium Digest*, pp. 929-932, 1997.

[137] V. Pauker, "GaAs Monolithic Microwave Active Gyrator," *IEEE GaAs IC Symposium*, pp. 82-84, 1986.

[138] Y. Cho, S. Hong, and Y. Kwon, "A Novel Active Inductor and Its Application to Inductance-Controlled Oscillator," *IEEE Transactions on Microwave Theory and Techniques*, vol. 45, pp. 1208-1213, August 1997.

[139] M. E. Kim, A. K. Oki, J. B. Camou, P. D. Chow, B. L. Nelson, D. M. Smith, J. C. Canyon, C. C. Yang, R. Dixit, and B. R. Allen, "12-40GHz Low Harmonic Distortion and Phase Noise Performance of GaAs Heterojunction Bipolar Transistors," *IEEE GaAs IC Symposium*, pp. 117-120, 1988.

[140] J. Cowles, L. Tran, T. Block, D. Streit, C. Grossman, G. Chao, and A. Oki, "A Comparison of Low Frequency Noise in GaAs and InP-based HBTs and VCOs," *IEEE MTT-S International Microwave Symposium Digest*, pp. 689-692, 1995.

[141] M. A. Khatibzadeh, B. Bayraktaroglu, and R. D. Hudgens, "High Power and High Efficiency Monolithic HBT VCO Circuit," *IEEE GaAs IC Symposium*, pp. 11-14, 1989.

[142] Y. Yamauchi, H. Kamitsuna, M. Nakatsugawa, H. Ito, M. Muraguchi, and K. Osafune, "A 15-GHz Monolithic Low-Phase-Noise VCO using AlGaAs/GaAs HBT Technology," *IEEE Journal of Solid State Circuits*, vol. 27, pp. 1444-1447, October 1992.

[143] S. R. Lesage, M. Madihian, N. Hayama, and K. Honjo, "15.6 GHz HBT Microstrip Oscillator," *Electronics Letters*, vol. 24, pp. 230-232, February 1988.

[144] N. Hayama, S. R. Lesage, M. Madihian, and K. Honjo, " A Low-Noise Ku-Band AlGaAs/GaAs HBT Oscillator," *IEEE MTT-S International Microwave Symposium Digest*, pp. 679-682, 1988.

[145] M. Madihian, N. Hayama, S. R. Lesage, and K. Honjo, "A Low-Noise Microwave Oscillator Employing Self-Aligned AlGaAs/GaAs HBT," *IEEE Transactions on Microwave Theory and Techniques*, vol. 37, pp. 1811-1814, November 1989.

[146] K. Sakuno, T. Yoshimasu, and T. Tomita, "A Miniature Low Current GaAs MMIC Downconverter for Ku-band Broadcast Satellite Applications," *IEEE Microwave and Millimeter-Wave Monolithic Circuits Symposium,* pp. 101-104, 1992.

[147] J. Portilla, M. Luisa, J.P. Pascual, and E. Artel, "Low-Noise Monolithic Ku-band VCO using pseudomorphic HEMT Technology," *IEEE Microwave and Guided Wave Letters,* vol. 7, no. 11, pp. 380-382, Nov. 1997.

[148] M. J. Howes and D. V. Morgan, *Microwave Device,* New York, John Wiley & Sons, 1976.

[149] T. Kashiwa, T. Ishida, T. Katoh, H. Kurusu, H. Hoshi, and Y. Mitsui, "V-band High-Power Low Phase-Noise Monolithic Oscillators and Investigation of Low Phase-Noise Performance at High Drain Bias," *IEEE Trans. on Microwave Theory and Techniques,* vol. 46, no. 10, pp. 1559-1565, Oct. 1998.

[150] E. Godshalk, "Phase Noise Issues in Wireless Systems," *ARFTG Conference Short Course on Measurement and Characterization of Broadband Access Technologies*, Atlanta, GA, 1999.

[151] P. B. Kennington, *High-linearity RF Amplifier Design*, Artech House, Boston, 2000.

[152] *EM Users Manual*, Sonnet Software Inc., Liverpool, NY

[153] M. T. Jones, and J. T. Bolljahn, "Coupled Strip Transmission Line Filters and Resonators," *IRE Trans. on Microwave Theory and*

Techniques, vol. 4, pp. 75-81, April 1956.

[154] S. B. Cohn, “Parallel Coupled Transmission Line Resonator Filters,” *IRE Trans. Microwave Theory and Techniques*, vol. 6, pp. 223-231, April 1958.

[155] S. B. Cohn, “Shielded Coupled-Strip Transmission Line,” *IRE Trans. Microwave Theory and Technique*, vol. 3, pp. 29-38, October 1955.

[156] A. Sutono, N. G. Cafaro, J. Laskar, and E. M. Tentzeris, “Experimental Study and Modeling of Bond Wire Interconnects for Microwave Integrated Circuits,” *IEEE AP-S*, vol. 4, pp. 2020-2023, Salt Lake City, UT, January 2000.

This page intentionally left blank

Index

Numerics

1/f noise 37, 52, 55, 65
1-dB compression point 19, 106, 109, 110, 114

A

AC simulation 21, 23
ACI 8
ACPR 5, 19, 20, 22, 26, 134, 136, 140
Air bridges 75
A1GaAs/GaAs ii, vii, 37, 55, 56, 67, 88, 89
AM noise 40
Amplifier efficiency 10

B

Balanced FET mixers 49
Balanced mixers 50
Barkhausen criterion 60
Behavioral model 19
BJT 37, 57, 67, 88
BPF vii, 4, 9, 12, 15, 16, 21, 22, 93, 97, 109, 111, 121, 127, 130, 131, 132, 139
BSS 2
Built-in potential, 34, 73

C

CAD, 19, 21, 26, 93, 124, 139
Cascode 49, 80, 82
Cavity filter, vi, 4, 16
CDMA, 10, 17
Circuit envelope co-simulation 20
Class A 93, 115, 116
Class AB 116
Class B 116
Common gate inductive feedback 62
Common source capacitive feedback 62
Common-drain 78
Common-source 54, 62, 79, 80, 82, 83, 85
Conversion compression 30
Conversion gain 29
Coupled line 122, 128

Coupled strip line 123
CPW 126, 127, 128, 131
Cross modulation 28
Cross talk 7, 15
CS/CG 53, 54

D

DAC. *See* digital to analog converter
Double Balanced 50
Doubly balanced diode-ring mixer 42
DBS v, 1, 3, 55, 134
DC offset 30
DDBM. *See* double doubly balanced mixer
DECT 9
DGFET. *See* dual gate FET
Digital to analog converter 15
Direct conversion 30
Direct to home v, 1, 3
Double conversion 15, 133
Double doubly balanced mixer 43, 44
Double double balanced Schottky mixer 56
Doubly Balanced FET mixers 50
Doubly balanced dual gate FET mixer 51
DQPSK 8
DR 87
Drain mixing 46
DTK. *See* direct to home
Dual gate FET 45, 46, 47
Dual gate mixer 21, 45, 46, 47, 49, 51, 93, 94, 97
Dynamic range, 30

E

E-B heterojunction 37
EM 117, 119, 124, 125
Epitaxial base 57
Even mode characteristic impedance 123
Exponential schemes 8

F

Feedback ii, 59, 60
Feedback oscillator ii, 59
Flicker noise 55
FM noise 64, 65, 70
f_{max} 39, 57, 88, 89
Folded edge coupled strip line filter 124
Free running VCOs 66
Front end 4, 13, 18, 134
FSS 2
f_t 4, 39, 57, 88, 89, 91

G

GaAs ion implantation 55
Sallium doped YIG 67
Generation recombination 37
Gilbert cell mixer, 52, 56
GSM 8
Gunn diode 60
Gyromagnetic 69

H

Harmonic balance 93, 116
HBT ii, vii, 36, 37, 38, 39, 55, 56, 57, 58, 65, 67, 88, 89, 91
HEMT 35, 36, 46, 52, 55, 57, 65
Heterojunction ii, 36
HTS 87

I

IDSVD 74, 75
IIP3 19, 95, 99, 108, 137, 139
Image 54, 140

Image rejection 4, 54
IMD 29, 31, 51
InGaAs 36
INTELSAT, 1
IP3 43, 55, 56, 57, 92, 95
ISM 9
Isolation i, 30, 99
ITU v, 3

J

JDC 8
Johnson noise 55

L

Lange couplers 46
Lattice matching 37, 55
LC 87, 99, 112
LC matching 112
Lesson 64
Link budget analysis 23
LMDS 2, 55
LNA vi
LNB 91
LO radiation, 16
LO rejection, 9, 41, 46, 125, 132
LO-RF isolation, 13, 30, 46, 98
Low temperature co fired ceramic iii, vi, vii, 4, 9, 16, 21, 93, 121, 124, 125, 127, 128, 129, 130, 131, 137, 139, 140
Low power tunable active inductor 82, 83
LPF 16
LPTAI. *See* low power tunable active inductor
LTCC. *See* low temperature co fired ceramic

M

Marchand balun 43
MBE 36
Mesa type 74, 75
MESFET ii, vi, vii, 4, 34, 35, 36, 46, 52, 55, 56, 57, 62, 66, 67, 71, 72, 73, 75, 77, 78, 81, 85, 86, 87, 88, 89, 91, 116, 119, 137, 139
Metal insulator metal 81, 91, 95, 99, 112
MIM. *See* metal insulator metal
Modulator, i, 7
Modulation accuracy, 7
MoM 101, 124, 125, 126
MSS 2
Multi layer vi, 127, 130, 139
LTCC substrate 127, 130, 139

N

NADC 8
Negative resistance ii, 60, 61
NF. *See* noise figure
NiCr resistors 91
Noise figure 24, 31, 36, 57
Non inverting amplifier 82

O

ODU 3
One port Model ii, 60
OQPSK 8
Orbital slots v, 3
Out of band Emission 25
Output power spectrum 65, 134, 135

P

PAE 119
PCS 8
Peak to average ratio 10, 115
Phase noise vi, 4, 14, 15, 21, 55, 60, 63, 64, 65, 67, 72, 78, 85,

87, 88, 89, 91, 92, 100, 101, 102, 103, 105, 116
Phased array 4
Physical models 47
PLL 17, 78, 89
Positive feedback amplifier 86
Post tuning drift ii, 63, 66
Pulling ii, 65, 66
Pushing ii, 65
Push pull 116

Q

QPSK 7, 8, 10, 19, 20, 23, 25, 115, 134
constellation 23
Quadrature hybrid 50

R

Reactive matching 108
Recessed gate 35
Re entrant self shielding magnetic circuit 69
Reflection coefficient line, vi, 4, 91, 99, 100
RF-IF isolation 97, 98
Rollet stability factor 61

S

Schottky barrier diode 29, 32, 33, 50, 57, 77
Self aligned 38
Self mixing 12, 30
Semi insulating substrate 38, 74
Si BJT 57, 67, 88
SiGe, 37, 38, 39, 55, 56, 57, 58
Signal to noise ratio 31, 54
Single crystal YIG 67
Single diode mixers 40, 41
Single Gate Mixer 45
Singly balanced mixer 41
SNR 31
Source follower 78
Spectral emission 9
Spurious ii, 25, 31
response, 43, 92
SSB 16, 64, 88
phase noise 64, 88
Strip line filter iii, vi, 4, 121
Surface state problem 88
System performance vi, 4, 19, 22, 25, 26, 139, 140

T

TAI 63, 81, 82, 83, 85, 87, 89
TCR 77
TDMA 17, 25
Third order products 31
Three terminal device, 32, 39, 60
TOM3 116
Transmitter, i, ii, 7, 19, 25, 26, 91, 92, 119, 121, 140
Trapping detrapping 37
Turn on voltages 44
Two port Model ii, 59
Two step transmitter 17
Two terminal device 32, 60
Two tone intercept point
intermodulation distortion 31

U

Up conversion, vi, 9, 11, 12, 13, 14, 15, 16, 17, 65, 93, 111
USB 109

V

Varactor diodes 88
Varactor tuned oscillator, 76, 77
VCO pulling 12, 16, 17
Voltage standing wave ratio 66
VSAT v, vi, 1, 2, 3, 4, 16, 23, 25, 129

VSWR. *See* voltage standing wave ratio

Y

YIG ii, 63, 67, 68, 69, 70, 71, 72, 73, 87, 88
sphere 67, 68, 69
tuned oscillator ii, 67